High-Throughput Operant Conditioning in *Drosophila* Larvae

Kristina Tenna Klein

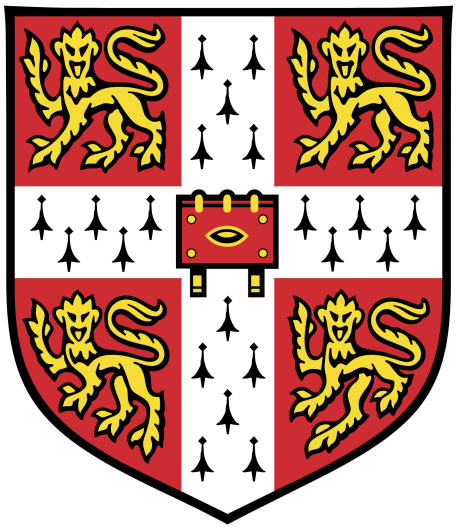

Department of Zoology

University of Cambridge

This thesis is submitted for the degree of Doctor of Philosophy.

Trinity College

September 2019

Preface

This thesis is the result of my own work and includes nothing which is the outcome of work done in collaboration except as declared in the Preface and specified in the text. It is not substantially the same as any that I have submitted, or, is being concurrently submitted for a degree or diploma or other qualification at the University of Cambridge or any other University or similar institution except as declared in the Preface and specified in the text. I further state that no substantial part of my thesis has already been submitted, or, is being concurrently submitted for any such degree, diploma or other qualification at the University of Cambridge or any other University or similar institution except as declared in the Preface and specified in the text. It does not exceed the prescribed word limit for the relevant Degree Committee.

Some of the work presented in this dissertation is the result of collaboration with Dr Lakshmi Narayan, Dr Jean-Baptiste Masson, Elise Croteau-Chonka, Dr Christopher McRaven, Dr Michael Winding, Dr Peter Polidoro, Monti Mercer, Dr Brandi Sharp and the HHMI Janelia FlyLight team as indicated in the relevant passages of the text.

Summary

Author: Kristina Tenna Klein

Title: High-Throughput Operant Conditioning in *Drosophila* Larvae

Operant conditioning is the process by which animals learn to associate their own behaviour with positive or negative outcomes, biasing future action selection in order to maximise reward and avoid punishment. It is an important strategy to ensure survival in an ever-changing environment. Although operant conditioning has been observed across vertebrate and invertebrate species, the underlying neural mechanisms are still not fully understood.

The *Drosophila* larva is an excellent model system to study neural circuits, since it is genetically tractable, with a variety of tools available. Although it is quite small, it is capable of a diverse range of behaviours and can achieve complex learning tasks. However, while the mechanisms underlying classical conditioning, where animals learn about the appetitive or aversive qualities of an external sensory cue, have been extensively studied in larvae, it has remained an open question whether they are capable of operant conditioning. This is in part due to the challenges which arise during the training process: in order to train an animal to associate its own actions with their outcomes, the experimenter needs to be able to deliver rewarding or punishing stimuli directly in response to behaviour.

In this thesis, I introduce a novel high-throughput tracker suitable for training up to 16 larvae simultaneously. I have developed a customised software for real-time detection of various actions that larvae perform: left and right bend, forward crawl, roll and back-up. Light and heat stimuli can be administered at individual animals with minimal delay, enabling optogenetic or thermogenetic activation of circuits encoding reward or punishment in response to behaviour. Using this system, I show that *Drosophila* larvae are capable

of operant conditioning. Pairing bends to one direction, e. g. the left, with optogenetic activation of a large group of reward-encoding dopaminergic and serotonergic neurons is sufficient to induce a learned preference for bending towards this side after training. I explore whether there are other types of actions which larvae can learn to associate with valence, and introduce a second operant conditioning paradigm, in which larvae modify their behaviour following pairing of the stimulus with forward crawls.

To identify new candidate neurons signalling valence in a learning context, I also conduct a classical conditioning screen, in which I pair an odour with optogenetic activation of distinct neuron types covered by different driver lines. While activation of many types of gustatory sensory neurons paired with the odour was insufficient for memory formation, I find that the serotonergic neurons of the brain and the subesophageal zone (SEZ) can induce strong appetitive learning. Finally, I show that activity of serotonergic rather than dopaminergic neurons is sufficient for memory formation in the operant bend direction paradigm, and that operant conditioning is impaired when restricting activation to the serotonergic neurons of the brain and the SEZ.

My results suggest a novel role of serotonergic neurons for learning in insects as well as the existence of learning circuits outside of the mushroom body. Different subsets of serotonergic neurons mediate classical and operant conditioning. This works lays a foundation for future studies of the function of serotonin and the mechanisms underlying operant conditioning at both circuit level and cellular level.

Quidquid agis, prudenter agas et respice finem.

Whatever you do, choose your actions wisely and consider their outcomes.

—Gesta Romanorum

凡事预则立，不预则废。

Success depends upon previous preparation, and without such preparation there will be failure.

—Confucius

Acknowledgements

This project would not have been possible without the help of many people. First and foremost, I would like to thank my supervisor, Dr Marta Zlatic, for planning this project together with me and for providing the necessary resources. Our many useful discussions contributed significantly to the success of the experiments.

I would also like to express my gratitude to Dr Lakshmi Narayan, Dr Jean-Baptiste Masson, Elise Croteau-Chonka, Dr Christopher McRaven, Dr Michael Winding, Dr Peter Polidoro and the HHMI Janelia FlyLight team, with whom I have collaborated on various aspects of this project and who have taught me invaluable skills which have proven useful throughout my work. I am also grateful to Monti Mercer and Dr Brandi Sharp for their help with setting up some of the fly crosses. Of course, special thanks go to the tens of thousands of larvae who have paid for their involuntary participation in my experiments with their lives.

I would further like to thank Dr Greg Jefferis, Dr Matthias Landgraf and Dr Jimena Berni for providing additional guidance and for welcoming me in Cambridge after my move. I am also grateful to the many researchers at Janelia Research Campus and in Cambridge, especially all the members of the Zlatic lab, who have asked stimulating questions and facilitated new ideas.

My studies were generously funded by a Gates Cambridge Scholarship. I would also like to express my gratitude to Howard Hughes Medical Institute and the Janelia Visiting Scientist programme for allowing me to spend the first two years of my studies at Janelia Research Campus, where I had access to invaluable resources, and to the Department of Zoology for providing me lab and office space despite ongoing renovations.

I would also like to thank Trinity College and especially the BA Society for making my time in Cambridge truly unforgettable. In addition, I would like to express my thanks to all

my friends from outside my academic environment, who have supported me with frequent Skype calls and occasional visits. Finally, I am deeply grateful to my mother, Cornelia Klein, for boundless support during my degree and throughout my entire life.

List of Figures

List of Tables

Abbreviations

C. elegans *Caenorhabditis elegans*.

CNS central nervous system.

CS conditioned stimulus.

CSD contralaterally projecting serotonin-immunoreactive deutocerebral.

DLL dynamic link library.

DMD digital micromirror device.

DPM dorsal paired medium.

EM electron microscopy.

FPGA field-programmable gate array.

GFP Green Fluorescent Protein.

IR infrared.

KC Kenyon cell.

MBON mushroom body output neuron.

MWT Multi-Worm Tracker.

NPF neuropeptide F.

PI performance index.

PKC protein kinase C.

ROS Robot Operating System.

SEZ subesophageal zone.

US unconditioned stimulus.

VNC ventral nerve cord.

Contents

1 Introduction

Animals need to be able to rapidly alter their behaviour in response to changes in their environment. An important strategy of adaptation to novel circumstances is by forming associations between events through a process called associative learning (Dickinson, 1981; Rescorla, 1988). As a result, an animal learns to predict an unconditioned stimulus (US) by the occurrence of a conditioned stimulus (CS) (Fig. 1.1a). The US often takes the form of a punishing or rewarding event, such as pain or the discovery of a new food source (Pavlov, 1927). Based on the nature of the CS, one can distinguish between two major types of associative learning: classical conditioning (Pavlov, 1927) and operant conditioning (Skinner, 1938; Thorndike, 1911).

For classical conditioning, the CS is an external stimulus from the environment, such as a sound, an odour or a visual cue. Pairing with an appetitive or aversive US leads to approach or avoidance of the CS in the future (Fig. 1.1b). Perhaps the most famous example is the experiment by Ivan Pavlov (1927), in which he conditioned dogs to predict food by the sound of a tone. However, classical conditioning is not limited to dogs. Many different species, including humans (Andreatta and Pauli, 2015; Austin and Duka, 2010; Kershaw and Running, 2018), are able to associate a previously neutral stimulus with reward or punishment, resulting in approach or avoidance. Rodents can learn to predict a food reward by the occurrence of an acoustic (Bouton and Peck, 1989; Holland and Rescorla, 1975) or a visual cue (Holland and Rescorla, 1975; McDannald et al., 2011). They are also capable of aversive classical conditioning as induced by a punishing US such as an electric shock (Brown et al., 1951; Jones et al., 2005). Zebrafish can form associations between a variety of sensory stimuli and subsequent food reward (Braubach et al., 2009; Mueller and Neuhauss, 2012; Sison and Gerlai, 2010).

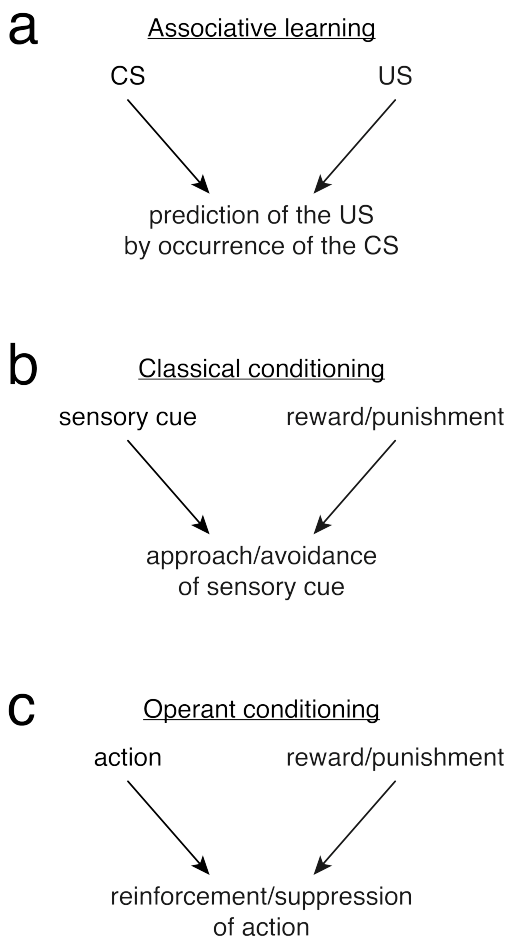

Figure 1.1: Associative learning. a. Associative learning is the process in which an animal learns to predict a previously neutral conditioned stimulus (CS) by the occurrence of an unconditioned stimulus (US). One can distinguish between two major forms of associative learning, classical conditioning and operant conditioning. **b.** For classical conditioning, the CS is an external sensory cue. Association with a rewarding or punishing US results in learned approach or avoidance of the sensory cue. **c.** In the case of operant conditioning, the CS is one of the animal's own actions. Resulting reward or punishment leads to reinforcement or suppression of the action in the future.

Invertebrates are often more accessible to investigating neural circuits due to the relative simplicity of their nervous system. They are also capable of classical conditioning, which makes them a powerful model system to study learning (Hawkins and Byrne, 2015). There are many examples of classical conditioning in insects. For example, honeybees show enhanced proboscis extension when presented with an odour after it was paired with sucrose reward (Bitterman et al., 1983; Takeda, 1961). Similarly, they exhibit the sting extension reflex as an aversive response to a previously neutral odour after training with electric shock as a US (Giurfa et al., 2009). Mosquitoes are able to form long-term olfactory memory when the odour is followed by a blood reward (Vinauger et al., 2014). The fruit fly *Drosophila* is capable of associating olfactory (Cognigni et al., 2018; Davis, 2005; Scherer et al., 2003; Tully and Quinn, 1985), visual (Gerber et al., 2004; Menne and Spatz, 1977; Schnaitmann et al., 2010; Vogt et al., 2014; von Essen et al., 2011) and gustatory (Masek and Scott, 2010) cues with reward or punishment. The pond snail *Lymnaea* provides an example of a mollusc which shows classical conditioning by reward (Alexander et al., 1984). Even the nematode *Caenorhabditis elegans*, whose nervous system only comprises 302 neurons (White et al., 1986), is capable of forming both long-term and short-term memory (Amano and Maruyama, 2011; Kauffman et al., 2010; Nishijima and Maruyama, 2017; Wen et al., 1997). In many species across the animal kingdom, specific circuits have been identified as the sites of conversion and association of the external CS and the rewarding or punishing US (Caroni, 2015; Gründemann and Lüthi, 2015; Hawkins and Byrne, 2015; Heisenberg et al., 1985; Owald and Waddell, 2015; Tonegawa et al., 2015).

On the other hand, in the case of operant conditioning, the CS is one of the animal's own actions (Skinner, 1938; Thorndike, 1911). As a result of memory formation, the animal learns to predict the outcomes of its behaviour and biases future action selection accordingly, usually in order to maximise reward and avoid punishment (Skinner, 1938; Fig. 1.1c). This is a phenomenon which can be observed in many species. Mice learn to press a lever at very high frequencies to obtain a sugar reward (Jin and Costa, 2010). Both rats (Corbett and Wise, 1980; Olds and Milner, 1954) and monkeys (Lovell et al., 2015; Mora et al., 1979) can be conditioned to perform simple actions at a high rate to self-stimulate reward areas in their brain through an implanted electrode. Operant conditioning can also lead to the generation of novel action sequences. For example, dogs can be trained to imitate a series of complex actions presented to them by a human, using

access to their favourite toy as a reinforcer (Topál et al., 2006). Juvenile songbirds learn to produce stereotyped vocalizations highly similar to a tutor song which they hear early in development (Fee and Goldberg, 2011; Nottebohm, 1991). These examples demonstrate the relevance of operant conditioning to a variety of diseases, such as impaired language acquisition, obsessive-compulsive disorders and addiction (Balleine et al., 2015; Drash and Leibowitz, 1973; Everitt et al., 2018; Joel, 2006; Pickett et al., 2009; Sturdy and Nicoladis, 2017).

The ability to adapt one's behaviour in response to reward or punishment is not limited to vertebrate species but has also been demonstrated in invertebrates (Brembs, 2003; Hawkins and Byrne, 2015). For example, locusts are able to associate their leg position with relief of an aversive tone or with the provision of a food reward (Hoyle, 1979). Honeybees can be trained to enhance the activity of antennal muscles to obtain a sucrose reward (Erber et al., 2000; Kisch and Erber, 1999), and they are also capable of learning new actions in order to reach a food source (Abramson et al., 2016).

In adult *Drosophila*, operant conditioning by punishment or reward has been demonstrated in various experimental settings. In a reward learning paradigm by Nuwal et al. (2012), flies walking on a rotating ball were conditioned to develop a directional preference for turning movements to one side. They can also learn to adjust their leg position to avoid an electric shock (Booker and Quinn, 1981). They can further be trained to bias yaw torque in stationary flight to evade punishment by noxious heat (Wolf and Heisenberg, 1991).

Although there are countless examples of operant conditioning, using a variety of CS–US combinations, the underlying mechanisms are still not fully understood. During some operant conditioning tasks, classical conditioning takes place as well. Colomb and Brembs (2010) hence distinguish between the terms "world-learning" and "self-learning" to describe the processes of assigning value to a sensory cue or an action, respectively. For example, consider an operant conditioning paradigm in which mice learn to repeatedly press a lever to reach a reward source (Jin and Costa, 2010). While the animals associate the action of lever-pressing with its rewarding outcome (self-learning), they also learn about the reward-predicting properties of the lever (world-learning). By contrast, classical conditioning purely relies on world-learning (Colomb and Brembs, 2010). Therefore, to fully

understand the neural mechanisms driving operant conditioning, one needs to dissociate the self-learning component from the world-learning component.

In order for an animal to form an association between an action and its outcome, information about the action needs to converge with circuits encoding positive or negative valence. In vertebrates, basal ganglia-like structures constitute an example of such a convergence site in the brain, as they receive inputs from both motor efference copy and dopaminergic neurons conveying valence (Balleine et al., 2009; Fee and Goldberg, 2011; Redgrave et al., 2011). However, there are cases of learned associations between actions and outcomes in which the brain has turned out to be dispensable. For example, there is evidence for successful conditioning of leg position in decapitated flies, cockroaches and locusts (Booker and Quinn, 1981; Horridge, 1962). Analogous observations have been made in spinalised rats (Grau et al., 1998), suggesting that there may be more than just a single area in the central nervous system (CNS) where operant conditioning takes place.

It is unclear to what extent learning at these convergence sites is mediated by plasticity at the synaptic connections between neurons as opposed to by modulating intrinsic excitability of individual neurons. In mammals, there is evidence that dopamine signalling can modulate the synaptic strength of efference copy input to the basal ganglia (Lovinger, 2010; Reynolds and Wickens, 2002; Surmeier et al., 2007). Operant conditioning of leg position in rats involves spinal cord synaptic plasticity (Gómez-Pinilla et al., 2007; Joynes et al., 2004). However, molecular mechanisms for increased excitability of basal ganglia spiny neurons have been proposed as well (Dong et al., 2006; Shen et al., 2005). Furthermore, in the mollusc *Aplysia*, operant conditioning in a feeding circuit (Nargeot et al., 1997) leads to enhanced intrinsic excitability of neurons involved in action selection (Brembs et al., 2002) and initiation (Nargeot et al., 2009).

A few highly conserved genes have been linked to the memory formation process. The protein kinase C (PKC) is essential for operant conditioning in *Aplysia* (Lorenzetti et al., 2008), *Lymnaea* (Rosenegger and Lukowiak, 2010) and *Drosophila* (Brembs and Plendl, 2008), where it is specifically needed in motor neurons (Colomb and Brembs, 2016). Mutations in the *Drosophila* gene *FoxP* result in impaired operant self-learning in a flight simulator paradigm (Mendoza et al., 2014). Its vertebrate homologue *FOXP2* is associated with deficits in human speech acquisition (Lai et al., 2001), song learning in birds (Haesler et al., 2007) and motor learning in mice (Groszer et al., 2008).

These examples suggest that the principles of operant conditioning are conserved across species. To fully understand the underlying neural mechanisms at a circuit level, there is the need for a simple learning paradigm in a model system which offers a variety of easily accessible neurobiological tools. In this thesis, I will investigate the neural circuits of operant conditioning in the *Drosophila* larva, a small model organism which combines substantial advantages, such as complex behaviour, the ability to learn, a wide range of genetic tools and an emerging connectome.

1.1 The *Drosophila* larva as a model system for learning

The larva of the fruit fly *Drosophila melanogaster* is a particularly well-suited model organism to study the neural circuits underlying learning and memory. Despite being small in size, larvae are capable of a wide range of different actions. This becomes most apparent when they leave their natural food source and navigate their environment on a two-dimensional surface. Larvae move around their substrate through peristaltic forward crawling (Heckscher et al., 2012; Fig. 1.2a). Occasionally, they stop to explore their environment by bending their head to the left or right one or more times, usually resulting in a change of crawling direction (Gomez-Marin et al., 2011; Kane et al., 2013; Luo et al., 2010; Fig. 1.2b).

In the presence of an unpleasant stimulus, larvae exhibit a variety of escape behaviours. Most commonly, they increase their bend rate to navigate away from undesirable conditions such as extreme temperature (Lahiri et al., 2011; Luo et al., 2010), light (Kane et al., 2013) or wind (Jovanic et al., 2019). Another typical avoidance response is by moving away from the aversive source with one or more backward peristaltic waves (back-up; Fig. 1.2c) (Heckscher et al., 2012; Jovanic et al., 2017; Kernan et al., 1994; Vogelstein et al., 2014). In response to mechanical stimuli such as touch (Kernan et al., 1994; Tsubouchi et al., 2012) or an air current (Jovanic et al., 2017, 2016), larvae often show head retraction behaviour (hunch; Fig. 1.2d). Perhaps the most drastic escape response is rolling, where the animal curls into a C-like shape and turns around its own body axis with a fast sideways movement (Hwang et al., 2007; Ohyama et al., 2013; Robertson et al., 2013; Fig. 1.2e). Under natural conditions, rolling is only observed in the presence of a strong noxious stimulus, such as heat or a predator attack (Ohyama et al., 2015; Robertson et al., 2013;

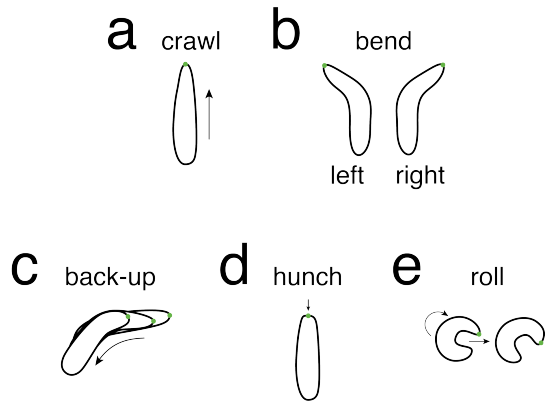

Figure 1.2: Behavioural repertoire of *Drosophila* larvae. Schematics of the five most prominent actions displayed by *Drosophila* larvae are shown. The contour of the larva is displayed as a black outline, the green dot marks the head. **a.** crawl, **b.** left and right bend, **c.** back-up, **d.** hunch, **e.** roll.

Tracey et al., 2003). This variety of actions facilitates studying the neural mechanisms of behaviour in the larva.

Furthermore, the large number of genetic tools which are available in adult *Drosophila* can be accessed in the larva as well. The GAL4-UAS system allows for targeted expression of a protein in any tissue of interest. To achieve this, the transcription factor GAL4 is expressed under a tissue-specific promoter. Expression of the gene controlled by the UAS promoter is then activated in those cells where GAL4 is present (Brand and Perrimon, 1993; Fischer et al., 1988; Fig. 1.3). The power of this toolkit lies in its design as a binary system: a variety of GAL4 driver and UAS effector constructs can each be maintained in separate, homozygous fly strains, which makes it possible to obtain any driver–effector combination in the offspring through a single cross.

The GAL4-UAS system has become especially useful in neuroscience. In *Drosophila*, individual neurons are uniquely identifiable and identical in morphology and function across animals (Bate et al., 1981; Jefferis et al., 2007; Marin et al., 2002; Skeath and Thor, 2003; Wong et al., 2002). Therefore, neuron-specific GAL4 drivers reproducibly target the same group of cells in each individual. Jenett et al. (2012) have developed a large collection of GAL4 driver lines, each specific to a distinctive subset of neurons. The split-GAL4 system allows to narrow down GAL4 expression to an even sparser subset of neurons (Luan et al., 2006; Pfeiffer et al., 2010).

There are a variety of effectors which can be expressed under control of the UAS promoter to investigate the function of individual neurons in the nervous system. To assess

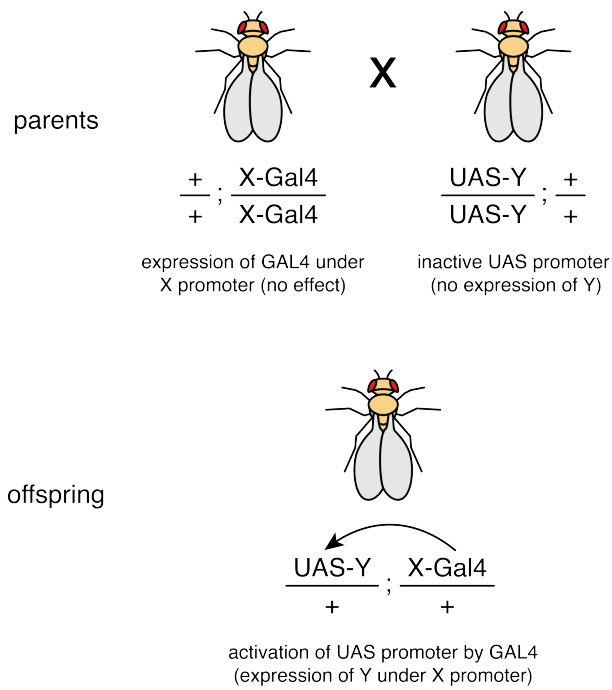

Figure 1.3: GAL4-UAS system. Parents are homozygous for either the GAL4 construct (expression of GAL4 under promoter X) or the UAS construct (expression of protein Y under the UAS promoter). The UAS promoter is inactive, since no GAL4 is present in the same flies. Therefore, protein Y is not expressed. The offspring contains genetic copies of both the GAL4 construct and the UAS construct. GAL4 activates the UAS promoter in the cells controlled by promoter X, leading to expression of protein Y. Figure inspired by St Johnston (2002).

the location and anatomical features of the neurons targeted by the GAL4 driver, one can use the Green Fluorescent Protein (GFP) (Lee and Luo, 1999) as a marker.

An especially powerful technique is optogenetics, by which neurons can be activated with light at high temporal resolution (Lima and Miesenböck, 2005; Zemelman et al., 2002). Klapoetke et al. (2014) have developed the red-shifted channelrhodopsin *CsChrimson*, which can be expressed under control of a GAL4 driver. Neurons expressing *CsChrimson* cannot only be activated with blue light, as is the case for many traditional channelrhodopsins (Boyden et al., 2005; Dawydow et al., 2014), but also with red light. Since *Drosophila* larvae can sense and will innately avoid blue light, but not red light (Xiang et al., 2010), *CsChrimson* is currently one of the most widely used channelrhodopsins for optogenetic activation of neurons in this model system.

Neural activity can also be modulated with heat through an approach called thermogenetics. The warmth-sensing ion channel *dTrpA1* (Hamada et al., 2008) can be used for targeted activation of neurons by exposing the animals to higher temperatures. It is also possible to use heat to silence a set of neurons expressing Shi^{ts}, a temperature-sensitive *Shibire* allele, through the GAL4-UAS system (Kitamoto, 2001).

This broad availability of tools has made the *Drosophila* larva a powerful model organism for studying the neural basis of learning and memory. There is overwhelming evidence that larvae are capable of classical conditioning. For example, they can be trained to approach an odour which is paired with gustatory reward such as sugar (Hendel et al., 2005; Neuser et al., 2005; Rohwedder et al., 2012; Schipanski et al., 2008; Schleyer et al., 2011) or amino acids (Kudow et al., 2017). Salt can serve as both a positive and a negative reinforcer in olfactory conditioning in a concentration-dependent manner (Niewalda et al., 2008; Schleyer et al., 2011). In addition, electric shock (Aceves-Piña and Quinn, 1979; Khurana et al., 2009; Pauls et al., 2010; Tully et al., 1994), heat (Khurana et al., 2012), vibration (Eschbach et al., 2011) and the bitter compound quinine (Apostolopoulou et al., 2014; Gerber and Hendel, 2006) can be used as a punishing US in aversive olfactory conditioning.

Not just an odour, but also light can serve as a CS for classical conditioning. Larvae innately avoid light and prefer darkness (Sawin-McCormack et al., 1995). This negative phototaxis can be modulated when light or darkness are paired with reward or punishment

(Gerber et al., 2004; von Essen et al., 2011). Similarly, light can act as a negatively reinforcing US in learning paradigms where the CS is an odour (von Essen et al., 2011).

Many studies have addressed the neural mechanisms underlying classical conditioning in *Drosophila*. In both larval and adult flies, the CS and the US converge in a brain area called mushroom body (Cognigni et al., 2018; Heisenberg, 2003; Heisenberg et al., 1985; Owald and Waddell, 2015; Rohwedder et al., 2016; Saumweber et al., 2018; Vogt et al., 2014). In each hemisphere, the CS is encoded by a subset of the approximately 110 Kenyon cells (KCs) (Aso et al., 2014a; Berck et al., 2016; Campbell et al., 2013; Eichler et al., 2017; Honegger et al., 2011; Lin et al., 2014; Owald and Waddell, 2015; Turner et al., 2008), which converge onto 24 mushroom body output neurons (MBONs) driving approach or avoidance (Aso et al., 2014b; Eichler et al., 2017; Owald et al., 2015; Perisse et al., 2016; Plaçais et al., 2013; Saumweber et al., 2018; Séjourné et al., 2011; Shyu et al., 2017).

The strength of the connection between individual KCs and MBONs is modulated by dopaminergic and octopaminergic neurons, which represent the rewarding or punishing US (Honjo and Furukubo-Tokunaga, 2009; Saumweber et al., 2018; Schroll et al., 2006; Schwaerzel et al., 2003; Vogt et al., 2014; Waddell, 2013). The four dopaminergic neurons of the PAM cluster, which innervate the mushroom body, are both necessary and sufficient to signal reward for classical conditioning (Cognigni et al., 2018; Liu et al., 2012; Rohwedder et al., 2016; Vogt et al., 2014; Waddell, 2013).

The compactness of the larval CNS has made it feasible to manually reconstruct neurons and their synaptic partners from an electron microscopy (EM) volume (Berck et al., 2016; Eichler et al., 2017; Fushiki et al., 2016; Jovanic et al., 2016, 2019; Larderet et al., 2017; Ohyama et al., 2015; Schlegel et al., 2016). This technique has given rise to a full wiring diagram of the larval mushroom body (Eichler et al., 2017).

Despite the abundance of studies addressing learning in the *Drosophila* larva, it has remained an open question whether it is capable of operant conditioning. If larvae are indeed able to associate their own actions with the respective outcomes, this would bring up the question where in the CNS the memory is formed. Previous work in adult flies suggests that the association of behaviour with punishment does not require the mushroom body (Booker and Quinn, 1981; Colomb and Brembs, 2010, 2016; Wolf et al., 1998) and

may instead involve plasticity in motor neurons (Colomb and Brembs, 2016). However, the neural correlates of operant conditioning in *Drosophila* are still not fully understood.

1.2 Automated high-throughput operant conditioning in multiple animals

To potentially induce operant conditioning in the larva, one needs to be able to pair one of its actions with reward or punishment. This requires detecting its behaviour in real time, such that the US can be administered with minimal delay. Such an experimental set-up would be most efficient if it could deliver reward or punishment in a fully automated way, and if it operated at high throughput, allowing to condition multiple animals simultaneously.

Automated operant conditioning in freely behaving animals often relies on an external read-out of behaviour, such as a lever (Corbett and Wise, 1980; Fernando et al., 2015; Jin and Costa, 2010) or a touch sensor (He et al., 2015). Due to the stereotypic nature of behaviour and limited visual sensation in *Drosophila* larvae, it would be challenging to design such a sensor in a way that would allow to unambiguously induce operant conditioning.

An alternative approach is to use immobilised animals in a virtual environment. For example, walking direction in adult *Drosophila* can be conditioned in a set-up where a single fly is walking on a rotating ball (Nuwal et al., 2012). To condition yaw torque in stationary flight, flies are usually tethered in a flight simulator (Brembs, 2011; Wolf and Heisenberg, 1991; Wolf et al., 1998). Such designs have limitations, since they require restricting the animal in its freedom to move.

A third option would be to detect actions in freely behaving animals using computer vision. Such a behaviour detection would have to operate in real time and would need to control the delivery of the US in closed loop, i. e. directly in response to behaviour.

Several algorithms for real-time animal tracking already exist. For example, the position and orientation of single dragonflies in three-dimensional space can be tracked at high speed (Mischiati et al., 2015). Stowers et al. (2017) have developed software for tracking the head position of freely behaving mice in a virtual reality in real time. There are numerous tracking frameworks for adult *Drosophila*, some of which require the flies to be moving within a two-dimensional plane (Donelson et al., 2012; Straw and Dickinson,

2009), while others can detect the position of single (Fry et al., 2008) or multiple (Grover et al., 2008; Straw et al., 2011) flies in a three-dimensional environment. The Multi-Worm Tracker (MWT) software developed by Swierczek et al. (2011) is suitable for simultaneously tracking a large number of *C. elegans*. It has been adopted for use in *Drosophila* larvae, where it has become a powerful tool for analysing the reaction in response to a variety of stimuli (Jovanic et al., 2019; Ohyama et al., 2013; Vogelstein et al., 2014).

However, the above techniques can only provide limited online analysis of animal behaviour, such as position, orientation and sometimes velocity. The targeted delivery of reward or punishment in response to an action, as would be needed to induce operant conditioning, requires a more advanced behaviour detection. Offline classification algorithms exist for a small number of behaviours in bees (Veeraraghavan et al., 2008), *C. elegans* (Huang et al., 2006) and zebrafish larvae (Mirat et al., 2013). By contrast, much more detailed behaviour detection methods have been developed for *Drosophila*. There are a variety of approaches for detecting a wide range of actions in adult flies (Branson et al., 2009; Katsov and Clandinin, 2008; Robie et al., 2017). More targeted frameworks exist for studying behaviours such as courtship or aggression, which involve several interacting flies (Dankert et al., 2009; Hoyer et al., 2008). In the larva, offline behaviour detection pipelines cover the majority of distinguishable actions and have become increasingly sophisticated over time (Denisov et al., 2013; Gershow et al., 2012; Gomez-Marin et al., 2011; Jovanic et al., 2017; Luo et al., 2010; Ohyama et al., 2013, 2015; Vogelstein et al., 2014).

An important limitation of these behaviour detection frameworks is run time. Many approaches require complicated mathematical models, which are too costly to be executed online. Furthermore, detection of certain actions has turned out to be much more reliable when it is based on the integration of both past and future information (Gomez-Marin et al., 2011; Jovanic et al., 2017). There are hence only a few examples in which both tracking and behaviour detection have been achieved in real time, which are usually limited to detecting simple actions in single animals (Schulze et al., 2015; Zabala et al., 2012).

In order to study operant conditioning in freely behaving *Drosophila* larvae at high throughput, a novel computer vision-based real-time behaviour detection software for multiple animals is needed. Optimising execution time is crucial when designing such a system. Field-programmable gate arrays (FPGAs) can reach high processing speeds because of their large potential for parallelisation (Li et al., 2011; Soares dos Santos and

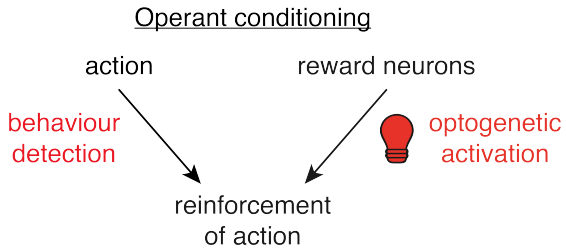

Figure 1.4: Automated operant conditioning. To induce operant conditioning in a fully automated way, one can detect an animal's behaviour in real time and reinforce an action of interest by optogenetically activating reward circuits in response to this action (light bulb).

Ferreira, 2014), up to an extent where they outperform other processor types such as CPUs or GPUs (Asano et al., 2009; Draper et al., 2003; Nurvitadhi et al., 2016). This has led to many implementations for image processing (Li et al., 2011; Zhang et al., 2017), with real-time applications becoming increasingly popular (Chiuchisan, 2013; Shirvaikar and Bushnaq, 2009; Uzun et al., 2005; Yasukawa et al., 2016). In neuroscience, FPGAs have been adopted for real-time tracking of zebrafish larvae (Cong et al., 2017) and rats (Chen et al., 2005). Karagyozov et al. (2018) have used an FPGA for updating the position of a real-time calcium imaging objective by tracking fluorescent neurons in a freely behaving *Drosophila* larva. An FPGA could therefore provide a solution for high-speed real-time behaviour detection of multiple *Drosophila* larvae.

To pair an action with reward or punishment, one needs to be able to administer the US to each larva individually, depending on its behaviour. A possible US for automated operant conditioning is the optogenetic activation of reward circuits in response to detection of an action of interest (Fig. 1.4). In single-larva experiments, closed-loop optogenetic stimulation is not hard to achieve: one only needs to use the output of the behaviour detection to control an LED (Schulze et al., 2015) which illuminates the animal. However, existing optogenetic set-ups for multiple larvae have been restricted to illuminating the entire arena (Klein et al., 2015; Ohyama et al., 2015; Vogelstein et al., 2014), and thus cannot be used to deliver the stimulus to only a subset of larvae which are performing the conditioned behaviour at a given point in time. Similar limitations apply to the control of a thermogenetic stimulus (Honda et al., 2016; Tastekin et al., 2015).

Bath et al. (2014) have used a two-axis galvanometer set-up to rapidly direct an infrared (IR) laser beam at a walking adult fly, which is sufficient to heat it up for thermogenetic

stimulation. In an experiment involving two freely behaving flies, a similar approach was used by Wu et al. (2014) to achieve optogenetic stimulation of one, but not the other fly. Since galvanometers can be used to move around a light beam at very high velocities, they may provide a perspective for individually targeting a US at multiple animals simultaneously. If combined with behaviour detection, such a set-up would fulfil the requirements of a high-throughput operant conditioning paradigm.

1.3 Aim of this thesis

The aim of this thesis is to establish the *Drosophila* larva as a powerful model system to study the neural mechanisms underlying operant conditioning, and to identify neurons involved in the learning process.

In Chapter 3, I will lay the technical foundations which are necessary to study operant conditioning at high throughput. I will introduce a novel experimental set-up which can track multiple larvae using an FPGA and detect their behaviour in real time. Optogenetic and thermogenetic stimuli can be independently administered at subsets of larvae with minimal delay directly in response to their behaviour. In Chapter 4, I will use this set-up to introduce a first operant conditioning paradigm, in which larvae learn to associate bend direction with reward. In Chapter 5, I will then explore whether other behaviours can be associated with the US.

Chapters 6 and 8 will be dedicated to investigating the neural circuits underlying operant conditioning in the bend direction paradigm. In Chapter 6, I will assess the role of the brain and the mushroom body in the learning process. In Chapter 7, I will perform a classical conditioning screen to identify novel candidate neurons for signalling reward or punishment in a learning context. Finally, I will test whether the newly identified candidate neurons can drive the formation of operant memory in Chapter 8.

2 Materials and Methods

2.1 Fly strains and handling

Fly stocks were maintained in vials filled with standard cornmeal food (Wirtz and Semey, 1982; 49.2 ml of molasses, 19.9 g of yeast, 82.2 g of cornmeal, 7.4 g of agarose, 9.8 ml of 20% Tegosept solution in 95% ethanol and 5.2 ml of propionic acid in 1 litre of water).

Larvae were reared on standard cornmeal food plates at 25 ℃ and 65% humidity using similar conditions as in previous studies (Eschbach et al., 2019; Jovanic et al., 2016, 2019; Ohyama et al., 2013, 2015). For learning and behaviour experiments, eggs were collected overnight for approximately 12–18 hours. A small amount of dry yeast was added to the food plates to increase egg laying. Learning experiments were performed using foraging-stage third-instar larvae (72–96 hours after egg laying). For immunohistochemistry, eggs were collected at daytime on food plates with yeast for approximately four hours. Dissections were performed using wandering-stage third-instar larvae (118–122 hours after egg laying). For experiments involving optogenetics, larvae were raised in the dark and 1:200 retinal solution, obtained by diluting 1 g of powdered all-*trans*-retinal (Toronto Research Chemicals, #R240000) in 35.2 ml of 95% ethanol, was added to the food unless indicated otherwise.

A full list of fly strains used in this thesis is shown in Table 2.1. Some of the crosses were set up with the help of Monti Mercer and Dr Brandi Sharp.

Table 2.1: Fly strains. For each fly strain, the short genotype (used as an alias in this thesis), the full genotype and the source of the stock are provided.

Short genotype	Detailed genotype	Source
30A08-Gal4	w^{1118}; $P\{y^{+t7.7}$ w^{+mC}=*GMR30A08-Gal4*$\}$@*attP2*	Bloomington #49513

Table 2.1: Fly strains (continued).

Short genotype	Detailed genotype	Source
58E02-Gal4	*w^{1118}; P{$y^{+t7.7}$ w^{+mC}=GMR58E02-Gal4}@attP2*	Bloomington #41347
69F06-Gal4	*w^{1118}; P{$y^{+t7.7}$ w^{+mC}=GMR69F06-Gal4}@attP2*	Bloomington #39497
72F11-Gal4	*w^{1118}; P{$y^{+t7.7}$ w^{+mC}=GMR72F11-Gal4}@attP2*	Bloomington #39786
attP2	*w^{1118}; ; attP2*	Pfeiffer et al. (2008)
C1-Gal4	*w^{1118}; Sp/CyO; C1-Gal4*	Dr Simon Sprecher
c346-Gal4	*P{$w^{+mW.hs}$=GawB}c346, w^{1118}*	Bloomington #30831
C5-Gal4	*w^{1118}; wg^{Sp-1}/CyO; C5-Gal4*	Dr Simon Sprecher
C6-Gal4	*w^{1118}; ; C6-Gal4*	Dr Simon Sprecher
Ddc-Gal4	*w^{1118}; ; Ddc-Gal4-HL8-3D*	Li et al. (2000)
dp2-Gal4	*w^{1118}; dp2-Gal4*	Dr Simon Sprecher
eg^{Mz360}-Gal4	w^{1118}; P{$w^{+mW.hs}$=GawB}eg^{Mz360}	Bloomington #8758
Gr2a-Gal4	*w^{1118}; Gr2a-Gal4; D2/TM3*	Dr Simon Sprecher
Gr43a-Gal4 line 1	*w^{1118}; wg^{Sp-1}/CyO; P{w^{+mC}=Gr43a-Gal4.5.3}17*	Bloomington #57637
Gr43a-Gal4 line 2	*Gr43a-Gal4 (II, knock-in)*	Miyamoto et al. (2012)
Gr5a-Gal4	*w^{1118}; wg^{Sp-1}/CyO; P{w^{+mC}=Gr5a-Gal4.8.5}2/TM3,Sb^1*	Bloomington #57591
Gr64a-Gal4	*w^{1118}; wg^{Sp-1}/CyO; P{w^{+mC}=Gr64a-Gal4.1.6}4*	Bloomington #57662
Gr64f-Gal4	*w^{1118}; UAS-mCD8::GFP; Gr64f-Gal4/TM3, Sb^1*	Bloomington #57668
Ir25a-Gal4	*w^{1118}; P{w^{+mC}=Ir25a-Gal4.A}236.1; TM2/TM6B, Tb^1*	Bloomington #41728
Ir76b-Gal4	*w^{1118}; Ir76b-Gal4; TM2/TM6B, Tb^+*	Bloomington #41730
Ir94e-Gal4	*w^{1118}; ; Ir94e-Gal4*	Dr Simon Sprecher
NPF-Gal4	*$y^1 w^{76c23}$; NPF-Gal4*	Wen et al. (2005)

Table 2.1: Fly strains (continued).

Short genotype	Detailed genotype	Source
ppk11-Gal4	*w^{1118}; ; ppk11-Gal4*	Liu et al. (2003)
ppk19-Gal4	*w^{1118}; ppk19-Gal4*	Liu et al. (2003)
SS01989	*GMR_SS01989*	Dr Marta Zlatic
Tdc2-Gal4	*w^{1118}; P{Tdc2-Gal4.C}2*	Cole et al. (2005)
TH-Gal4	*TH-Gal4*	Friggi-Grelin et al. (2003)
Tph-Gal4	*+; Tph-Gal4; +*	Park et al. (2006)
Trh-Gal4	*Trh-Gal4*	Alekseyenko et al. (2010)
UAS-CsChrimson	*20xUAS-CsChrimson-mVenus@attP18*	Bloomington #55134
UAS-CsChrimson; tsh-LexA, LexAop-Gal80	*20xUAS-CsChrimson-mVenus@attP18; tsh-LexA, pJFRC20-8xLexAop2-IVS-Gal80-WPRE (su(Hw)attP5)/CyO, 2xTB-RFP; +*	Dr Stefan Pulver, Dr Yoshinori Aso
UAS-dTrpA1	*UAS-dTrpA1*	Dr Paul Garrity
UAS-GFP	*10XUAS-IVS-myr::smGFP-HA@attP18, 13XLexAop2-IVS-myr::smGFP-V5@su(Hw)attP8*	Nern et al. (2015)
VT57358-Gal4	*w^{1118}; ; VT057358-Gal4@attP2*	VDRC #203226
w^{1118}	*w^{1118}*	Hazelrigg et al. (1984)

2.2 Immunohistochemistry and confocal imaging

2.2.1 Experimental procedures

All dissections, immunohistochemical stainings and confocal imaging presented in this thesis were performed by the HHMI Janelia FlyLight team using a procedure adapted from Jenett et al. (2012) and Li et al. (2014).

Larval CNSs were dissected in cold 1x phosphate buffer saline (PBS, Corning Cellgro, #21-040) and transferred to tubes filled with cold 4% paraformaldehyde (Electron Microscopy Sciences, #15713-S) in 1x PBS. Tubes were incubated for one hour at room temperature. The tissue was washed four times in 1x PBS with 1% Triton X-100 (Sigma Aldrich, #X100) (PBT) and incubated in 1:20 donkey serum (Jackson Immuno Research, #017-000-121) in PBT for two hours at room temperature.

A primary antibody solution was prepared, consisting of mouse anti-Neuroglian (1:50, Developmental Studies Hybridoma Bank, #BP104 anti-Neuroglian), rabbit anti-GFP (1:500, Life Technologies, #A11122) and rat anti-N-Cadherin (1:50, Developmental Studies Hybridoma Bank, #DN-Ex #8) in PBT. The tissue was incubated with the primary antibody solution, first for four hours at room temperature and then for two nights at 4℃. The primary antibodies were removed and the tissue was washed four times in PBT. A secondary antibody solution was prepared, consisting of Alexa Fluor 568 donkey anti-mouse (1:500, Invitrogen, #A10037), FITC donkey anti-rabbit (1:500, Jackson Immuno Research, #711-095-152) and Alexa Fluor 647 donkey anti-rat (1:500, Jackson Immuno Research, #712-605-153) in PBT. The tissue was incubated with the secondary antibody solution, first for four hours at room temperature and then for two nights at 4℃. After removal of the secondary antibody, the tissue was washed again four times and mounted on a coverslip coated with poly-L-lysine (Sigma Aldrich, #P1524-25MG).

The coverslip with the CNSs was dehydrated by moving it through a series of jars containing ethanol at increasing concentrations (30%, 50%, 75%, 95%, 100%, 100%, 100%) for ten minutes each. The tissue was then cleared by soaking the coverslip with xylene (Fisher Scientific, #X5-500) three times for five minutes each. Finally, the coverslips were mounted in dibutyl phthalate in xylene (DPX, Electron Microscopy Sciences, #13512) with the tissue facing down on a microscope slide with spacers. At least two days were

allowed for the DPX to dry prior to confocal imaging with an LSM 710 microscope (Zeiss). Further details on the confocal imaging settings are provided in the respective figure captions.

2.2.2 Data analysis

Confocal images were analysed using Fiji (ImageJ). Neurons were counted by specifying regions of interest around the cell bodies using raw image stacks. All figures showing confocal images were derived from maximum intensity projections.

2.3 Single-larva operant conditioning

2.3.1 Experimental set-up

For single-larva operant conditioning experiments, I have used a closed-loop tracker with hardware identical to the one presented in Schulze et al. (2015) (Fig. 2.1a). A 617 nm red LED (Mightex Systems, #PLS-0617-030-S) was added for optogenetic excitation of *CsChrimson* (Klapoetke et al., 2014).

In this set-up, a single larva was freely moving on a 40 cm x 40 cm 1% agarose plate, which is prepared daily to ensure a high moisture level of the substrate. In praxis, the arena size was 34 cm x 38 cm, due to a limited range of movement of the moving stages on which the camera, the LED and the IR backlight are mounted.

All hardware was controlled by a customised software written by Dr Peter Polidoro using the Robot Operating System (ROS). A camera image was acquired and processed at 20 Hz. The contour of the larva was extracted by inverse binary thresholding and head, tail and spine were calculated and features were extracted as described in Chapter 3. The positions of the moving stages with the camera, the LED and the backlight were updated at 4 Hz to track the centroid of the larva. I have implemented all protocols which determine the delivery of the closed-loop optogenetic stimulus in a Python script connected with the ROS framework to control the LED at 10 Hz (Fig. 2.1b).

In collaboration with Elise Croteau-Chonka and Dr Jean-Baptiste Masson, I have developed a classifier for detecting left and right bends in real time on this tracker. This classifier was obtained by combining a two-layer neural network with input features $\mathbf{s}$,

`s_filtered`, `eig_reduced` and `eig_reduced_filtered`, a single hidden layer (five neurons, hyperbolic tangent activation function) and an output layer (one neuron, sigmoid activation function) with a linear threshold on `asymmetry` (for details on the features see Section 3.2.5). The classifier output was exponentially smoothed and post-processed as described in Section 3.2.6. The error rates were quantified using 60 minutes of video data containing a total number of 741 bends from ten larvae. The bend classifier has a precision of 97.6% and a recall of 100.0%. The bend direction was accurately detected in 99.2% of true-positive bends.

2.3.2 Data acquisition

A small number of larvae were washed out of the food using 15% sucrose solution. For any given larva, the time outside the food did not exceed 30 minutes prior to the start of the experiment. A single larva was gently picked up from the sucrose solution with a brush, rinsed with water to remove residual sucrose and placed in the centre of the agarose plate inside the single-larva tracker. The tracker door was shut and the larva was given at least one minute to accustom to its new environment before the experiment was started. All handling of larvae and all experiments were performed in the dark to avoid unintended optogenetic stimulation.

Optogenetic stimulation was performed following protocols specified in the respective results sections of the text. There was a delay of up to 100 ms between detection of a behaviour and closed-loop stimulation in response to this behaviour. The light intensity of the red light stimulus was 385 $\mu W/cm^2$.

2.3.3 Data analysis

Only data from larvae which did not reach the edge of the arena during the experiment was kept for analysis, since otherwise tracking was permanently interrupted. Data analysis was conducted using custom MATLAB (MathWorks) scripts.

The experiment time was equally split into bins with a duration of 60 s. To analyse data for operant conditioning of a directional preference for bend, the numbers of left and right bends initiated within each bin were counted to obtain the bend rate towards the respective direction. The probability of the larva to bend towards the side which was associated with

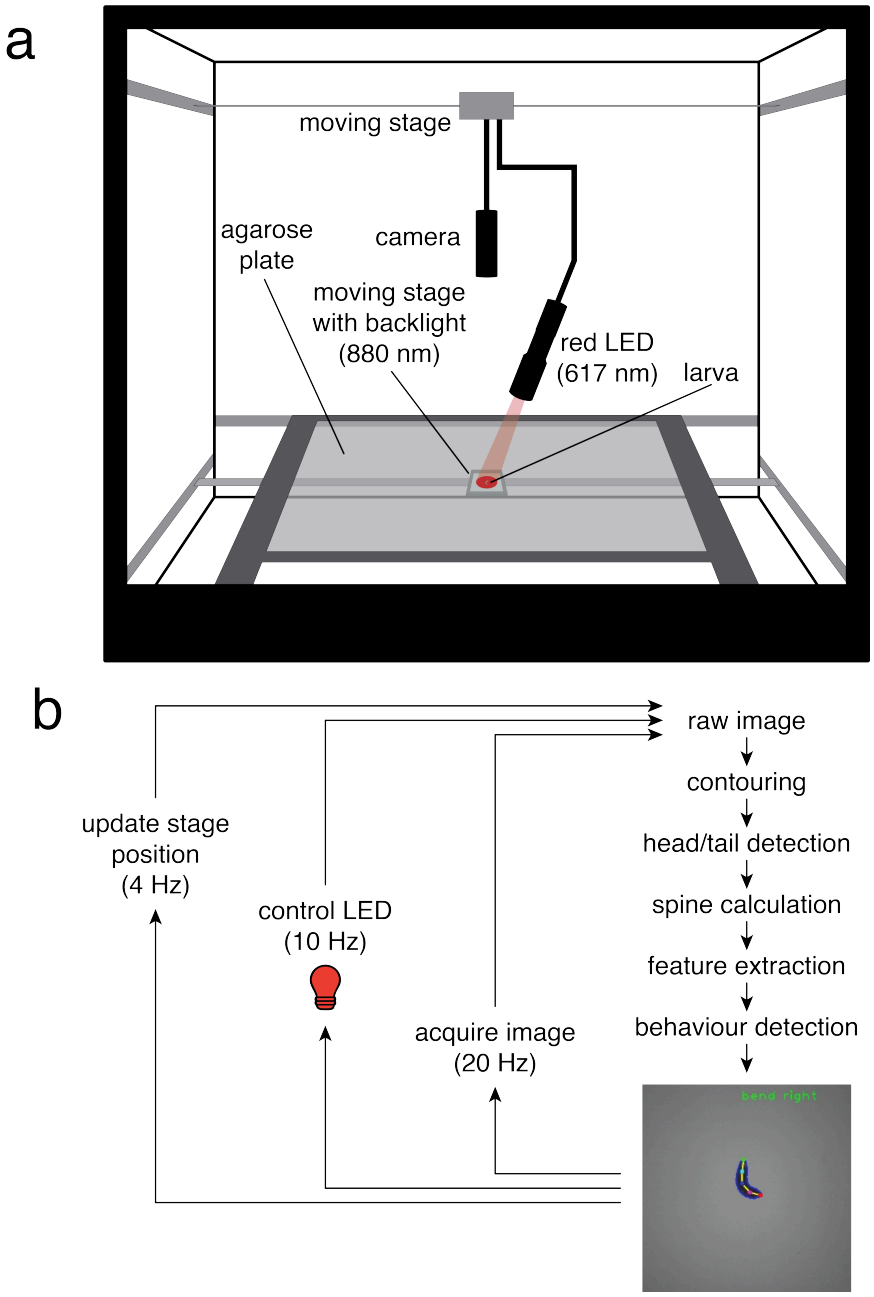

Figure 2.1: Single-larva closed-loop tracker with real-time behaviour detection. a. Schematic of the single-larva closed-loop tracker designed after Schulze et al. (2015). A single larva is freely crawling on an agarose plate. It is illuminated by an 880 nm backlight and tracked by a camera. An LED (617 nm) can be controlled to deliver optogenetic stimuli. The backlight, the camera and the LED are all mounted onto moving stages, which are following the larva. **b.** Data flow diagram of the behaviour detection software. A camera image is acquired at 20 Hz. The contour of the larva is extracted from the raw image, head and tail are detected and the spine is calculated. Features describing body shape, velocity and direction of movement are extracted and behaviours are detected in real time (see the text and Chapter 3 for details). Behaviour detection output is used to control the LED at 10 Hz for closed-loop stimulation. The stage positions are updated at 4 Hz according to the position of the larva within the camera image.

the optogenetic stimulus was calculated as the ratio of the number of bends towards the stimulated side over the total number of bends initiated in this bin.

Data of all larvae was pooled and it was accounted for the fact that bends to the left and to the right were each paired with the optogenetic stimulus for approximately half of the larvae. For each bin, mean and standard error were calculated for the bend rate to the stimulated side, the bend rate to the unstimulated side and the probability for bending towards the stimulated side. In the case of the control condition in which larvae received random stimulation during 50% of bends regardless of their direction, mean and standard error of the bend rates to the left and right and the probability for bending towards the left were calculated. Bend rates to the two sides were compared to each other using a two-sided Wilcoxon signed-rank test. The probability for bending to a given side was compared to chance level (0.5) using a two-sided Wilcoxon signed-rank test.

2.4 High-throughput operant conditioning

2.4.1 Experimental set-up

High-throughput operant conditioning experiments were performed using a multi-larva closed-loop tracker, which is described in detail in Chapter 3. Briefly, larvae were placed onto a 23 cm x 23 cm 4% agarose plate which was illuminated by a 30 cm x 30 cm 850 nm LED backlight (Smart Vision Lights, #SOBL-300x300-850) with intensity control (Smart Vision Lights, #IVP-C1). The larvae were recorded at 20 Hz by a high-resolution camera (Teledyne DALSA, #TEL-G3-CM10-M5105) with an 800 nm longpass filter (Midwest Optical Systems, #LP800-40.5) and the image was processed by an image acquisition FPGA device (National Instruments, #PCIe-1473R-LX110), which was programmed by Dr Lakshmi Narayan and is connected to a computer (Dell, #T7920) with a Windows 10 operating system (Microsoft Corporation).

In a custom software written in C++ by myself and in LabVIEW 2017 (National Instruments) by Dr Lakshmi Narayan, the contours of the larvae were extracted from the raw image and behaviour was detected in real time. Optogenetic and thermogenetic stimuli could be controlled in closed loop in response to behaviour.

Optogenetic stimulation was achieved using two digital micromirror devices (DMDs), one with 613 nm LED input (Digital Light Innovations, #CEL-5500-LED) and one with optic fibre input (Digital Light Innovations, #CEL-5500-FIBER) with a 625 nm LED source (Mightex Systems, #BLS-GCS-0625-38-A0710) controlled by a BioLED light source control module (Mightex Systems, #BLS-13000-1).

Thermogenetic stimulation was achieved by heating up the larvae with a custom IR laser set-up developed by Dr Christopher McRaven and Dr Michael Winding. The beam of a 1490 nm laser diode (SemiNex, #2CM-101) was fed into a two-axis galvanometer system (Thorlabs, #GVSM002), with which it could be targeted onto any spot on the agarose plate. The laser diode and the galvanometers were controlled by an analogue output device (National Instruments, #PCIe-6738). The system could be used to heat up four larvae simultaneously by alternating between the different locations at 80 Hz.

2.4.2 Data acquisition

Approximately 10–12 larvae were washed out of the food with water and immediately placed into the centre of the agarose plate with a brush, in such a way that they were not touching each other. The tracker door was shut and the larvae were given at least 30 s to accustom to their new environment before the experiment was started. All handling of larvae and all experiments were performed in the dark to avoid unintended optogenetic stimulation.

Stimuli were given following the protocols specified in the respective results sections of the text. The delay between detection of a behaviour and closed-loop stimulation in response to this behaviour did not exceed 50 ms for optogenetic stimuli and 100 ms for thermogenetic stimuli. The light intensity of the red light stimulus was 285 $\mu W/cm^2$.

For experiments including a control group which received stimulation uncorrelated from behaviour (yoked control), the experiment was split into 60 s time bins, and during each bin each larva was randomly allocated the stimulus train which a valid object (see Section 2.4.3) from a previous experiment with contingent stimulation had received in this respective time bin.

2.4.3 Data analysis

Data analysis was conducted using custom MATLAB (MathWorks) scripts. Since identity of detected objects is lost upon restarting an experiment, whenever a larva temporarily reaches the edge of the plate or when two or more larvae touch each other, individual objects are usually only detected for part of the experiment. Furthermore, the software sometimes recognises corrupted objects, such as scratches on the plate or residual food, as larvae.

The experiment time was equally split into bins with a duration of 60 s. To ensure high quality of the data, objects included into analysis for a given bin had to fulfil a number of criteria: i) the object must have been detected in every frame of the bin; ii) the initial detection of the object must have happened at least 20 s prior to the start of the bin; iii) at no point during the bin, `v_centroid_long_time` (the smoothed velocity of the centroid of the larval contour, see Section 3.2.5) exceeded 1.5 mm/s; and iv) the mean of `v_centroid_long_time` across the overall detection period of the object, excluding the first 20 s after initial detection, was at least 0.5 mm/s. 350 videos of objects flagged as valid for a given 60 s bin in this process were manually assessed to quantify the accuracy of this method. No severely corrupted objects could be detected. In one case (0.3%), a larva was briefly touching another larva. In another case (0.3%), head and tail of the larva were falsely detected for the majority of the time, leading to flipped detection of left and right bends (Table 3.2).

To analyse data for operant conditioning of a directional preference for bend, the numbers of left and right bends initiated within each valid bin were counted for each object to obtain the bend rate towards the respective direction. The probability of the larva to bend towards the side which was associated with the optogenetic stimulus was calculated as the ratio of the number of bends towards the stimulated side over the total number of bends initiated in this bin. For each bin, data of all larvae was pooled and it was accounted for the fact that bends to the left and to the right were each paired with the optogenetic stimulus for approximately half of the larvae. Mean and standard error were calculated for the bend rate to the stimulated side, the bend rate to the unstimulated side and the probability for bending towards the stimulated side. In the case of the control condition in which larvae received random stimulation during 50% of bends regardless of their direction,

mean and standard error of the bend rates to the left and right and the probability for bending towards the left were calculated. Bend rates to the two sides were compared to each other using a two-sided Wilcoxon signed-rank test. The probability for bending to a given side was compared to chance level (0.5) using a two-sided Wilcoxon signed-rank test.

To analyse data for operant conditioning of the frequency of bends or forward crawls, the number of left or right bends or crawl periods (using the `forward` classifier) initiated within each valid bin were counted for each object. Furthermore, the mean velocity and the mean duration of all bends and of all crawl periods initiated during the bin was calculated for each larva. Data from all valid objects was pooled and the mean and standard error were calculated for each bin. The behaviour characteristics of experimental animals were compared to the yoked control group using a two-sided Mann-Whitney *U* test.

2.5 Classical conditioning

2.5.1 Experimental procedures

CsChrimson (Klapoetke et al., 2014) was expressed under the control of driver lines targeting candidate valence-conveying neurons. Optogenetic activation of these neurons (US) was paired with an odour (CS) to induce olfactory memory (Fig. 2.2). For each driver line, data was acquired from at least two separate crosses.

Classical conditioning was performed using a procedure similar to the ones described in Gerber and Hendel (2006), Saumweber et al. (2011) and Eschbach et al. (2019). Approximately 40 third-instar larvae were transferred onto a petri dish filled with 4% agarose. Larvae were presented with an odour (1:10^4 ethyl acetate in ddH_2O) pipetted onto filter papers attached to the lid of the dish, and the dish was exposed to red light (630 nm, 350 µW/cm^2) for three minutes. Larvae were then transferred to a fresh petri dish and placed in the dark for three minutes without the odour (“air”). This training procedure was repeated three times, with alternating presentation of odour/light and air/dark (paired group).

An unpaired group receiving reciprocal stimulus presentation (odour paired with dark, air paired with light) was trained simultaneously to ensure that any observed effects

are due to learning as opposed to innate odour preference or avoidance. In half of the experiments, the order of training trials was reversed, starting with air presentation instead of odour presentation.

After training, larvae of both groups were immediately transferred to fresh agarose-filled petri dishes and lined up along a 1 cm middle zone in the centre of the dish, and the odour was presented on one side of the lid (odour side), but not on the other side (air side). After a three-minute test period in the dark, the number of larvae on the odour side, on the air side and in the middle zone were counted and stored in an Excel spreadsheet (Microsoft).

2.5.2 Data analysis

All data was manually entered into MATLAB (MathWorks) and analysed using customs scripts. For each experiment, a performance index (PI) was calculated as follows:

$$\mathrm{Pref}_{\mathrm{paired}} = \frac{\#(\text{larvae on odour side}) - \#(\text{larvae on air side})}{\#(\text{larvae on plate})} \quad \text{(paired dish)}$$

$$\mathrm{Pref}_{\mathrm{unpaired}} = \frac{\#(\text{larvae on odour side}) - \#(\text{larvae on air side})}{\#(\text{larvae on plate})} \quad \text{(unpaired dish)}$$

$$\mathrm{PI} = \frac{\mathrm{Pref}_{\mathrm{paired}} - \mathrm{Pref}_{\mathrm{unpaired}}}{2} \quad \text{(combined)}$$

PIs take values between -1 and +1, where a positive PI reflects appetitive learning, whereas a negative PI represents aversive learning. For each condition, mean and standard error were calculated. Statistical differences between two groups were tested using a two-sided Mann-Whitney *U* test with Bonferroni correction. Significances compared to zero were tested with a two-sided Wilcoxon signed-rank test with Bonferroni correction.

2.6 Software availability

All software which I have developed as part of this project is available in private repositories on GitHub (`https://www.github.com`), which can be shared upon request.

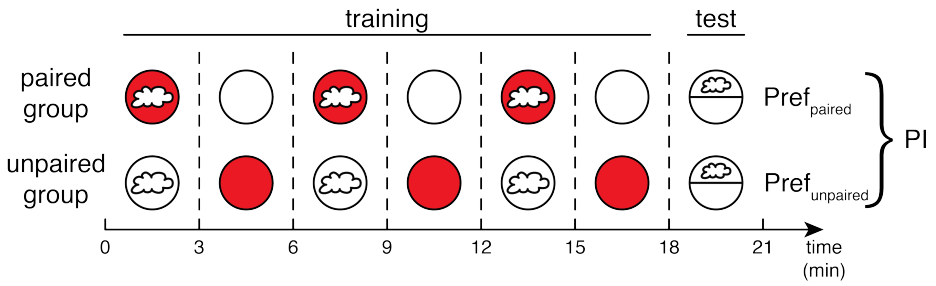

Figure 2.2: Schematic and timeline of the experimental protocol for olfactory conditioning. For training, two groups of larvae are each alternatingly presented with an odour (white cloud) and no odour ("air", no cloud). The paired group receives optogenetic stimulation with red light (solid red circles) paired with the odour and is placed in darkness (solid white circles) when presented air. The unpaired group receives reciprocal stimulus presentation (odour paired with dark, air paired with light). This procedure is repeated three times. In half of the experiments, the order of training trials is reversed, starting with air presentation instead of odour presentation. Both groups are then tested for learned odour preference in the dark with odour presentation on one side and no odour on the other side of the plate. The two preference indices are combined to calculate a performance index for olfactory conditioning (see text for details).

3 High-Throughput Tracker with Real-Time Behaviour Detection and Stimulation

3.1 Introduction

The first step towards establishing a fully automated high-throughput operant conditioning paradigm for *Drosophila* larvae is to lay the technical foundations. In this chapter, I will introduce a novel high-throughput tracker. This system combines three important features which distinguish it from existing experimental set-ups: first, it can detect complex actions for up to 16 freely behaving larvae simultaneously in real time and at high accuracy. Second, optogenetic stimuli can be administered to any subset of larvae in response to behaviour detection output with full intensity control and minimal delay. Third, thermogenetic stimuli can be targeted at individual animals in closed loop. At the moment, thermogenetic stimulation is available for up to four larvae at a time. However, the system could easily be upgraded to work for 16 larvae by adding more lasers.

3.2 Results

3.2.1 Hardware design

I have selected and tested all hardware components used for this set-up in collaboration with Dr Lakshmi Narayan (Fig. 3.1). All hardware is contained within an optically opaque enclosure to ensure that optogenetic experiments are performed in the absence of environmental light.

Up to 16 larvae are placed on a 23 cm x 23 cm agarose plate, where they can freely move. They are illuminated by a 30 cm x 30 cm 850 nm LED backlight. A high-resolution

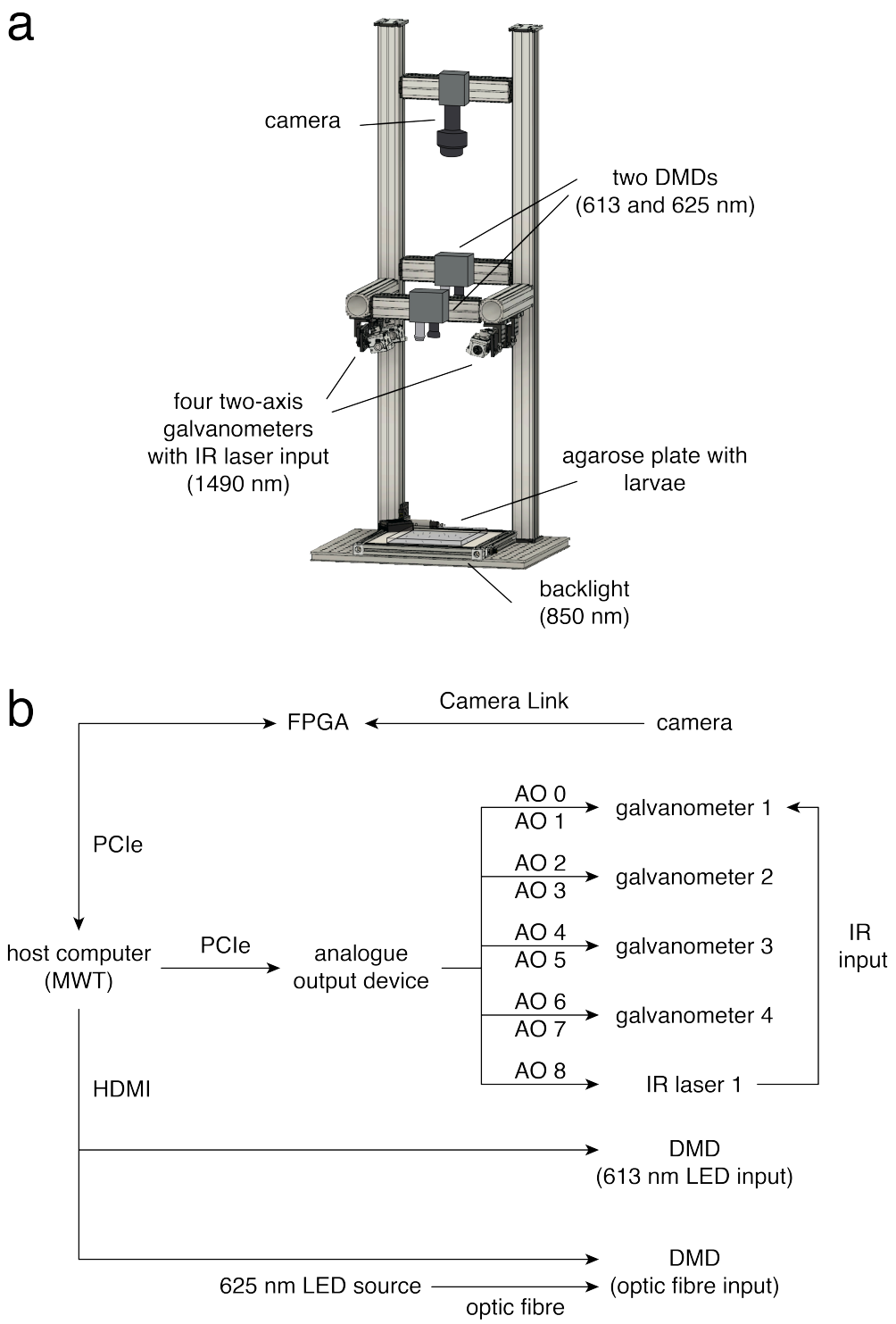

Figure 3.1: Hardware architecture of the high-throughput tracker. a. Schematic of the high-throughput tracker. Up to 16 freely moving larvae on an agarose plate are illuminated by an 850 nm backlight and monitored by a high-resolution camera. Two digital micromirror devices (DMDs) are used for optogenetic stimulation of individual larvae at 613 and 625 nm. For thermogenetic stimulation, four two-axis galvanometers can be used to heat up larvae with a 1490 nm infrared (IR) beam. **b.** Block diagram of hardware components. AO: analogue output, FPGA: field-programmable gate array.

camera (3072 x 3200 pixels) obtains an 8-bit greyscale image at 20 Hz. The camera is positioned such that the arena comprises most of the camera image. Each camera pixel corresponds to a section of the arena with a diameter of 72.92 µm, allowing for easy transformation between camera coordinates (in pixels) and world coordinates at plate level (in mm). An 800 nm longpass filter is installed within the camera to block all visible wavelengths, especially those used for optogenetic stimulation.

The camera is connected to an FPGA through a Camera Link interface. The FPGA interacts with a computer through a PCIe slot. Image processing, behaviour detection and stimulus calculation are performed on the FPGA and the host computer (see Section 3.2.2).

Optogenetic stimulation of individual larvae is achieved using two DMDs. One DMD operates with an integrated 613 nm LED input, whereas the other one is illuminated by a 625 nm LED source through an optic fibre. Both DMDs each cover the entire agarose plate and are used together in order to maximise the achievable light intensity. They are connected to the host computer through an HDMI output.

Thermogenetic stimulation is achieved using four two-axis galvanometers. Currently, one of the galvanometers receives IR input from a laser source (1490 nm). For future expansion, the remaining three galvanometers can easily be connected to additional laser sources. Both the galvanometers and the laser are controlled by an analogue output device, which is connected to the host computer through a PCIe slot.

3.2.2 Software architecture

Up to 16 larvae can be tracked simultaneously using a real-time adaptation of the MWT software (Swierczek et al., 2011). Some of the algorithms have been implemented on FPGA using LabVIEW, whereas other parts of the framework are executed on the host computer. The software package on the host computer consists of three interconnected components: a user interface written in LabVIEW, a LabVIEW application responsible for object detection and hardware control and a dynamic link library (DLL) written in C++ (Fig. 3.2). I was actively involved in the design and testing of all parts of this framework. All LabVIEW implementations have been carried out by Dr Lakshmi Narayan, while I have written all C++ code. A rough outline of the software architecture is given in this section. For details, please refer to Sections 3.2.3–3.2.6.

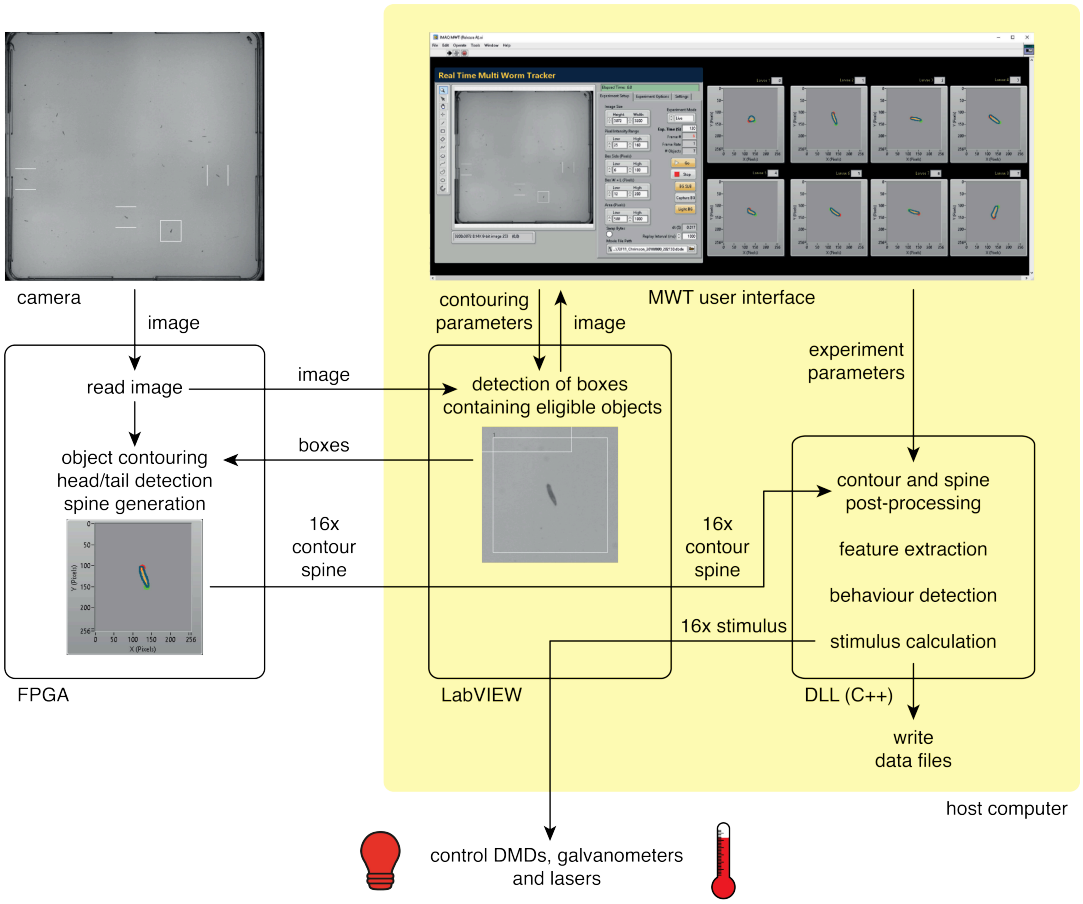

Figure 3.2: Data flow diagram of the high-throughput tracker software. The raw camera image is read by a field-programmable gate array (FPGA) at 20 Hz. Eligible objects are detected in a LabVIEW process on the host computer (highlighted in yellow) based on parameters specified on the multi-worm tracker (MWT) user interface. Object contouring, an initial head and tail detection and the generation of a raw spine are then performed on the FPGA. Up to 16 contours and spines are sent to a dynamic link library (DLL) on the host computer. Inside the DLL, post-processing of contour, spine, head and tail, feature extraction and behaviour detection are performed. In addition, data files are written to the hard drive. For each larva, a stimulus is calculated based on experiment parameters specified on the user interface. The stimulus information is sent back to a LabVIEW process which controls the digital micromirror devices (DMDs), galvanometers and lasers for optogenetic (red light bulb) and thermogenetic (red thermometer) stimulation.

Raw camera images are read by the FPGA at 20 Hz. They are then sent to the host computer. The LabVIEW application on the host computer detects larvae by finding eligible objects based on parameters defined on the user interface. Each object is assigned an ID to enable tracking of larvae over time. Up to 16 boxes containing eligible objects are sent back to the FPGA for processing. Since this LabVIEW process is slow, it is not executed in every frame.

In a parallel process, each raw image is also processed by the FPGA. Using the most recent set of up to 16 eligible objects obtained by the LabVIEW application on the host computer, contouring, an initial head and tail detection and the computation of a raw spine are performed. Contour and spine data is sent back to the host computer, where it is received by the LabVIEW application and sent to the DLL for further processing.

Inside the DLL, contour and spine are smoothed and the head and tail detection is improved for robustness over time. For each larva, a variety of features describing body shape, velocity and direction of movement are extracted. These features are used to detect behaviours in real time. Using experiment parameters specified on the user interface, closed-loop stimuli can be calculated for individual larvae based on their behaviour. All experiment parameters, contour, spine, behaviour and stimulation data are written to output files by the DLL. These output files can be processed for post-acquisition analysis by a framework written by myself in MATLAB but are also compatible with existing scripts written by Dr Jean-Baptiste Masson (Jovanic et al., 2017, 2016).

For each larva, the parameters for optogenetic and thermogenetic stimulation are sent back to the LabVIEW application, which controls the DMDs, galvanometers and lasers.

3.2.3 Multi-animal tracking

For tracking of multiple larvae, the raw image, which is acquired by the camera at 20 Hz, is processed in parallel on both the host computer and the FPGA. I have designed and tested these algorithms in collaboration with Dr Lakshmi Narayan, who has implemented the code in LabVIEW.

Detection of eligible objects on the host computer

On the host computer, eligible objects are detected using background subtraction and binary thresholding as well as the following parameters specified on the user interface:

- Pixel intensity range: specifies the range (minimum and maximum) of the brightness values for pixels which are selected by binary thresholding (between 0 and 255 for an 8-bit image). For each object, a rectangular box of minimal size with edges parallel to the image axes is constructed around the object.
- Box side length (pixels): specifies the range (minimum and maximum) of eligible values for width and height of the box.
- Box width + height (pixels): specifies the range (minimum and maximum) of eligible values for the sum of box width and height.
- Box area (pixels): specifies the range (minimum and maximum) of eligible values for the area of the box in pixels.

In addition to the background subtraction, which eliminates all motionless objects, these parameters are sufficient for filtering out most non-larval objects. The values to be chosen for pixel intensity range depend on the level of background illumination. Parameters characterising the box size are specific to larval stage. The default values for detecting third-instar larvae under the standard lighting conditions are a pixel intensity range of 25–170, a box side length of 6–100 pixels, a box width + height of 12–200 pixels and a box area of 300–900 pixels.

The eligible objects are sorted by object area in descending order, and up to 16 objects and their location (defined as the centre of the box) are sent to the FPGA. Since object detection on the host computer requires more than 50 ms of run time, this part of the code is not executed every frame. On average, the FPGA receives an updated set of object locations every three frames.

Assignment of larva IDs on the host computer

A larva ID is assigned on the host computer for each eligible object whose location is sent to the FPGA in a given frame. If in the previous frame an object has been detected

within the squared box with a radius of 40 pixels around the centroid of a given object in the current frame, the current object is assigned the same ID as the previous object. Otherwise, a new ID is assigned to the object.

This process ensures that larvae can be tracked over time. However, in the case of any ambiguity, e. g. when two or more larvae are touching or when a larva reaches the edge of the arena, larval identity is lost and the animal will be treated like a new object when it reappears.

Calculation of the contour on FPGA

This thread is only executed after the first set of object locations is received from the host computer. Contours of up to 16 eligible objects are extracted based on the most up-to-date list of object locations.

For each object, a 256 x 256 pixel box is considered around the object centre. Since the camera image has a size of 3072 x 3200 pixels, which contains an arena with a size of approximately 23 cm x 23 cm, the box covers an image section of about 2 cm x 2 cm. Due to the small size of the larvae and the rapid update cycle of the object locations, each larval object will always be fully contained inside its respective box.

First, a binary threshold is applied to all pixels inside the box using the pixel intensity range specified on the user interface. For edge detection, both a vertical and a horizontal convolution with a 2 x 1 XOR kernel are applied to the resulting binary image. The edge is obtained by overlaying the two convoluted images using a pixelwise OR operation (Fig. 3.3a).

Next, the contour is constructed using an iterative process. The algorithm starts with the edge pixel which is located closest to the centre of the box by selecting it as the first point of the raw contour and removing it from the edge. In each step, the eight neighbouring pixels of the most recently added contour point are considered one at a time by moving clockwise around this contour point, starting with the pixel directly above. For each neighbouring pixel, the algorithm checks whether it is part of the edge. If this is the case, the pixel is appended to the contour and removed from the edge. The process is then repeated on the neighbouring points of this pixel. If none of the neighbouring eight pixels are part of the remaining edge, the contour has been completely reconstructed (Fig. 3.3b).

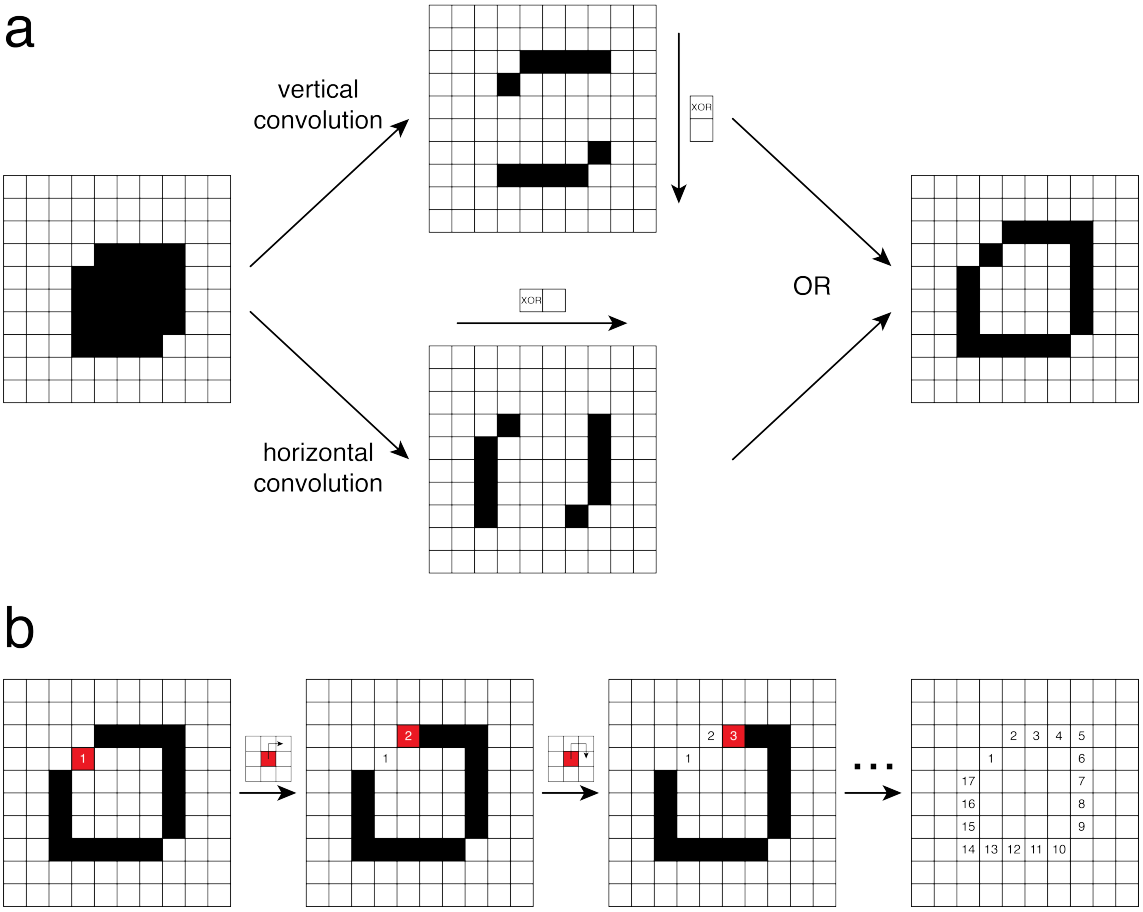

Figure 3.3: Calculation of the contour on FPGA. A simplified example is shown using a 10 x 10 pixel box containing a small object. **a.** The object (black) is detected against the background (white) using binary thresholding. The edge is detected by combining the results of a vertical and a horizontal image convolution with a 2 x 1 XOR kernel using an OR operator. **b.** The contour points are reconstructed in an iterative process. Starting with the closest edge pixel to the centre of the box, the next contour point is found by checking for each neighbouring pixel whether it is part of the edge, starting from the pixel directly above and going clockwise until an edge pixel is found. The process ends when no eligible edge pixels can be found.

It is possible that this process yields a contour which ends prematurely or contains small loops. If this happens, the construction process can be reversed by up to 16 contour points to find an alternative contour. The maximum time span allowed for contour construction is 10,000 FPGA clock cycles, where each pixel comparison has a run time of one clock cycle. In the rare event that this time span is exceeded, the algorithm returns the contour points which have been reconstructed up to this point.

Only contours with a minimum number of 63 points are considered as valid and processed further. If less than 63 contour points are found, the FPGA returns the last valid contour which was detected for a given larva ID.

3.2.4 Contour processing and landmark detection

Detection of head and tail

The initial detection of head and tail was implemented on FPGA by Dr Lakshmi Narayan using an algorithm originally developed for use on the single-larva closed-loop tracker (Schulze et al., 2015) by Dr Jean-Baptiste Masson, Elise Croteau-Chonka and myself. I have designed some necessary adaptations for this high-throughput implementation and conducted all testing and validation.

The idea underlying this algorithm is that head and tail are the contour points with the sharpest and second-sharpest curvature, respectively. To find these points, let C_{raw} denote the raw contour as obtained from the FPGA and let $n_{C_{raw}}$ be the number of contour points. Let C_i^{raw} denote the i^{th} point on C_{raw}. If $i \leq 0$ or $i > n_{C_{raw}}$, then $C_i^{raw} := C_j^{raw}$ with $i \equiv j \mod n_{C_{raw}}$ and $1 \leq j \leq n_{C_{raw}}$.

First, for $i = 1, ..., n_{C_{raw}}$, let ϑ_i denote the angle between the contour points $C^{raw}_{i-\left\lfloor \frac{n_{C_{raw}}}{8} \right\rfloor}$, C_i^{raw} and $C^{raw}_{i+\left\lfloor \frac{n_{C_{raw}}}{8} \right\rfloor}$, i. e.

$$\vartheta_i = \angle C^{raw}_{i-\left\lfloor \frac{n_{C_{raw}}}{8} \right\rfloor} C_i^{raw} C^{raw}_{i+\left\lfloor \frac{n_{C_{raw}}}{8} \right\rfloor}.$$

The preliminary head `head_initial` is defined as the contour point $C^{raw}_{i_{head}}$ with the sharpest angle, i. e.

$$i_{head} = \operatorname*{argmin}_i \vartheta_i.$$

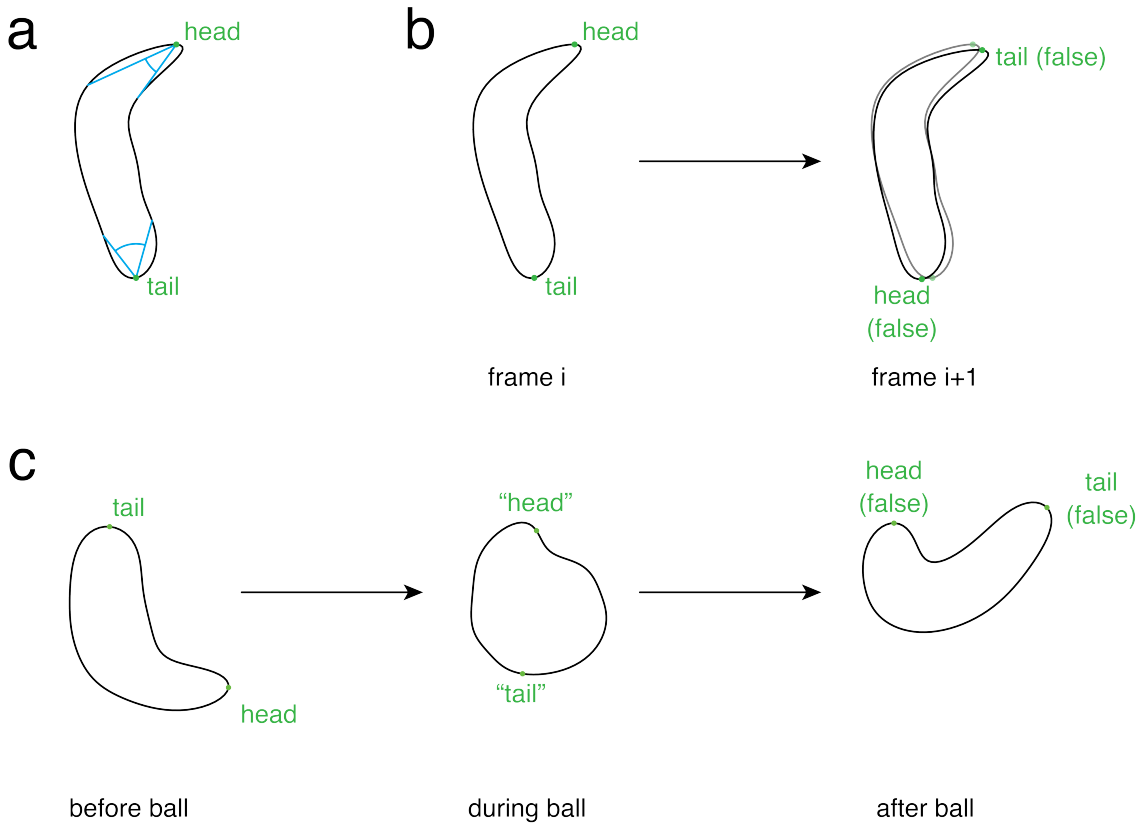

Figure 3.4: Detection of head and tail. The contour of the larva (black outline) and head and tail (green) are shown. **a.** Initial detection of head and tail. The head is the contour point with the sharpest curvature. The tail is the contour point with the next-sharpest curvature which does not lie in close proximity to the head. **b.** The initial detection of head and tail is not correct in all cases. False detections can be corrected by swapping head and tail to minimise the distances of head and tail in the current frame (solid contour) to head and tail in the previous frame (transparent contour). **c.** The correction described in **b** fails if larvae curl together such that the contour appears to be circular ("ball"). To eliminate this source of false detection, these events need to be detected using a `ball` classifier.

The preliminary tail `tail_initial` is defined as the contour point $C^{raw}_{i_{tail}}$ with the sharpest angle among those remaining contour points which are separated by the head by at least $\left\lfloor \frac{n_{C_{raw}}}{8} \right\rfloor$ contour points (Fig. 3.4a):

$$i_{tail} = \underset{i \notin \left[i_{head} - \left\lfloor \frac{n_{C_{raw}}}{8} \right\rfloor,\ i_{head} + \left\lfloor \frac{n_{C_{raw}}}{8} \right\rfloor \right]}{\operatorname{argmin}} \vartheta_i$$

This initial detection of `head_initial` and `tail_initial` is correct in most cases but leads to a flipped detection of the two body ends in some cases. I identify and correct these false detection events at run time in the DLL code. To ensure correct detection of head and tail in all frames, the locations of `head_initial` and `tail_initial` are compared

to the locations head_prev and tail_prev of the final smooth head and tail detection in the previous image frame. The following four distances are calculated:

$$\texttt{head\_initial\_to\_head\_prev} = |\texttt{head\_initial} - \texttt{head\_prev}|$$

$$\texttt{head\_initial\_to\_tail\_prev} = |\texttt{head\_initial} - \texttt{tail\_prev}|$$

$$\texttt{tail\_initial\_to\_head\_prev} = |\texttt{tail\_initial} - \texttt{head\_prev}|$$

$$\texttt{tail\_initial\_to\_tail\_prev} = |\texttt{tail\_initial} - \texttt{tail\_prev}|$$

Next, the smallest of these four distances is found. Since head and tail do not move very far from one frame to the next frame, a flipped detection has occurred if this smallest distance is either head_initial_to_tail_prev or tail_initial_to_head_prev (Fig. 3.4b).

This comparison cannot be drawn in the first frame in which a larva is detected. Therefore, the final head_raw and tail_raw have to be set to head_initial and tail_initial for this frame. Since it is possible that the initial detection fails in this frame, there needs to be a mechanism to correct head and tail over time. For this purpose, I have employed a vote system which measures whether the detection in the first frame was likely to be correct and which I have improved based on an algorithm by Dr Jean-Baptiste Masson.

The underlying idea is that if head_initial and tail_initial are flagged as flipped more often than they are flagged as correct, it is likely that the detection in the first frame of that larva was false. Two votes, vote_correct and vote_flipped, are both initialised to zero when a larva is first detected. At the end of the first frame, vote_correct is incremented by one. In all following frames, vote_correct is incremented by one and vote_flipped remains unchanged if the smallest distance is either head_initial_to_head_prev or tail_initial_to_tail_prev. vote_flipped is incremented by one and vote_correct remains unchanged otherwise.

If the Boolean the comparison vote_correct $\geq$ vote_flipped remains unchanged between two consecutive frames, then the final positions for head and tail are chosen as head_raw $=$ head_initial and tail_raw $=$ tail_initial if the smallest of the four distances is head_initial_to_head_prev or tail_initial_to_tail_prev, and as head_raw $=$ tail_initial and tail_raw $=$ head_initial otherwise.

Whenever the Boolean value of vote_correct $\geq$ vote_flipped changes between two frames, the data suggests that the final head and tail detection in the previous frame was false, such that the final positions of head and tail in the current frame are defined

as head_raw = tail_initial and tail_raw = head_initial if the smallest of the four distances is either head_initial_to_head_prev or tail_initial_to_tail_prev, and to head_raw = head_initial and tail_raw = tail_initial otherwise.

This correction using the vote system fails if the assumption that head and tail do not move far from one frame to the next frame is not met. This is the case when a larva bends very strongly in one direction, such that parts of its body wall are touching and the contour appears to take a circular shape. This causes the curvature to be almost identical across all contour points, and head_initial and tail_initial are detected in arbitrary locations. When the larva evolves from this "ball"-like shape, there is a high chance that head and tail are detected incorrectly (Fig. 3.4c). The solution to this problem is to detect these ball events (see Section 3.2.6) and to reset vote_correct and vote_flipped to zero whenever they occur.

Generation of a smooth spine

Next, $n_S = 11$ spine points are generated from the contour points. The spine defines a body axis which runs from head to tail. Initially, a raw spine S_{raw} is calculated. Let S_i^{raw} denote the i^{th} point of S_{raw} with $i = 1, ..., n_S$. To generate the remaining spine points, the contour is split into a left and a right body half as defined by head_raw and tail_raw. Let $L_1, ..., L_{n_S}$ and $R_1, ..., R_{n_S}$ be contour point on the left and right halves, respectively, such that $L_1 = R_1 =$ head_raw and $L_{n_S} = R_{n_S} =$ tail_raw. The remaining points L_i and R_i are chosen as contour points C_j^{raw} with j equally spaced out among the indices of C^{raw} between L_1 and L_{n_S} on the left half and R_1 and R_{n_S} on the right half, respectively. Then each raw spine point S_i^{raw} is defined as the centre between L_i and R_i as given by

$$S_i^{raw} = \frac{L_i + R_i}{2}$$

for $i = 1, ..., n_S$ (Fig. 3.5a).

C_{raw} and S_{raw} are transformed from camera coordinates (in pixels) to world coordinates (in mm) inside the DLL. If a given larva has already been detected in the past, the Boolean value of vote_correct $\geq$ vote_flipped has not changed from the previous to the current frame and no ball has been detected within the past 1.5 s, all spine points are temporally smoothed using exponential smoothing (Fig. 3.5b). Let S_{prev} be the smooth spine of the

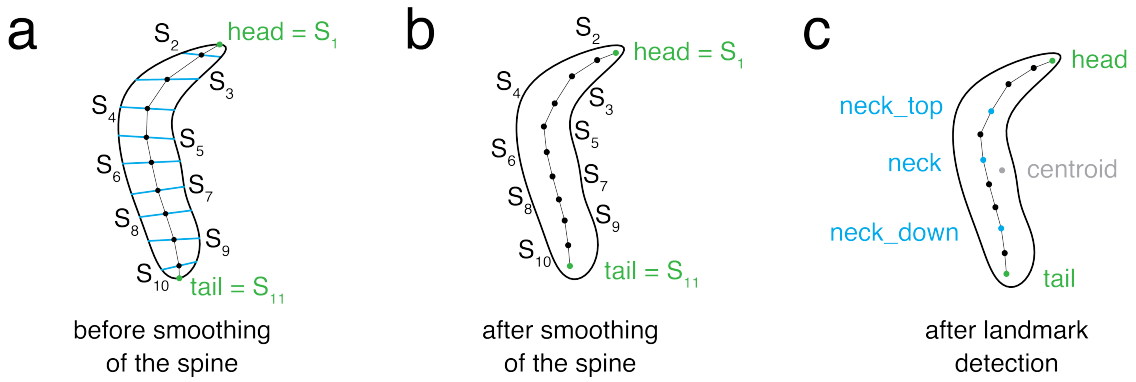

Figure 3.5: Calculation of a smooth spine and landmark points. The contour of the larva is shown (black outline). The spine is composed of eleven points (black), including head and tail (green). **a.** The points of the raw spine S_{raw} are obtained by finding the centres between equally spaced contour points on either half of the contour as defined by head and tail. The first spine point is the head, the last spine point is the tail. **b.** The smooth spine S is obtained by exponential smoothing of S_{raw}. **c.** Four landmark points, `neck_top`, `neck` and `neck_down` (blue) and the `centroid` of the contour (grey), are calculated.

previous frame. Let further S_i and S_i^{prev} denote the i^{th} points of S and S_{prev}, respectively. Then

$$S_i = \gamma \cdot S_i^{raw} + (1-\gamma) \cdot S_i^{prev}$$

with $\gamma = 0.8$. The final smooth `head` and `tail` are given by $\texttt{head} = S_1$ and $\texttt{tail} = S_{11}$.

Obtaining a smooth contour with a fixed number of points

The number $n_{C_{raw}}$ of raw contour points obtained by the original contouring algorithm implemented on the FPGA varies across larvae and frames. For behaviour detection, it is desirable to work with a smooth contour with a fixed number of contour points. This is achieved inside the DLL by applying Fourier decomposition to the raw contour C_{raw} to obtain a small number of coefficients $F_{i,j}$, and by then reconstructing a smooth contour C with $n_C = 100$ contour points from these coefficients.

Fourier decomposition is performed as follows:

$$F_{i,1} = \frac{2}{n_{C_{raw}}} \sum_{k=1}^{n_{C_{raw}}} \left(x_k^{raw} \cdot \cos \frac{i \cdot 2\pi \cdot (k-1)}{n_{C_{raw}}} \right)$$
$$F_{i,2} = \frac{2}{n_{C_{raw}}} \sum_{k=1}^{n_{C_{raw}}} \left(x_k^{raw} \cdot \sin \frac{i \cdot 2\pi \cdot (k-1)}{n_{C_{raw}}} \right)$$
$$F_{i,3} = \frac{2}{n_{C_{raw}}} \sum_{k=1}^{n_{C_{raw}}} \left(y_k^{raw} \cdot \cos \frac{i \cdot 2\pi \cdot (k-1)}{n_{C_{raw}}} \right)$$
$$F_{i,4} = \frac{2}{n_{C_{raw}}} \sum_{k=1}^{n_{C_{raw}}} \left(y_k^{raw} \cdot \sin \frac{i \cdot 2\pi \cdot (k-1)}{n_{C_{raw}}} \right)$$

with $i = 0, ..., 6$. Here, x_k^{raw} and y_k^{raw} denote the x and y coordinates, respectively, of the k^{th} point of C_{raw}. A deviating definition is used for $F_{0,1}$ and $F_{0,3}$, which correspond to the coordinates of the centroid:

$$F_{0,1} = \frac{1}{n_{C_{raw}}} \sum_{k=1}^{n_{C_{raw}}} x_k^{raw}$$
$$F_{0,3} = \frac{1}{n_{C_{raw}}} \sum_{k=1}^{n_{C_{raw}}} y_k^{raw}$$

Next, C is obtained by Fourier reconstruction:

$$x_k = \sum_{i=0}^{6} \left(F_{i,1} \cdot \cos \left(i \cdot \left(-\pi + \frac{(k-1) \cdot 2\pi}{n_C} \right) \right) + F_{i,2} \cdot \sin \left(i \cdot \left(-\pi + \frac{(k-1) \cdot 2\pi}{n_C} \right) \right) \right)$$
$$y_k = \sum_{i=0}^{6} \left(F_{i,3} \cdot \cos \left(i \cdot \left(-\pi + \frac{(k-1) \cdot 2\pi}{n_C} \right) \right) + F_{i,4} \cdot \sin \left(i \cdot \left(-\pi + \frac{(k-1) \cdot 2\pi}{n_C} \right) \right) \right)$$

where x_k and y_k denote the x and y coordinates, respectively, of the k^{th} point of C.

Calculation of landmark points

In addition to `head` and `tail`, four landmark points are extracted inside the DLL, which are used for feature extraction and for defining the position of a larva on the plate (Fig. 3.5c):

- `centroid`

  This is the centroid of the contour, describing the position of the larva. Let C_i denote the i^{th} point of the contour. Then

$$\texttt{centroid} = \frac{1}{n_C} \sum_{i=1}^{n_C} C_i.$$

- `neck`

  Let $k_{\texttt{neck}}$ be the minimum k such that $3 \leq k \leq n_S - 2$ and

  $$\sum_{i=2}^{k} |S_i - S_{i-1}| > \frac{1}{2} \sum_{i=2}^{n_S} |S_i - S_{i-1}|,$$

  then

  $$\texttt{neck} = S_{k_{\texttt{neck}}}.$$

  If no integer k fulfils the above conditions, then

  $$\texttt{neck} = S_{\lfloor \frac{n_S}{2} \rfloor}$$

  (i. e. $\texttt{neck} = S_5$ in the case $n_S = 11$).

- `neck_top`

  Let $k_{\texttt{neck\_top}}$ be the minimum k such that $2 \leq k_{\texttt{neck\_top}} \leq k_{\texttt{neck}} - 1$ and

  $$\sum_{i=2}^{k} |S_i - S_{i-1}| > \frac{1}{4} \sum_{i=2}^{n_S} |S_i - S_{i-1}|,$$

  then

  $$\texttt{neck\_top} = S_{k_{\texttt{neck\_top}}}.$$

  If no integer k fulfils the above conditions, then

  $$\texttt{neck\_top} = S_{\lfloor \frac{k_{\texttt{neck}}+1}{2} \rfloor}.$$

- `neck_down`

  Let $k_{\texttt{neck\_down}}$ be the minimum k such that $k_{\texttt{neck}} + 1 \leq k_{\texttt{neck\_down}} \leq n_S - 1$ and

  $$\sum_{i=2}^{k} |S_i - S_{i-1}| > \frac{3}{4} \sum_{i=2}^{n_S} |S_i - S_{i-1}|,$$

  then

  $$\texttt{neck\_down} = S_{k_{\texttt{neck\_down}}}.$$

  If no integer k fulfils the above conditions, then

  $$\texttt{neck\_down} = S_{\lfloor \frac{k_{\texttt{neck}}+n_S}{2} \rfloor}.$$

3.2.5 Feature extraction

Training behaviour classifiers directly on the contour and spine data with a supervised learning approach would cause several problems. A complex model would be necessary to successfully process the large amount of raw data. For example, when using a neural network classifier, a large number of hidden layers would be needed in order for the network to extract meaningful features. This, in turn, requires a large tagged dataset for training the classifier. The quality of the tagged data would need to be very high, such that behaviours would need to be annotated manually. This approach is very time-consuming. Furthermore, the larger the network architecture, the more computations would have to be performed at inference time, making it infeasible to detect behaviour in real time.

To circumvent this problem, a number of meaningful features describing body shape, velocity and direction of movement are extracted from the contour and spine data inside the DLL using explicit calculations. I have designed these features inspired by Jovanic et al. (2017) as well as previous work on the behaviour detection software for the single-larva closed-loop tracker, which I have carried out in collaboration with Dr Jean-Baptiste Masson and Elise Croteau-Chonka. Not all of these features are currently used to obtain behaviour classifiers on the high-throughput tracker, but I have already implemented their calculations since they may become important for the development of future behaviour classifiers.

Direction vectors

- `direction_vector`

  This is the normalised vector describing the main body axis spanning from `neck_down` to `neck`, defined by $\texttt{direction\_vector} = \frac{\texttt{neck}-\texttt{neck\_down}}{|\texttt{neck}-\texttt{neck\_down}|}$ (Fig. 3.6a).

- `direction_head_vector`

  This is the normalised vector describing the head axis spanning from `neck_top` to `head`, defined by $\texttt{direction\_head\_vector} = \frac{\texttt{head}-\texttt{neck\_top}}{|\texttt{head}-\texttt{neck\_top}|}$ (Fig. 3.6b).

- `direction_tail_vector`

  This is the normalised vector describing the tail axis spanning from `tail` to `neck_down`, defined by $\texttt{direction\_tail\_vector} = \frac{\texttt{neck\_down}-\texttt{tail}}{|\texttt{neck\_down}-\texttt{tail}|}$ (Fig. 3.6c).

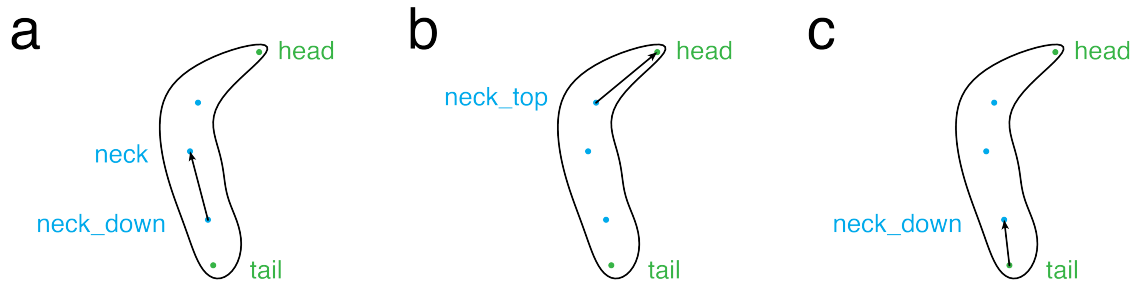

Figure 3.6: Direction vectors. Three direction vectors are calculated based on `head`, `tail` and the landmark points. **a.** `direction_vector` is the normalised vector from `neck_down` to `neck`, **b.** `direction_head_vector` is the normalised vector from `neck_top` to `head`, and **c.** `direction_tail_vector` is the normalised vector from `tail` to `neck_down`.

Features describing body shape

- `skeleton_length`

  This feature describes the total length of the spine as defined by the sum of the distances between consecutive spine points:

$$\texttt{skeleton\_length} = \sum_{i=2}^{n_S} |S_i - S_{i-1}|$$

- `perimeter`

  The perimeter of the contour is calculated as the sum of the distances between neighbouring contour points:

$$\texttt{perimeter} = \sum_{i=1}^{n_C} |C_i - C_{i-1}|,$$

  where $C_0 \equiv C_{n_C}$.

- `larva_arc_ratio`

  This feature uses the convex hull H of the contour C (Fig. 3.7a). It is defined as the ratio between the perimeter of the contour and the perimeter of the convex hull.

$$\texttt{larva\_arc\_ratio} = \frac{\sum_{i=1}^{n_C} |C_i - C_{i-1}|}{\sum_{i=1}^{n_H} |H_i - H_{i-1}|},$$

  where n_H denotes the number of points of the convex hull. Because of the properties of the convex hull, $\texttt{larva\_arc\_ratio} \geq 1$. The value is close to 1 when the larva is either in a straight or in a ball-like body shape.

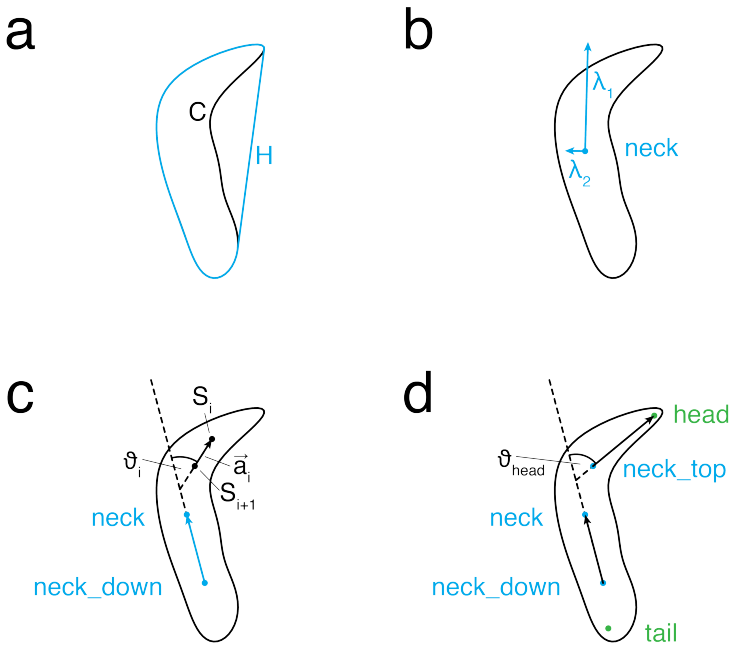

Figure 3.7: Schematics for features describing body shape. a. Outline of a larva with contour C (black) and its convex hull H (blue). *b.* The eigenvectors (blue) of the structure tensor of the larval contour (black) with respect to the `neck` and their corresponding eigenvalues λ_1 and λ_2 are shown. **c.** ϑ_i is defined as the angle between `direction_vector` (blue) and the vector $\vec{a}_i$ passing through spine points S_i and S_{i+1} (black). **d.** $\vartheta_{\texttt{head}}$ is defined as the angle between `direction_vector` and `direction_head_vector`. `head` and `tail` are shown in green.

- `larva_area_ratio`

  The areas A_C and A_H enclosed by the contour and its convex hull, respectively, are calculated using the shoelace formula (Zwillinger, 2003). Briefly, the area A of a polygon with vertices (x_i, y_i), $i = 1, ..., n$, is obtained by

  $$A = \frac{1}{2}\sum_{i=1}^{n} x_i y_{i+1} - x_{i+1} y_i,$$

  where $(x_{n+1}, y_{n+1}) \equiv (x_1, y_1)$. `larva_area_ratio` is defined as the ratio of A_C and A_H:

  $$\texttt{larva\_area\_ratio} = \frac{A_C}{A_H}$$

  Because of the properties of the convex hull, $0 \leq$ `larva_area_ratio` ≤ 1. The value is close to 1 when the larva is either in a straight or in a heavily curved or ball-like body shape.

- `eig_reduced`

  Let λ_1, λ_2 be the eigenvalues of the structure tensor of the larval contour with respect to the `neck` (Fig. 3.7b). Then `eig_reduced` is defined as the normalised difference between the two eigenvalues: `eig_reduced` $= \frac{|\lambda_1 - \lambda_2|}{\lambda_1 + \lambda_2}$. The structure tensor S is given by the matrix

  $$S = \begin{pmatrix} \frac{mom_{x^2}}{mom_{x^2}+mom_{y^2}} & \frac{mom_{xy}}{mom_{x^2}+mom_{y^2}} \\ \frac{mom_{xy}}{mom_{x^2}+mom_{y^2}} & \frac{mom_{y^2}}{mom_{x^2}+mom_{y^2}} \end{pmatrix},$$

  where

  $$mom_{x^2} = \frac{1}{n_C}\sum_{i=1}^{n_C} (x_i - x_{\texttt{neck}})^2,$$

  $$mom_{y^2} = \frac{1}{n_C}\sum_{i=1}^{n_C} (y_i - y_{\texttt{neck}})^2$$

  and

  $$mom_{xy} = \frac{1}{n_C}\sum_{i=1}^{n_C} (x_i - x_{\texttt{neck}})(y_i - y_{\texttt{neck}}).$$

  Here, x_i and y_i denote the x and y coordinates, respectively, of contour point C_i. Note that $0 \leq$ `eig_reduced` ≤ 1 is always satisfied. Typically, `eig_reduced` will decrease as the bend amplitude of the larva increases.

- `s`

  To calculate this feature, the spine is partitioned into $n_S - 1$ segments $\vec{a}_1, ..., \vec{a}_{n_S-1}$ as defined by the n_S spine points, such that $\vec{a}_1$ points from S_2 to the head, whereas $\vec{a}_{n_S-1}$ originates at the tail. For each $i = 1, ..., n_S - 1$, the angle between $\vec{a}_i$ and `direction_vector` is denoted by ϑ_i (Fig. 3.7c). The nematic spine `s` is defined as follows:

$$s = \frac{1}{n_S - 1} \sum_{i=1}^{n_S-1} \frac{3\cos^2\vartheta_i - 1}{2}$$

  `s` can take values between –0.5 and 1. Values are typically close to 1 when the larva is in a straight body shape ($\vartheta_i \simeq 0^\circ$) and become significantly smaller with increasing bend amplitude.

- `asymmetry`

  This is the sine of the angle $\vartheta_{\texttt{head}}$ between `direction_vector` and `direction_head_vector` (Fig. 3.7d). It takes positive values when the larva is bending its head to the left and negative values when it is bending its head to the right.

$$\begin{aligned}\texttt{asymmetry} &= \sin(\vartheta_{\texttt{head}}) \\ &= x_{\texttt{direction\_vector}} \cdot y_{\texttt{direction\_head\_vector}} \\ &\quad - y_{\texttt{direction\_vector}} \cdot x_{\texttt{direction\_head\_vector}}\end{aligned}$$

  This identity is derived from the subtraction formula for the sine function, making use of the fact that `direction_vector` and `direction_head_vector` are normalised.

- `angle_upper_lower`

  This is the absolute angle between `direction_vector` and `direction_head_vector` (Fig. 3.7d).

$$\begin{aligned}\texttt{angle\_upper\_lower} &= |\vartheta_{\texttt{head}}| \\ &= \cos^{-1}(\texttt{direction\_vector} \cdot \texttt{direction\_head\_vector})\end{aligned}$$

  `asymmetry` and `angle_upper_lower` are very similar, since they both directly depend on $\vartheta_{\texttt{head}}$. Nevertheless, they can develop very different dynamics after temporal smoothing, which is valuable for a stable detection of left and right bends.

Features describing velocity

Velocities are calculated using information from previous frames, which is stored in buffers. When a larva ID first occurs during the experiment, all buffers for previous landmark locations are initialised to 0.

- `head_speed`
  This is the velocity of the `head`, measured in mm/s over a time interval of dt $= 0.2$ s (four frames).

- `tail_speed`
  This is the velocity of the `tail`, measured in mm/s over a time interval of dt $= 0.2$ s (four frames).

- `neck_speed`
  This is the velocity of the `neck`, measured in mm/s over a time interval of dt $= 0.2$ s (four frames).

- `neck_top_speed`
  This is the velocity of `neck_top`, measured in mm/s over a time interval of dt $= 0.2$ s (four frames).

- `neck_down_speed`
  This is the velocity of `neck_down`, measured in mm/s over a time interval of dt $= 0.2$ s (four frames).

- `v_centroid`
  This is the velocity of the `centroid`, measured in mm/s over a time interval of dt $= 0.2$ s (four frames).

- `v_norm`
  This feature is calculated as the arithmetic mean of `neck_down_speed`, `neck_speed` and `neck_top_speed`, passed through a hyperbolic tangent activation function to suppress excessively large values.

$$\texttt{v\_norm} = 15 \tanh\left(\frac{1}{15} \cdot \frac{\texttt{neck\_down\_speed} + \texttt{neck\_speed} + \texttt{neck\_top\_speed}}{3}\right)$$

- `speed_reduced`

  This feature describes the relative contribution of `neck_top_speed` to `v_norm`, passed through a hyperbolic tangent activation function to suppress excessively large values. A small positive number, 0.001, is added to both the enumerator and the denominator in order to avoid potential division by zero. The value of `speed_reduced` increases when the front part of the larval body is moving fast compared to the rest of the body, e. g. when a bend is initiated.

$$\texttt{speed\_reduced} = \tanh\left(\frac{\texttt{neck\_top\_speed} + 0.001}{3 \cdot \texttt{v\_norm} + 0.001}\right)$$

- `damped_distance`

  This feature reflects the distance in mm travelled by the neck, giving more weight to recent events compared to past events ($\gamma < 1$; here: $\gamma = 0.9$). For any given frame i, the distance d_i is calculated as

$$d_i = \texttt{neck}_i - \texttt{neck}_{i-1}.$$

  Then we define

$$\texttt{damped\_distance}_t = \sum_{i=1}^{t} \gamma^{t-i} d_i,$$

  where t denotes the current frame. Algorithmically, `damped_distance` can be obtained through a recursion:

$$\texttt{damped\_distance}_t = d_t + \gamma \cdot \texttt{damped\_distance}_{t-1}$$

Features related to direction of movement

- `crab_speed`

  This is the sideways velocity of the larva measured in mm/s, calculated as the component of `neck_velocity` which is orthogonal to `direction_vector_filtered`, the smoothed normalised vector from `neck_down` to `neck` (Fig. 3.8a):

$$\texttt{crab\_speed} = \left|\texttt{neck\_velocity} \times \texttt{direction\_vector\_filtered}\right|$$

- `parallel_speed`

  This describes the forward velocity of the larva measured in mm/s, defined as

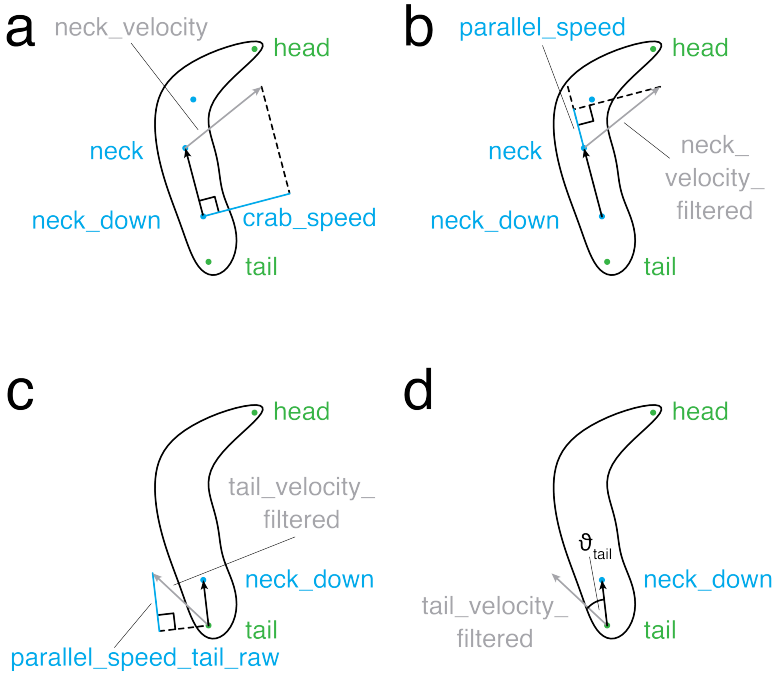

Figure 3.8: Schematics for features related to direction of movement. The larval contour is shown in black, `head` and `tail` are shown in green. **a.** `crab_speed` (blue) is defined as the component of `neck_velocity` (grey) which is orthogonal to `direction_vector_filtered` (black). **b.** `parallel_speed` (blue) is defined as the component of `neck_velocity_filtered` (grey) which is parallel to `direction_vector_filtered` (black). **c.** `parallel_speed_tail_raw` (blue) is defined as the component of `tail_velocity_filtered` (grey) which is parallel to `direction_tail_vector_filtered` (black). **d.** $\vartheta_{\texttt{tail}}$ is defined as the angle between `tail_velocity_filtered` (grey) and `direction_tail_vector_filtered` (black).

the component of the smoothed neck velocity, `neck_velocity_filtered`, which is parallel to `direction_vector_filtered` (Fig. 3.8b):

$$\texttt{parallel\_speed} = \texttt{neck\_velocity\_filtered} \cdot \texttt{direction\_vector\_filtered}$$

- `parallel_speed_tail_raw`

  This is the forward velocity of the tail measured in mm/s, defined as the component of the smoothed tail velocity, `tail_velocity_filtered`, which is parallel to `direction_tail_vector_filtered` (Fig. 3.8c):

$$\begin{aligned}\texttt{parallel\_speed\_tail\_raw} = \texttt{tail\_velocity\_filtered} \\ \cdot \texttt{direction\_tail\_vector\_filtered}\end{aligned}$$

- `parallel_speed_tail`

  This feature is similar to `parallel_speed_tail_raw`, with the difference that the smoothed tail velocity, `tail_velocity_filtered`, is normalised prior to calculating the dot product. `parallel_speed_tail` is hence purely a measure of direction of tail movement, since it is the cosine of the angle $\vartheta_{\texttt{tail}}$ between `tail_velocity_filtered` and `direction_tail_vector_filtered` (Fig. 3.8d). It can take values between -1 (corresponding to backward movement of the tail) and +1 (corresponding to forward movement of the tail).

$$\begin{aligned}\texttt{parallel\_speed\_tail\_raw} &= \frac{\texttt{tail\_velocity\_filtered}}{|\texttt{tail\_velocity\_filtered}|} \\ &\cdot \texttt{direction\_tail\_vector\_filtered} \\ &= \cos(\vartheta_{\texttt{tail}})\end{aligned}$$

Temporal smoothing

For each feature, a `filtered` version is calculated using exponential smoothing over time. In the first frame in which a certain larva ID occurs during the experiment, all buffers for previous filtered feature values are initialised to 0.

For a given feature `f`, the smoothed feature `f_filtered` is calculated as follows:

$$\texttt{f\_filtered}_t = (1-\alpha) \cdot \texttt{f\_filtered}_{t-\Delta t} + \alpha \cdot \texttt{f}_t$$

where t is unitless, but derived from the experiment time in seconds, $\Delta t = 0.05$ and $\alpha = \frac{\Delta t}{\tau}$ with $\tau = 0.25$ (Fig. 3.9a, b).

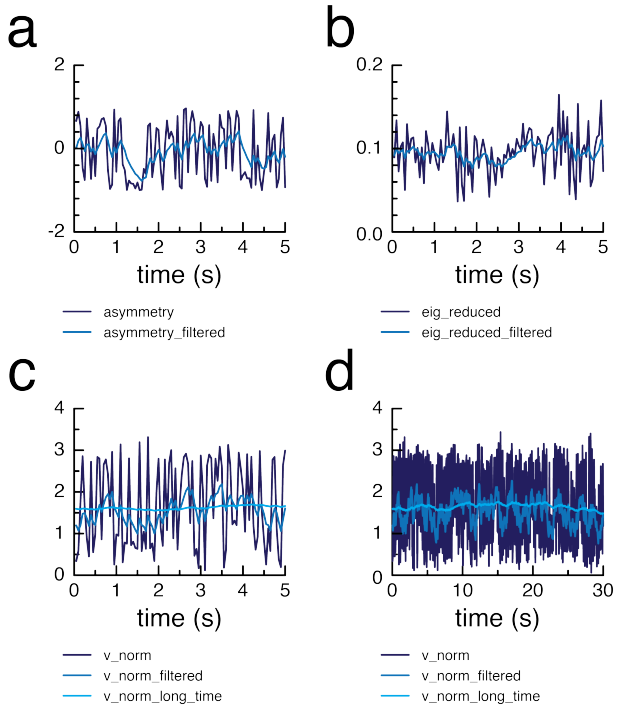

Figure 3.9: Temporal smoothing of features. a–b. Raw (dark blue) and filtered (mid blue) example graphs of `asymmetry` (**a**) and `eig_reduced` (**b**) over time. **c–d.** Raw (dark blue), filtered (mid blue) and long-time filtered (light blue) example graphs of `v_norm` over a short (**c**) and a long (**d**) period of time.

An exception is `v_norm_filtered`, which uses a different formula. This is necessary because when a larva ID is initialised, `v_norm` can take very high values, which can be bounded using a hyperbolic tangent activation function:

$$\texttt{v\_norm\_filtered}_t = (1-\alpha) \cdot \texttt{v\_norm\_filtered}_{t-\Delta t} + \alpha \cdot \sigma \cdot \tanh\left(\frac{\texttt{v\_norm}_t}{\sigma}\right)$$

where $\sigma = 5$.

In addition, `v_norm_long_time` and `v_centroid_long_time` are calculated as versions of `v_norm` and `v_centroid` which are smoothed over a longer time window using the general formula for exponential smoothing:

$$\texttt{v\_norm\_long\_time}_t = (1-\alpha_{long}) \cdot \texttt{v\_norm\_long\_time}_{t-\Delta t} + \alpha_{long} \cdot \texttt{v\_norm}_t$$

$$\texttt{v\_centroid\_long\_time}_t = (1-\alpha_{long}) \cdot \texttt{v\_centroid\_long\_time}_{t-\Delta t} + \alpha_{long} \cdot \texttt{v\_centroid}_t$$

where $\alpha_{long} = \frac{\Delta t}{\tau_{long}}$ with $\tau_{long} = 5$ (Fig. 3.9c, d).

Table 3.1: Value of k by feature.

Feature	k
angle_upper_lower	1,000
asymmetry	1,000
crab_speed	500
damped_distance	1,000
eig_reduced	100,000
parallel_speed	1,000
parallel_speed_tail	1,000
perimeter	1,000
s	1,000
skeleton_length	1,000
speed_reduced	1,000
v_norm	50

Differentiation by convolution

A convolution is used to approximate a smoothed squared derivative for each feature. The underlying mathematical concepts are motivated by Masson et al. (2012). Calculating these convolved_squared versions of features is a useful way to integrate information over time without the need for a larger expansion of the feature space.

In the first frame in which a certain larva ID occurs during the experiment, all buffers for previous feature values are initialised to 0. For a given feature f at a point in time t, f_convolved_squared is calculated as follows:

$$\begin{aligned} \mathtt{f1}_t &= (1-\lambda\Delta t)\cdot \mathtt{f1}_{t-\Delta t} + \frac{1}{2}\Delta t\cdot(\mathtt{f}_{t-\Delta t}+\mathtt{f}_t) \\ \mathtt{f2}_t &= \lambda\Delta t\cdot \mathtt{f1}_{t-\Delta t} + (1-\lambda\Delta t)\cdot \mathtt{f2}_{t-n\Delta t} \\ \mathtt{f\_convolved\_squared}_t &= k\cdot(\mathtt{f1}_t-\mathtt{f2}_t)^2, \end{aligned}$$

where t is unitless, but derived from the experiment time in seconds, $\Delta t = 0.05$, $\lambda = \frac{1}{\tau}$, $\tau = 0.25$ and $n = 5$. Values for k are empirically chosen for each feature (Table 3.1). Example trajectories of the convolved_squared version of several features are shown in Fig. 3.10.

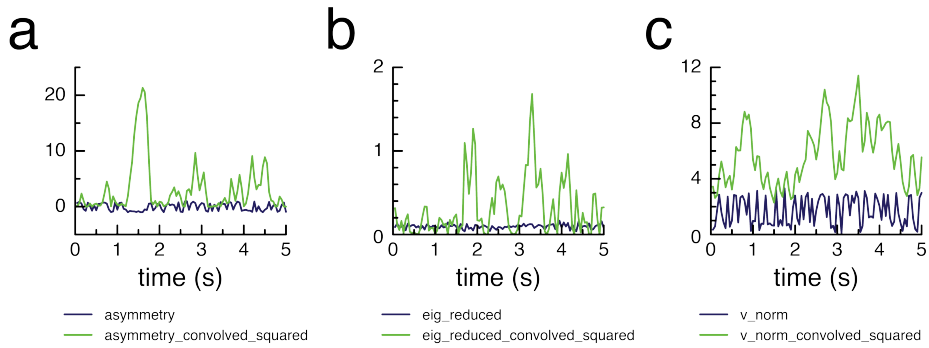

Figure 3.10: Differentiation by convolution. Raw (dark blue) and convolved squared (green) example graphs of **a.** `asymmetry`, **b.** `eig_reduced` and **c.** `v_norm` over time.

3.2.6 Behaviour classifiers

The behaviour classifiers described below were developed using a modified version of JAABA (Kabra et al., 2013). I have developed the user interface with functions for manual annotation, data visualisation and machine learning using the Neural Network Toolbox, the Deep Learning Toolbox and the Statistics and Machine Learning Toolbox in MATLAB. A combination of trained neural networks and empirically determined linear thresholds is used for behaviour detection.

Ball

As described in Section 3.2.4, the votes for head and tail detection need to be reset when a larva is curling up such that the contour takes a circular shape. I have developed the `ball` classifier, which detects these events.

The classifier uses a feed-forward neural network with a single fully connected hidden layer, which receives normalised values of `eig_reduced`, `larva_arc_ratio` and `larva_area_ratio` as inputs. The hidden layer consists of five neurons with a hyperbolic tangent activation function. The output layer contains a single neuron and uses a sigmoid activation function (Fig. 3.11). The neural network was trained on a manually annotated dataset for 500 epochs in MATLAB using a cross-entropy loss function and scaled conjugate gradient backpropagation. `ball` is set to true if the network output is greater than 0.8.

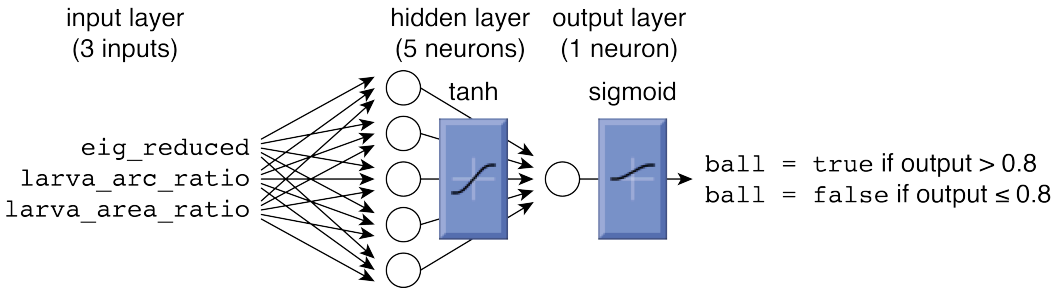

Figure 3.11: Neural network architecture for `ball` detection. Three input features (`eig_reduced`, `larva_arc_ratio` and `larva_area_ratio`) are processed by a feed-forward neural network consisting of a fully connected hidden layer (five neurons) with hyperbolic tangent activation function and an output layer (one neuron) with sigmoid activation function. A `ball` is detected if the output is greater than 0.8. Schematics of the activation functions have been obtained using the `view` function of the MATLAB R2018b Deep Learning Toolbox (MathWorks).

Left and right bend

The initial `bend` classifier is set to `true` if all of the following criteria are met:

- `s_filtered` < 0.85
- `eig_reduced_filtered` < 0.85
- `angle_upper_lower_filtered` > 0.4

`bend_smooth` is then obtained by exponential smoothing of `bend` over time. `bend_smooth` is set to `true` if

$$\texttt{bend\_filtered}_t > 0.7$$

for

$$\texttt{bend\_filtered}_t = (1-\alpha)\cdot \texttt{bend\_filtered}_{t-\Delta t} + \alpha \cdot \text{int}(\texttt{bend}_t),$$

where t is unitless, but derived from the experiment time in seconds, $\Delta t = 0.05$, $\alpha = \frac{\Delta t}{\tau}$ with $\tau = 0.06$, $\text{int}(\texttt{true}) \equiv 1$ and $\text{int}(\texttt{false}) \equiv 0$.

Independent classifiers are used for an initial detection of bending direction. `left` is set to `true` if all of the following criteria are met:

- `angle_upper_lower_filtered` > 0.4
- `asymmetry` $\geq$ 0.4

`right` is set to `true` if all of the following criteria are met:

- `angle_upper_lower_filtered` > 0.4
- `asymmetry` $\leq$ –0.4

If for a larva `ball == true` at any point during the previous 1.5 s, the `left` and `right` classifiers are overwritten to match the last detected bend direction prior to the beginning of the `ball` event.

Left and right bends are detected by combining `bend_smooth` with `left` or `right`, respectively, using an AND conjunction. The raw time series of left and right bends is further smoothed post acquisition using a custom MATLAB script. First, whenever two bends to the same side were separated by a break of less than 200 ms, they are combined into a single long bend. Next, short bends with a duration of less than 200 ms are removed from analysis.

I have manually validated the performance of the final classifier (Table 3.2).

Forward crawl and forward peristaltic waves

Two different classifiers are used for detection of crawl. `forward` is designed to detect longer forward crawl periods. It is set to `true` if all of the following conditions are met:

- `parallel_speed_tail_filtered` > 0.6
- `parallel_speed_tail_raw_filtered` > 0.6
- `ball == false` for all frames in the previous 1.5 s

The second classifier, `forward_peristaltic`, is designed to detect individual forward peristaltic waves. It is set to `true` if all of the following conditions are met:

- `forward == true`
- `parallel_speed_tail_raw` > 0.8

I have manually validated the performance of the `forward` and `forward_peristaltic` classifiers (Table 3.2).

Table 3.2: Accuracy of behaviour detection based on manual quantification.

Contour (350 valid objects, each with 60 s video data)	
Severely corrupted objects	100.0%
Two touching larvae detected as one object	0.3%
Long period of flipped `head` and `tail` detection	0.3%
`bend` (714 events from 24 larvae in 60 minutes of video data)	
Precision	95.6%
Recall	96.4%
Correct `left` and `right` detection (true-positive bends)	97.3%
`forward` (425 events from 24 larvae in 60 minutes of video data)	
Precision	97.8%
Recall	94.1%
`forward_peristaltic` (2954 events from 24 larvae in 60 minutes of video data)	
Precision	99.5%
Recall	93.6%
Events which are falsely combined with another event	10.7%
Events which are detected as more than one event	1.2%
`back` (268 events from 24 larvae in 60 minutes of video data)	
Precision	86.5%
Recall	88.4%
`roll` (240 events from 24 larvae in 60 minutes of video data)	
Precision (rolls and roll-like events)	96.6%
Recall (rolls)	86.7%
Recall (roll-like events)	25.8%

Back-up

The `back` classifier is designed to detect individual backward peristaltic waves during back-up. It is set to true if all of the following conditions are met:

- `parallel_speed_tail_filtered` < –0.6
- `parallel_speed_tail_raw_filtered` < –0.45
- `ball == false` for all frames in the previous 1.5 s

I have manually validated the performance of the classifier (Table 3.2).

Roll

In order for the preliminary `roll` classifier to be set to `true`, all of the following criteria have to be met:

- 1 < `angle_upper_lower_filtered` < 1.8
- `crab_speed_filtered` > 1
- `damped_distance_filtered` > 0.64
- `v_norm_filtered` > 1.2
- $|\texttt{asymmetry\_filtered}| > 0.65$
- `s` < 0.8
- `s_filtered` > 0.2
- `eig_reduced_filtered` < 0.7
- $\texttt{eig\_reduced\_filtered} > -1.5 \cdot \texttt{s\_filtered} + 0.45$
- `v_norm_long_time` > 0.5
- `parallel_speed_tail_filtered` > –0.6
- `parallel_speed_tail_filtered` > –0.4
  or `asymmetry_convolved_squared` > 10

- `speed_reduced_filtered` < 0.38
- `ball == false`

If for a larva `roll == true` at any point during the previous 1.5 s, the values of the classifiers for `forward`, `forward_peristaltic` and `back` are overwritten and set to `false`. This serves to reduce the number of false-positive detections for these classifiers.

In addition, a smooth classifier `roll_smooth` is obtained by exponential smoothing of `roll` over time. `roll_smooth` is set to `true` if

$$\texttt{roll\_filtered}_t > 0.6$$

for

$$\texttt{roll\_filtered}_t = (1-\alpha) \cdot \texttt{roll\_filtered}_{t-\Delta t} + \alpha \cdot \text{int}(\texttt{roll}_t),$$

where t is unitless, but derived from the experiment time in seconds, $\Delta t = 0.05$, $\alpha = \frac{\Delta t}{\tau}$ with $\tau = 0.1$, $\text{int}(\texttt{true}) \equiv 1$ and $\text{int}(\texttt{false}) \equiv 0$. `back` is overwritten to `false` when `roll_smooth == true` to further reduce false-positive back-up detection.

I have manually validated the performance of the classifier (Table 3.2). When larvae are rolling, unusual behaviour patterns such as rapid bending or twitching can be observed in addition to true rolls. I call these behaviours "roll-like behaviours".

3.2.7 Optogenetic stimulation

Optogenetic stimulation is controlled for each larva individually based on a custom protocol which can be defined by the user inside the DLL and which operates on the output of the behaviour detection. DMDs are used to project light patterns onto a subset of larvae on the agarose plate. The DMDs operate like monochrome red light projectors with an image size of 768 x 1024 pixels, in which a large number of individually rotatable micromirrors are used to each modulate the intensity of a single image pixel.

During the process of hardware design, two different DMD models were tested. The first DMD is illuminated by an integrated LED (613 nm), whereas the second DMD receives input from an external LED source (625 nm) through an optic fibre. The two DMDs achieve similar light intensities, which based on empirical values are on their own insufficient for optogenetic stimulation of larvae. Both devices were installed on the final system,

such that they each cover the entire agarose plate. With this set-up, the sum of the light intensities of the two DMDs can be reached at each location on the agarose plate.

Optogenetic stimulation of individual larvae is achieved by commanding both DMDs to project a square with a size of 1 cm^2 at the location of the larval `centroid` (Fig. 3.12a). The light intensity can be controlled for each larva independently at a resolution of 8 bits, which is constrained by the normalisation step performed to achieve uniform light intensity across the plate (see below). If two or more larvae are located close enough to each other such that the corresponding squares overlap, the light intensity in the overlapping region is set to the smallest value to avoid undesired stimulation. Since the DMD images are updated at 20 Hz, the delay between behaviour detection and optogenetic stimulation does not exceed 50 ms.

In collaboration with Dr Lakshmi Narayan, I have developed two necessary calibration methods. To aim light stimuli at larvae crawling at plate level, a map between world coordinates (in mm) and DMD pixel locations needs to be created. For each DMD, a small number of squared spots is projected at fixed DMD pixel locations and visualised in the camera image at the level of the agarose plate by removing the optical filter from the camera. The location of the spots in the image in camera coordinates (in pixels) is manually recorded and used to fit a linear regression model to obtain the parameters for camera-to-DMD transformation. World-to-DMD transformation is performed using the existing camera-to-world coordinate transform.

One problem with optogenetic stimulation using DMDs is that illumination using the default output is not uniform at plate level. The maximum light intensity which can be achieved around the edge of the plate is only approximately 40% as high as the peak value at the centre of the arena. Since this can cause very different degrees of optogenetic stimulation depending on where a given larva is located, I have calibrated the pixel intensity of the DMD image by normalising it to the level of the highest possible intensity which can be achieved anywhere on the plate. Based on approximately 100 light intensity values measured across the plate, a look-up table containing the normalisation factor for each DMD pixel is calculated using bilinear interpolation.

To accommodate for possible differences in the levels of nonuniformity between the two DMDs, intensity calibration is performed for both DMDs simultaneously following spatial

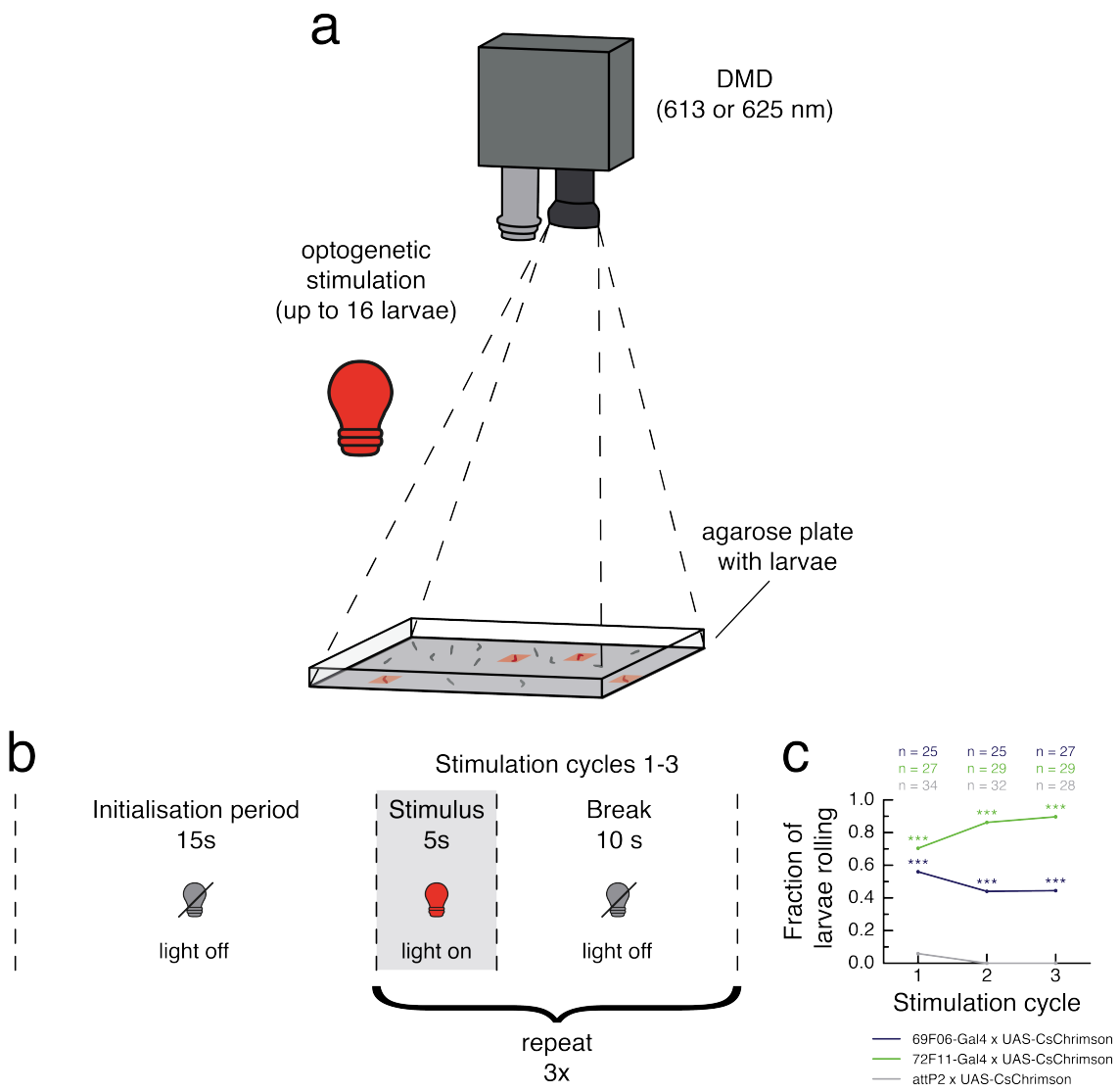

Figure 3.12: Optogenetic stimulation of individual larvae. a. Schematic of the hardware design for optogenetic stimulation. There are two digital micromirror devices (DMDs), only one of which is shown in the illustration for simplicity. The DMD operates like a red light movie projector (613 or 625 nm) and is positioned such that the entire agarose plate can be covered. It is configured to project small squares of light with a size of 1 cm^2 onto the desired subset of larvae as defined by the stimulation protocol and the behaviour detection output. **b.** Protocol of a proof-of-principal experiment for optogenetic stimulation. After a 15 s initialisation period to stabilise behaviour detection and to allow the larvae to accommodate to their environment, the reaction of the larvae to the optogenetic stimulus is tested in three 15 s stimulation cycles. Each cycle consists of a 5 s open-loop red light stimulus directed at all detected objects on the plate (red light bulb), followed by a 10 s period without stimulation (grey light bulb). **c.** For each stimulation cycle, the fraction of larvae for which a `roll` was detected in at least six frames during the 15 s period is shown. *69F06-Gal4 x UAS-CsChrimson* and *72F11-Gal4 x UAS-CsChrimson* larvae (*CsChrimson* expression in neurons triggering roll behaviour; experimental groups) were compared to *attP2 x UAS-CsChrimson* larvae (no *CsChrimson* expression; control group). Only larvae which received stimulation for more than 90% of the 5 s stimulation period are included into analysis. Statistical differences between the experimental groups and the control group are tested with a Fisher's exact test; *** $p < 0.001$.

calibration. With the fully calibrated system, a uniform light intensity of 285 µW/cm^2 can be achieved across the plate.

I have conducted a proof-of-principle experiment to verify that this set-up can be successfully used for optogenetic stimulation. Ohyama et al. (2015) have identified two GAL4 lines expressed in neurons whose activation triggers strong rolling behaviour. *69F06-Gal4* drives expression in command neurons for rolling, whereas *72F11-Gal4* is specific to the Basin neurons, which integrate mechanosensory and nociceptive stimuli.

In a one-minute experiment, I tested rolling responses upon optogenetic stimulation of *69F06-Gal4 x UAS-CsChrimson* and *72F11-Gal4 x UAS-CsChrimson* larvae using the maximum available light intensity of 285 µW/cm^2. In the beginning of the experiment, larvae were allowed to get used to the arena in a 15 s initialisation period. Excluding this time window from analysis also increases robustness of the behaviour classifier for `roll`. In three 15 s stimulation cycles, all detected larvae on the plate received a 5 s optogenetic stimulus followed by a 10 s period without a stimulus (Fig. 3.12b).

For each larva, I assessed whether a `roll` was detected for at least six frames during a given 15 s stimulation cycle. This threshold was set to eliminate noise in the behaviour classifier caused by rapid bending in response to the stimulus. Since the frame rate of the behaviour detection is 20 Hz, it corresponds to a behaviourally relevant total `roll` duration of at least 300 ms. Only larvae which received stimulation for more than 90% of the 5 s stimulation period were included into analysis. For each stimulation cycle, above-threshold rolling behaviour was observed for over 40% of *69F06-Gal4 x UAS-CsChrimson* larvae and over 70% of *72F11-Gal4 x UAS-CsChrimson* larvae. By contrast, less than 6% of *attP2 x UAS-CsChrimson* control larvae, which do not express *CsChrimson*, were rolling during any given stimulation cycle (Fig. 3.12c).

3.2.8 Thermogenetic stimulation

Thermogenetic stimulation can be controlled for each larva individually based on a custom protocol which is defined by the user inside the DLL and which operates on the output of the behaviour detection. For stimulation of up to 16 larvae, four two-axis galvanometers are installed on the system. Each galvanometer can receive input from a laser source and contains two mirrors, which can be rotated around orthogonal axes to project a laser beam onto different spots on the agarose plate with full two-dimensional coverage. A

single galvanometer can target up to four larvae within a 50 ms frame. Therefore, the delay between behaviour detection and thermogenetic stimulation does not exceed 100 ms.

The laser source, which was developed by Dr Christopher McRaven and Dr Michael Winding, operates at 1490 nm. This wavelength is well absorbed by water (Curcio and Petty, 1951). Because larvae are transparent objects which contain a large amount of water, they are rapidly heated up by the laser beam. In the present set-up, only a single laser source has been built, such that only one of the galvanometers is functional. Therefore, up to four larvae can currently receive the thermogenetic stimulus. However, the system can easily be expanded to work for all 16 larvae by adding three more lasers.

To achieve thermogenetic stimulation of four larvae with a single galvanometer, four locations are specified inside the DLL at 20 Hz. The galvanometer mirrors can be rotated within less than 1 ms to move the laser beam from one location on the plate to another location. Therefore, the available 50 ms time window is split up as follows: every 12.5 ms, the galvanometer receives a command to move to a new location. To account for fluctuations in the movement time and to avoid undesired stimulation of other parts of the plate, the laser input is switched off for 1.5 ms. During the remaining 11 ms, the laser beam is targeted at the specified location (Fig. 3.13a). For each larva, the laser intensity can be controlled relative to the maximum laser power which is uniformly available across the arena after intensity calibration (see below). If less than 16 objects are detected in a given frame, the remaining target locations for the galvanometers are set to the centre of the arena and the corresponding laser intensity is set to zero.

The mirror position of the galvanometers is controlled by two integrated motors, which receive a voltage input through an analogue output device. The combination of the two voltages clearly defines the location on the agarose plate at which the laser beam is aimed. To obtain the parameters which are necessary to map larval locations in world coordinates to input voltages for the galvanometer, I have calibrated the system in collaboration with Dr Lakshmi Narayan and Elise Croteau-Chonka. First, the existing world-to-camera transform is used to calculate the location of the larval `centroid` in camera coordinates. This location is then mapped to a pair of voltages using two look-up tables (i. e. one for each voltage value), which are obtained through bilinear interpolation from a set of measured values. These values are acquired by scanning a visible aiming beam across different locations on the plate using a fixed set of voltage inputs to the galvanometer. The

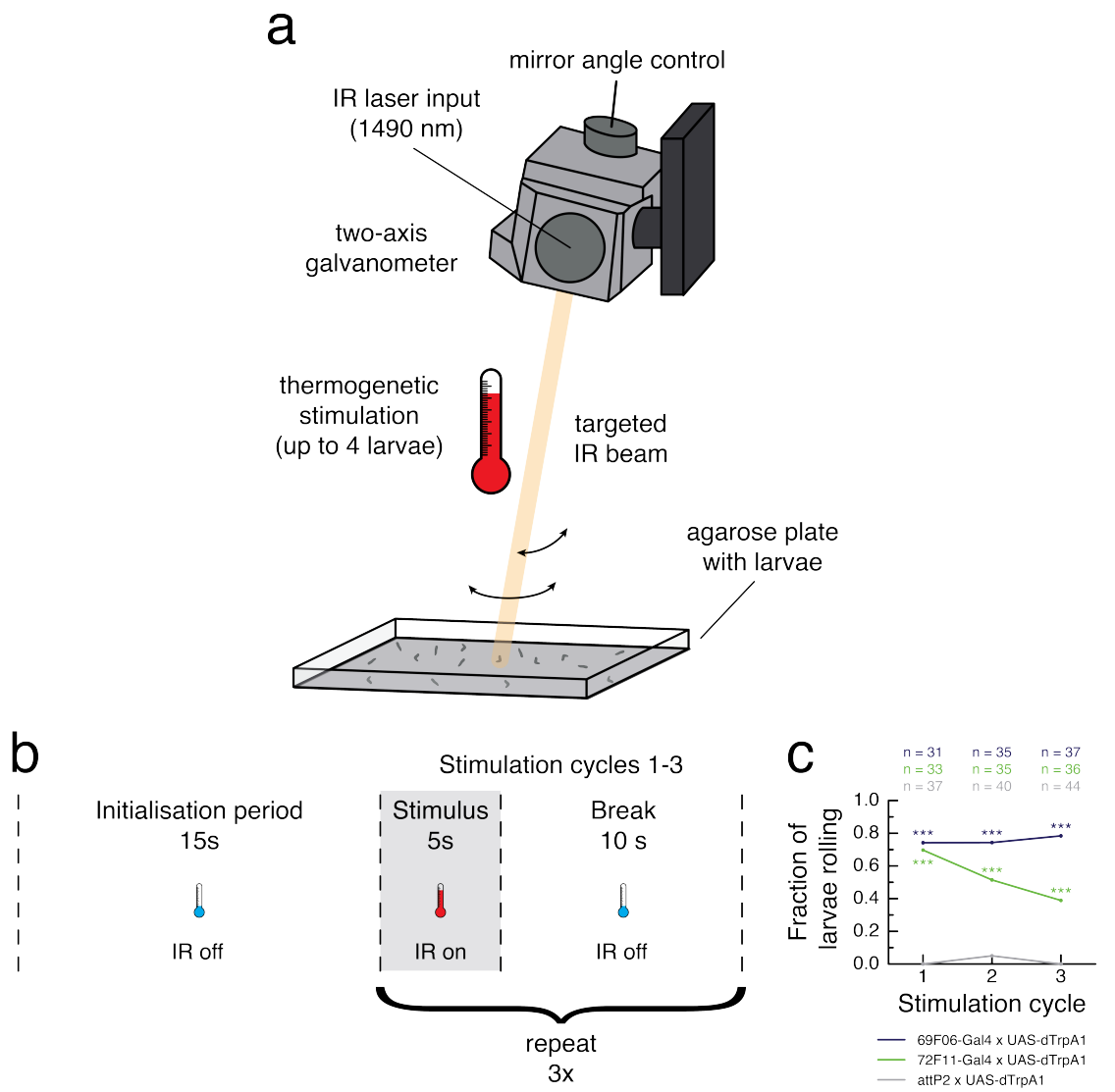

Figure 3.13: Thermogenetic stimulation of individual larvae. a. Schematic of the hardware design for thermogenetic stimulation. There are four two-axis galvanometers, only one of which is shown in the illustration for simplicity. The galvanometer receives input from an infrared (IR) laser source (1490 nm) and can be used to target IR beam spots with a diameter of about 5 mm at a user-defined location on the agarose plate. The mirror angles of the galvanometer can be updated at 80 Hz to move to a new location. The galvanometer is configured to cycle between up to four larvae at 20 Hz as defined by the stimulation protocol and the behaviour detection output. The IR beam temporarily heats up the larvae, enabling thermogenetic stimulation. **b.** Protocol of a proof-of-principal experiment for thermogenetic stimulation. After a 15 s initialisation period to stabilise behaviour detection and to allow the larvae to accommodate to their environment, the reaction of the larvae to the thermogenetic stimulus is tested in three 15 s stimulation cycles. Each cycle consists of a 5 s open-loop stimulation period, in which the galvanometer targets the IR beam at up to four larvae in an alternating way (red thermometer), followed by a 10 s period without stimulation (blue thermometer). **c.** For each stimulation cycle, the fraction of larvae for which a `roll` was detected in at least six frames during the 15 s period is shown. *69F06-Gal4 x UAS-dTrpA1* and *72F11-Gal4 x UAS-dTrpA1* larvae (*dTrpA1* expression in neurons triggering roll behaviour; experimental groups) were compared to *attP2 x UAS-dTrpA1* larvae (no *dTrpA1* expression; control group). Only larvae which received stimulation for more than 90% of the 5 s stimulation period are included into analysis. Statistical differences between the experimental groups and the control group are tested with a Fisher's exact test; *** $p < 0.001$.

optical filter is removed from the camera, such that the corresponding locations in camera coordinates can be automatically extracted from the image using binary thresholding.

Since the laser beam is projected at the agarose plate at different angles depending on the location of the larva, the illuminated spot at plate level takes an elliptical shape with variable size. As the power of the laser beam is constant, but the area of the spot changes, the amount of IR light covering the larva is not consistent. To ensure that all larvae receive the same amount of stimulation regardless of their position in the arena, I have calibrated the intensity of the laser output in collaboration with Dr Lakshmi Narayan and Elise Croteau-Chonka. The spot size of a visible aiming beam was measured at various locations across the plate and used to normalise the desired laser intensity to achieve constant power per area. Based on these measurements, a look-up table which contains the required laser power value corresponding to each pixel location of the larval `centroid` was calculated using bilinear interpolation. In addition, a map between the input voltage to the laser source and the total laser power output was created based on manual measurements by Elise Croteau-Chonka to account for nonlinearity in the voltage-to-power relationship. By combining these transformations, the voltage input to the laser source necessary to produce uniform stimulation can be calculated for any location in the arena. At the location on the plate where the area of the laser spot reaches its minimum, the maximum laser power of 5.26 W is reduced to 67.3% after this intensity calibration when using the temporal pattern of galvanometer position updates described above.

I performed a proof-of-principle experiment to verify that the galvanometer set-up can be successfully used for thermogenetic stimulation. Since currently only one galvanometer is connected to a laser source and stimulation is hence only available for up to four larvae, I performed the experiment using three larvae per run. This is necessary because of the residual risk of detecting one or more non-larval objects. If the total number of detected objects exceeds four, it is possible that a valid larva is excluded from stimulation.

In a one-minute experiment, I tested rolling responses upon thermogenetic stimulation of *69F06-Gal4 x UAS-dTrpA1* and *72F11-Gal4 x UAS-dTrpA1* larvae using 40% of the maximum available laser intensity. The experimental protocol consists of a 15 s initialisation period without stimulation and three 15 s stimulation cycles. In each stimulation cycle, the laser beam was cycled between the first four object locations which are output from the

DLL for 5 s, heating up each larva for an 11 ms period every 50 ms, followed by a 10 s period without a stimulus (Fig. 3.13b).

For each larva, I assessed whether a `roll` was detected for at least six frames during a given 15 s stimulation cycle. Only larvae which received stimulation during more than 90% of frames in the 5 s stimulation period were included into analysis. For each stimulation cycle, above-threshold rolling behaviour was observed for over 70% of *69F06-Gal4 x UAS-dTrpA1* larvae and over 35% of *72F11-Gal4 x UAS-dTrpA1* larvae. By contrast, not more than 5% of *attP2 x UAS-dTrpA1* control larvae, which do not express *dTrpA1*, were rolling during any given stimulation cycle, suggesting that larvae do not perceive strong pain under the heating conditions used in this experiment (Fig. 3.13c).

It should be pointed out that additional increases to the laser power do not necessarily result in more efficient thermogenetic stimulation. In fact, raising the laser power to 45% while keeping all other conditions unchanged results in irreversible changes in the behaviour pattern, reflecting tissue damage. Increasing it even further to 50% causes larvae to die immediately. Similar effects can be observed when extending the duration of the stimulation period beyond a certain threshold. Three parameters characterise the temperature increase following illumination with the IR beam: i) the laser power, ii) the total duration of the stimulus, and iii) the temporal arrangement in which the galvanometer cycles between locations in its 80 Hz movement pattern. Preliminary experiments suggest that these parameters can be adjusted in a way which allows simultaneous thermogenetic stimulation of eight or even twelve larvae with a single galvanometer, which may eliminate the need to install a total number of four lasers to target all 16 larvae.

3.3 Conclusions

The novel experimental set-up introduced in this chapter can track up to 16 objects simultaneously. A number of complex behaviours of *Drosophila* larvae, including left and right bend, forward crawl, back-up and roll, can be detected in real time. The output of this detection can be used to independently administer both optogenetic and thermogenetic stimuli at individual larvae in closed loop, based on customisable criteria and with small latency. This allows for targeted activation or inhibition of neurons in response to the

occurrence of an action or action sequence or the position of a larva on the plate in a fully automated, high-throughput manner.

In the following chapters, I will take advantage of this system to investigate the neural circuits underlying operant conditioning.

4 Operant Conditioning of Bend Direction

4.1 Introduction

In the previous chapter, I have introduced a novel multi-animal tracker for *Drosophila* larvae with real-time behaviour detection and closed-loop stimulation. In this chapter, I will use this set-up to introduce a first operant conditioning paradigm in the larva by pairing an action with optogenetic activation of neurons which are presumed to signal reward.

Perhaps the largest challenge in designing such a paradigm is to choose a suitable set of reward neurons. Since it has been an open question whether *Drosophila* larvae are capable of operant conditioning, there is no information available about the underlying neural circuits. It is hence unclear which neurons would need to be activated to convey a reinforcement signal sufficient to induce this type of learning.

Across the animal kingdom, it has been observed that biogenic amines can provide such a learning signal (Fee and Goldberg, 2011; Giurfa, 2006; Hawkins and Byrne, 2015; Meneses and Liy-Salmeron, 2012). In flies, the PAM cluster dopaminergic neurons, which innervate the mushroom body, are both necessary and sufficient to signal reward in classical conditioning (Cognigni et al., 2018; Liu et al., 2012; Rohwedder et al., 2016; Vogt et al., 2014; Waddell, 2013). It would be conceivable that the reward circuits of classical and operant conditioning are shared. However, operant conditioning in adult flies does not require the mushroom body (Booker and Quinn, 1981; Colomb and Brembs, 2010, 2016; Wolf et al., 1998).

Therefore, I have decided to try to induce operant conditioning by using optogenetic stimulation of a rather broad set of dopaminergic and serotonergic neurons as a US. If valence signalling relevant for operant conditioning is mediated by one of these two

neurotransmitters, activation of this large set of neurons paired with behaviour should be sufficient to cause learning.

4.2 Results

I have expressed *UAS-CsChrimson* under the control of the *Ddc-Gal4* driver, which covers the majority of dopaminergic and serotonergic neurons in the CNS (Li et al., 2000; Sitaraman et al., 2008), including the PAM cluster neurons (Aso et al., 2012; Liu et al., 2012 for evidence in adult flies; Chapter 6 for evidence in larvae). Although the function of most of these neurons is unknown, *Ddc* neurons seem to collectively convey a positive net valence in at least some learning paradigms, since their activation can substitute for reward in olfactory conditioning in adult flies (Aso et al., 2012; Liu et al., 2012; Shyu et al., 2017).

While the high-throughput closed-loop tracker introduced in Chapter 3 was still under development, I initially tested experimental conditions for operant conditioning in *Ddc-Gal4 x UAS-CsChrimson* larvae at low throughput using a single-larva closed-loop tracker (Schulze et al., 2015; Section 2.3). Here, I will introduce a paradigm for inducing a learned directional preference for bends, which I have developed using this single-larva tracker. The aim was to condition larvae to bend more often to one predefined side than to the other side. For simplicity, I will describe the experimental procedure where this predefined side was chosen to be the left, however, approximately 50% of the experimental animals were trained to develop a preference for bending towards the right.

For two three-minute training sessions, the larva received an optogenetic stimulus whenever a left bend was detected, for the entire duration of the behaviour. No stimulus was given when the larva was bending to the right or when it was in a straight body position. The two training sessions were separated by a three-minute break, in which the larva did not receive any optogenetic stimulus, regardless of behaviour. Larvae were not exposed to any stimulus before or after training (Fig. 4.1).

For each larva, I used two measures as a read-out for bend direction preference: i) the bend rate, measured as the absolute number of bends per minute performed towards each side, and ii) the probability for a given bend to be directed towards the stimulated side. This second measure is obtained by normalising the bend rate with the total number

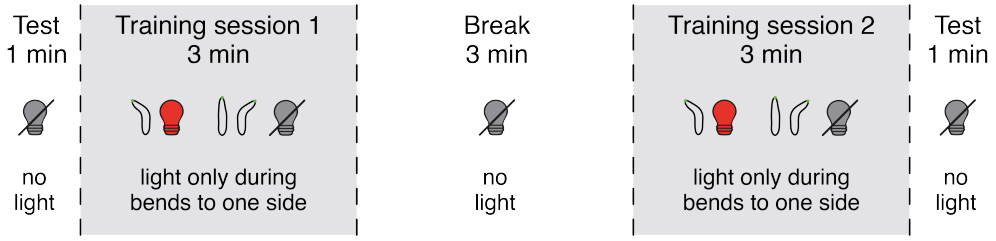

Figure 4.1: Experimental protocol for conditioning bend direction using the single-larva closed-loop tracker. The training protocol consists of one minute of test directly before training, two three-minute training sessions (highlighted in grey) interrupted by a three-minute break, and one minute of test immediately after training. Behaviours are depicted as larval contours (black) with head (green). During training, the larva receives an optogenetic stimulus (red light bulb) whenever it is bending to one predefined side (here depicted as the left for simplicity), and light is switched off during all other behaviours (grey light bulb).

of bends to both sides. Because there is variation in the overall bend rates across larvae, these two measures can yield different results at population level.

In the one-minute test directly prior to the beginning of the first training session, there was no difference in the rates of left and right bends. Bend direction preference was tested again in a one-minute time window following the end of the second training session. After training, larvae performed more bends towards the side which was paired with optogenetic stimulation during training than to the other side (Fig. 4.2a). Similarly, naïve larvae, prior to training, were equally as likely to bend to the side which would later be paired with *Ddc* neuron activation as they were to bend towards the other side. Following training, the probability of bending towards the previously stimulated side was significantly greater than 50% (Fig. 4.2b). No significant difference could be detected between the bend rates of larvae which received paired training compared to larvae which received uncorrelated training (two-sided Mann-Whitney *U* test; $p \geq 0.05$ for all comparisons).

To confirm that this preference for bends to the previously stimulated side after training is indeed due to the pairing of bends to one direction with light, I conducted a control experiment, which like the previous experiments consisted of two three-minute training sessions, with the difference that larvae received random stimulation during 50% of bends regardless of bend direction. There was neither a difference in absolute left and right bend rates, nor did larvae show a higher probability for choosing one of the two sides over the other in the one-minute test period after the end of the second training session (Fig. 4.2a, b).

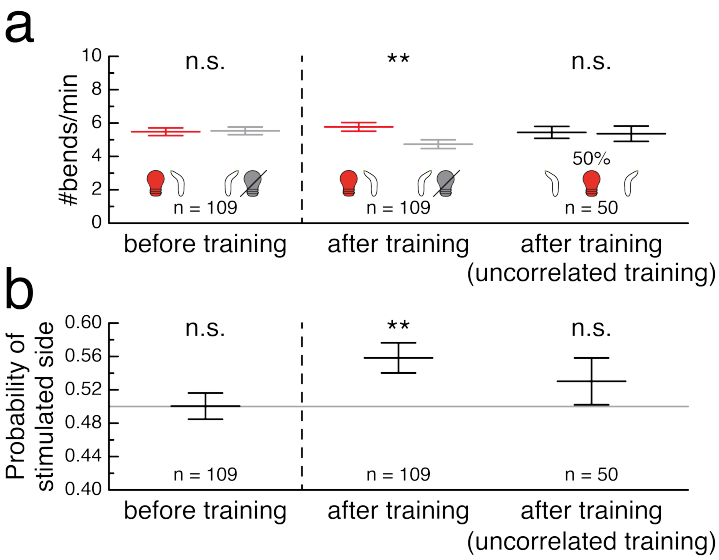

Figure 4.2: Single-larva operant conditioning of bend direction in *Ddc-Gal4 x UAS-CsChrimson* larvae. Experiments are performed using *Ddc-Gal4 x UAS-CsChrimson* larvae and the protocol described in Fig. 4.1. Data is shown for the test before training (left), the test after training (centre) and the test after training for control larvae receiving uncorrelated training with random stimulation during 50% of bends (right). **a.** The graph shows the bend rate in number of bends per minute split up by bend direction. The bend rate to the stimulated side (depicted as a left bend with a red light bulb for simplicity) is shown in red and the bend rate to the other side (depicted as a right bend with a grey light bulb for simplicity) is shown in grey. For larvae receiving random stimulation during 50% of bends, the bend rates to the left and right (black) are shown. **b.** The graph shows the probability that a given bend is directed towards the stimulated side (contingent training) or towards the left (uncorrelated training with random stimulation of 50% of bends). The grey line indicates equal probability of 0.5 for bends to either side. **a–b.** All data is shown as (mean $\pm$ s. e. m.). Statistical differences are tested with a two-sided Wilcoxon signed-rank test; n. s. $p \geq 0.05$ (not significant), ** $p < 0.01$.

These experiments indicate that larvae are capable of associating the direction in which they initiate a bend with a US, leading to learned modification of their future behaviour. Since this shift in behaviour was only observed when the CS, here bends to one predefined side, and the US, in this case an optogenetic light stimulus, were paired during training, it is due to operant conditioning. As pairing bends to one side with the US induced a learned preference for bends to this side, the optogenetic stimulus serves as a rewarding signal.

Upon completion of the high-throughput closed-loop tracker (Chapter 3), I have reproduced the paradigm described above using this novel set-up. High-throughput experiments presented in this chapter were kindly performed by Elise Croteau-Chonka. Design of the experimental conditions, implementation of the stimulus protocol as part of the tracker software and analysis of all data were performed by myself.

Due to the design of the high-throughput tracker, the agarose plate on which the larvae are freely behaving is significantly smaller than the one used in the single-larva tracker (see Chapter 2 for details). As a consequence, when using the experimental design shown in Fig. 4.1, the majority of larvae are located very close to the edge of the plate by the beginning of the second training session. Tracking of animals which touch the edge of the plate is often disrupted, such that the object is temporarily lost. Although these larvae can be detected again as new objects when they move back towards the centre of the plate, they do not receive an optogenetic stimulus while they are not being tracked. Therefore, a prolonged experiment with freely behaving larvae on a small agarose plate not only causes the sample size to shrink with increasing experiment time, but also affects the efficiency of training by decreasing the proportion of animals which are receiving the stimulus.

To circumvent this problem, the experiment was interrupted one minute after the end of each three-minute training session, and a brush was used to gently move all larvae back to the centre of the plate. The experiment was then restarted, and the larvae were given 30 s to recover before the beginning of the next training session (Fig. 4.3). Under these modified experimental conditions, no operant conditioning was observed after the end of the second training session (Fig. 4.4). It is possible that this is due to the disruptive process of moving the larvae. Therefore, I extended the conditioning procedure to four training sessions to give larvae more time to experience the pairing of the optogenetic stimulus with the behaviour and to potentially compensate for the disruption (Fig. 4.3).

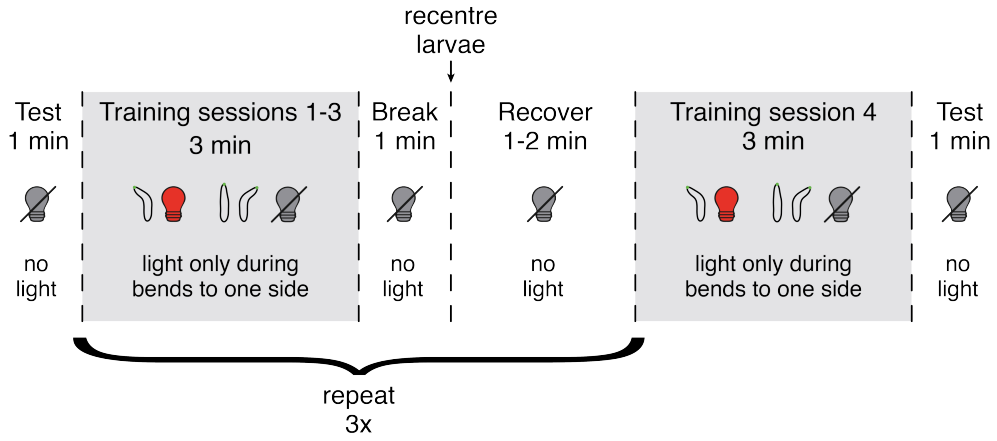

Figure 4.3: Experimental protocol for conditioning bend direction using the high-throughput closed-loop tracker. The training protocol consists of a one-minute test directly before training, four training sessions (highlighted in grey) a one-minute test immediately after the end of the last training session. Each training session lasts for three minutes. The first three training sessions are followed by one minute without stimulation, after which the experiment is stopped and the larvae are placed back to the centre of the plate. Afterwards, they are allowed a period of one to two minutes for recovery before the next training session begins. Behaviours are depicted as larval contours (black) with head (green). During training, the larva receives an optogenetic stimulus (red light bulb) whenever it is bending to one predefined side (here depicted as the left for simplicity), and light is switched off during all other behaviours (grey light bulb).

In the one-minute test period following the fourth training session, larvae indeed showed a preference for bends towards the side which had been paired with *Ddc* neuron activation during training. No directional preference was observed in naïve animals or in animals which had received random stimulation during 50% of all left and right bends, regardless of their direction (Fig. 4.4). The operant conditioning effect observed on the single-larva tracker could hence be replicated using the high-throughput set-up.

In the training procedure described in this chapter, *Ddc-Gal4 x UAS-CsChrimson* larvae receive a red light stimulus paired with the conditioned behaviour. The red light optogenetically activates *Ddc* neurons, which express *CsChrimson*. In order to be able to conclude that this activation of *Ddc* neurons and not purely the red light has served as the rewarding US which induced learning, a control is needed in which larvae of identical genotype receive a red light stimulus paired with behaviour which does not activate any neurons.

The light-dependent activation of neurons using *CsChrimson* requires a cofactor, retinal, which is supplemented to the food during development (Klapoetke et al., 2014; Section 2.1). A control group of larvae which were raised on food without retinal showed

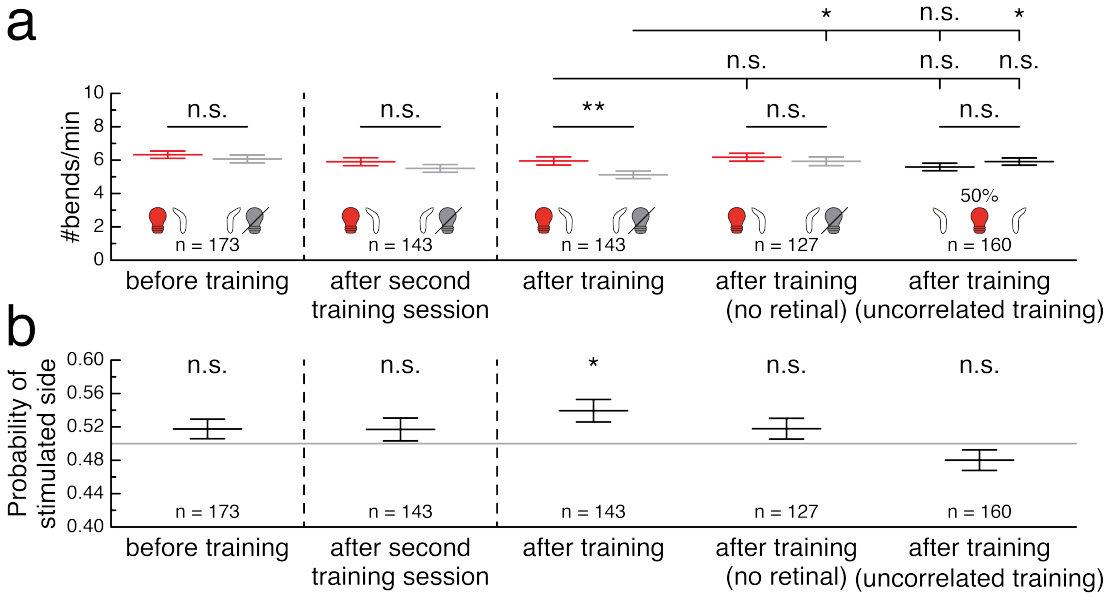

Figure 4.4: High-throughput operant conditioning of bend direction in *Ddc-Gal4 x UAS-CsChrimson* larvae. Experiments are performed using *Ddc-Gal4 x UAS-CsChrimson* larvae and the protocol described in Fig. 4.3. Data is shown for the test before training (left), the one-minute period following the second training session (second from the left) and the test after training (centre), the test after training for control larvae which receive retinal through their food (second from the right) and the test after training for control larvae receiving uncorrelated training with random stimulation during 50% of bends (right). **a.** The graph shows the bend rate in number of bends per minute split up by bend direction. The bend rate to the stimulated side (depicted as a left bend with a red light bulb for simplicity) is shown in red and the bend rate to the other side (depicted as a right bend with a grey light bulb for simplicity) is shown in grey. For larvae receiving random stimulation during 50% of bends, the bend rates to the left and right (black) are shown. **b.** The graph shows the probability that a given bend is directed towards the stimulated side (contingent training) or towards the left (uncorrelated training with random stimulation of 50% of bends). The grey line indicates equal probability of 0.5 for bends to either side. **a–b.** All data is shown as (mean $\pm$ s. e. m.). Statistical differences within a group are tested with a two-sided Wilcoxon signed-rank test; statistical differences between two groups are tested with a two-sided Mann-Whitney *U* test; n. s. $p \geq 0.05$ (not significant), * $p < 0.05$, ** $p < 0.01$.

the same absolute rate and probability for bends to the stimulated side and bends to the other side throughout the experiment, suggesting that the US which triggered a learned directional preference for bends was indeed the activation of *Ddc* neurons and not the red light alone (Fig. 4.4). The collective activation of all *Ddc* neurons therefore serves as the reward in this paradigm.

Next, I assessed whether there were differences between the bend rates of the three groups after training. No change in the bend rate towards the stimulated side could be detected for larvae which received paired training compared to larvae which did not receive retinal. The bend rate towards the stimulated side of larvae which received paired training was also indistinguishable from the bend rates towards the left and right of larvae which received uncorrelated training. However, the bend rate towards the unstimulated side of larvae which received paired training was significantly reduced compared to larvae which did not receive retinal and compared to the right bend rate of larvae which received uncorrelated training (Fig. 4.4a).

4.3 Conclusions

In this chapter, I have successfully trained larvae to associate bend direction with a US, using both a single-larva and a multi-larva experimental set-up. After pairing of *Ddc* neuron activation with bends to one predefined side, larvae showed a significant learned preference for bending towards this side, even though no stimulus was given during test. This provides, to my knowledge, the first evidence that *Drosophila* larvae are capable of operant conditioning.

Furthermore, I have shown that activation of *Ddc* neurons serves as a rewarding US during this learning process. *Ddc-Gal4* drives expression in dopaminergic and serotonergic neurons (Li et al., 2000; Sitaraman et al., 2008), therefore it can be concluded that a set of neurons expressing one or both of these neurotransmitters is involved in memory formation under the given experimental conditions.

In the high-throughput paradigm, larvae which received paired training show a decreased bend rate towards the unstimulated side, but no change of bend rate toward the stimulated side compared to the control groups. This brings up the question whether larvae learn to prefer the side which is paired with the rewarding US, or rather to avoid

the side without the stimulus. With an increased sample size, one could test whether there is also a currently undetectable change in the bend rate towards the stimulated side. The smaller sample size could also explain why the decreased in bend rate towards the unstimulated side is not currently observed in the single-larva paradigm.

The conditioned behaviour in the presented paradigm was the direction of bends. In Chapter 5, I will pair other types of behaviour with activation of *Ddc* neurons and test whether operant conditioning can be induced. The aim of Chapter 6 will be to pinpoint the observed operant conditioning effect to a smaller subset of neurons. *Ddc* is broadly expressed across the CNS, including neurons in the brain, the subesophageal zone (SEZ) and the ventral nerve cord (VNC). Using genetic methods, I will express *CsChrimson* in only the brain and SEZ subset of *Ddc* neurons and test whether operant conditioning can be induced. I will then investigate the role of the mushroom body in this type of learning.

5 Operant Conditioning of Other Behaviours

5.1 Introduction

In the previous chapter, I have introduced a first operant conditioning paradigm, in which I have trained larvae to associate bends to one side, but not the other side, with the activation of *Ddc* neurons, which served as a rewarding US. As a result, larvae developed a preference for bending towards the side which was associated with the stimulus. In this chapter, I will test whether the same US can be used to reinforce other behaviour patterns. I will train larvae by pairing optogenetic activation of *Ddc* neurons with actions such as bending and forward crawling, with the aim to increase the spontaneous rate of these behaviours after training.

5.2 Results

First, I tested whether the frequency of bends could be increased by pairing bends to both sides with optogenetic activation of *Ddc* neurons. I trained *Ddc-Gal4 x UAS-CsChrimson* larvae using the high-throughput tracker. The conditioning procedure was similar to the one of the bend direction paradigm introduced in Chapter 4: the experiment consisted of an initial one-minute test period, four three-minute training sessions and a final one-minute test period. The first three training sessions were each followed by a one-minute break, after which the experiment was stopped and all larvae were gently placed back to the centre of the plate with a brush. The experiment was then restarted, and the larvae were given 30 s to recover before the beginning of the next training session. During training, all larvae for which a bend was detected received an optogenetic stimulus. The light stimulus stayed on for the entire duration of the bend and was switched off during other behaviours. No stimulus was given outside training (Fig. 5.1).

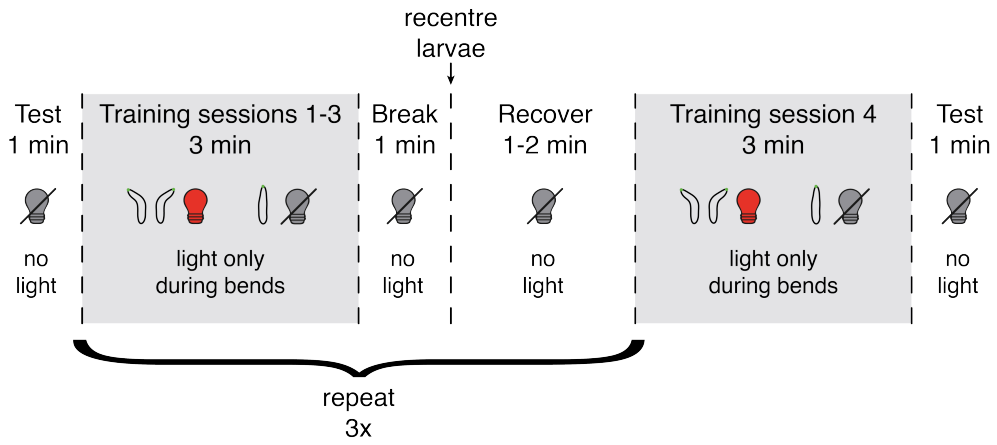

Figure 5.1: Experimental protocol for reinforcing bends using the high-throughput closed-loop tracker. The training protocol consists of a one-minute test directly before training, four training sessions (highlighted in grey) a one-minute test immediately after the end of the last training session. Each training session lasts for three minutes. The first three training sessions are followed by one minute without stimulation, after which the experiment is stopped and the larvae are placed back to the centre of the plate. Afterwards, they are allowed a period of one to two minutes for recovery before the next training session begins. Behaviours are depicted as larval contours (black) with head (green). During training, the larva receives an optogenetic stimulus (red light bulb) whenever it is bending, and light is switched off when it is in a straight body position (grey light bulb).

The bend rate of larvae which received contingent stimulation during bends as described above was compared to a yoked control group, which received an equivalent stimulus pattern during training, but uncorrelated from behaviour. No difference between the two groups was detected in the two test periods before and after training (Fig. 5.2a). A few other measures of behaviour, such as bend duration (Fig. 5.2b) and the number of forward peristaltic waves over time (Fig. 5.2c) were compared as well, but no difference could be found. These results suggest that no operant conditioning has occurred in this paradigm.

In a second set of experiments, I assessed whether larvae could be trained to associate forward crawling with reward. I used a training procedure analogous to the one described above, in which larvae received optogenetic activation of *Ddc* neurons paired with crawls during training. To ensure that only true forward crawls were rewarded, I restricted stimulation to those crawls which did not coincide with a bend (Fig. 5.3).

I compared several behaviour measures of larvae which underwent contingent stimulation during forward crawls as described above to a yoked control, which received stimulation uncorrelated from behaviour. First, I analysed frequency and duration of for-

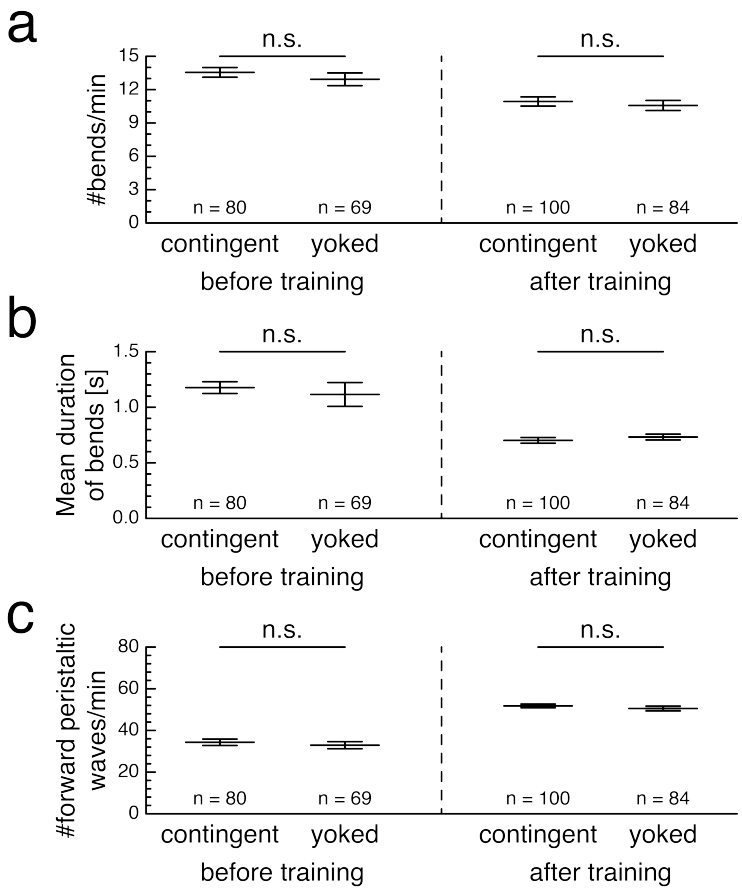

Figure 5.2: Analysis of bend rate using the high-throughput paradigm for reinforcing bends in *Ddc-Gal4 x UAS-CsChrimson* larvae. Experiments are performed using *Ddc-Gal4 x UAS-CsChrimson* larvae and the protocol described in Fig. 5.1. Several characteristics of behaviour are shown for the tests before (left) and after (right) training. A group of larvae receiving optogenetic stimulation correlated with bends during training (contingent) is compared to a control group receiving an equivalent stimulus train, but uncorrelated from behaviour (yoked). **a.** Bend rate in number of bends per minute, **b.** average duration of all bends which occurred during the test period for a given larva in seconds, **c.** number of forward peristaltic waves per minute. All data is shown as (mean $\pm$ s. e. m.). Statistical differences between the contingent group and the yoked group are tested with a two-sided Mann-Whitney *U* test; n. s. $p \geq 0.05$ (not significant).

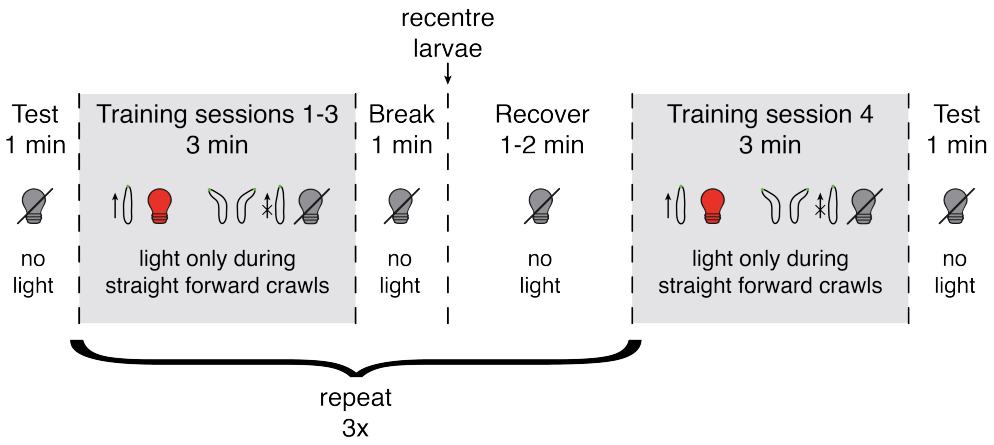

Figure 5.3: Experimental protocol for reinforcing forward crawls using the high-throughput closed-loop tracker. The training protocol consists of a one-minute test directly before training, four training sessions (highlighted in grey) a one-minute test immediately after the end of the last training session. Each training session lasts for three minutes. The first three training sessions are followed by one minute without stimulation, after which the experiment is stopped and the larvae are placed back to the centre of the plate. Afterwards, they are allowed a period of one to two minutes for recovery before the next training session begins. Behaviours are depicted as larval contours (black) with head (green). During training, the larva receives an optogenetic stimulus (red light bulb) whenever it is crawling forward in a straight body position, and light is switched off when it is bending or not crawling forward (grey light bulb).

ward crawls during which a larva was not bending. Before training, there was no difference between the contingent group and the yoked control. However, the number of forward crawls initiated during the test period after training was significantly higher in contingent group animals (Fig. 5.4a). On average, the duration of individual forward crawl periods was shorter than for the yoked control (Fig. 5.4b).

Since the number of forward crawl periods over time had increased, while the average duration of such events had decreased in animals of the contingent group, I analysed

Figure 5.4 *(facing page)*: Operant conditioning using the high-throughput paradigm for reinforcing forward crawls in *Ddc-Gal4 x UAS-CsChrimson* larvae. Experiments are performed using *Ddc-Gal4 x UAS-CsChrimson* larvae and the protocol described in Fig. 5.3. Several characteristics of behaviour are shown for the tests before (left) and after (right) training. A group of larvae receiving optogenetic stimulation correlated with bends during training (contingent) is compared to a control group receiving an equivalent stimulus train, but uncorrelated from behaviour (yoked). **a.** Forward crawl rate in number of forward crawl periods which did not coincide with bending per minute, **b.** average duration of all forward crawl periods which did not coincide with bending and which occurred during the test period for a given larva in seconds, **c.** fraction of time spent crawling forward while not bending, **d.** number of forward peristaltic waves per minute, **e.** bend rate in number of bends per minute, **f.** velocity in mm/s as defined by the feature `v_norm_filtered`. All data is shown as (mean $\pm$ s. e. m.). Statistical differences between the contingent group and the yoked group are tested with a two-sided Mann-Whitney *U* test; n. s. $p \geq 0.05$ (not significant), ** $p < 0.01$, *** $p < 0.001$.

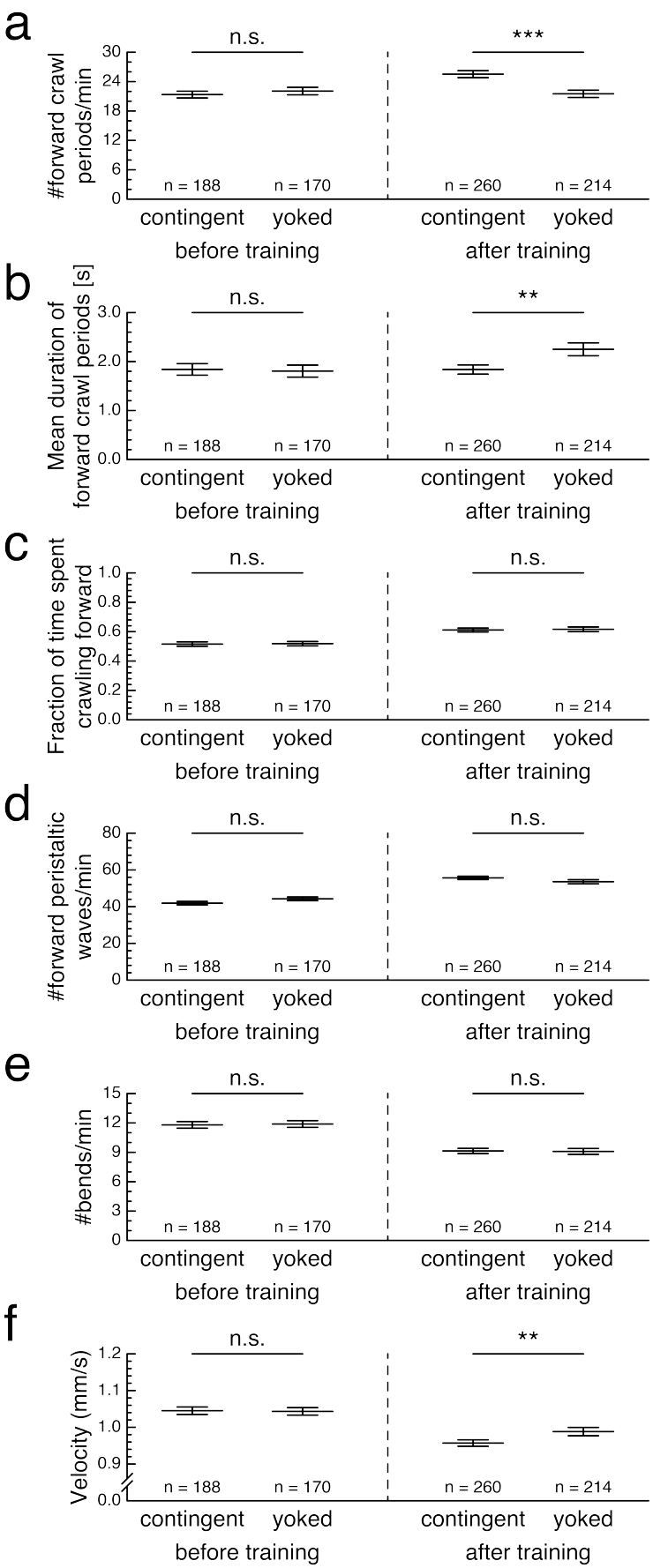
a
n.s.
***
#forward crawl periods/min
30
24
18
12
6
0
n = 188
n = 170
n = 260
n = 214
contingent
yoked
contingent
yoked
before training
after training
b
n.s.
**
Mean duration of forward crawl periods [s]
3.0
2.0
1.0
0.0
n = 188
n = 170
n = 260
n = 214
contingent
yoked
contingent
yoked
before training
after training
c
n.s.
n.s.
Fraction of time spent crawling forward
1.0
0.8
0.6
0.4
0.2
0.0
n = 188
n = 170
n = 260
n = 214
contingent
yoked
contingent
yoked
before training
after training
d
n.s.
n.s.
#forward peristaltic waves/min
80
60
40
20
0
n = 188
n = 170
n = 260
n = 214
contingent
yoked
contingent
yoked
before training
after training
e
n.s.
n.s.
#bends/min
15
12
9
6
3
0
n = 188
n = 170
n = 260
n = 214
contingent
yoked
contingent
yoked
before training
after training
f
n.s.
**
Velocity (mm/s)
1.2
1.1
1.0
0.9
0.0
n = 188
n = 170
n = 260
n = 214
contingent
yoked
contingent
yoked
before training
after training

whether a shift in the overall fraction of time which a larva spent in a forward crawling state while not bending had occurred. No such difference could be detected (Fig. 5.4c). Furthermore, no difference in the number of forward peristaltic waves over time was observed (Fig. 5.4d).

The increase in the forward crawl rate could potentially be explained by an increased number of bends, since forward crawling and bending are the most frequent behaviours in larvae. If a larvae stops more often to bend, then the number of times where it initiates a new forward crawl movement will also increase. On average, these forward crawl periods would become shorter. Therefore, I assessed whether there a change in the bend rate occurred. No difference in the frequency of bends between the two groups could be detected both before and after training (Fig. 5.4e).

An alternative explanation for an increased number of detected forward crawls, each with a shorter duration, would be that the larvae are stopping more often or are generally moving at a slower speed after training. In order for a forward crawl period to be detected, the temporally smoothed velocity of the tail needs to exceed a certain threshold. If a larva is moving slowly, several short crawling events will be detected instead of a single, longer crawling period. Indeed, the average velocity as defined by the feature `v_norm_filtered` (see Section 3.2.5) in the one-minute test period after training was significantly reduced in larvae which had received contingent training compared to the control group (Fig. 5.4f).

Since differences between the contingent group and the yoked control could be detected for several behaviour characteristics after training, a learned shift in behaviour has occurred, which is due to the pairing of the US with forward crawls. Therefore, the results shown here provide evidence of operant conditioning.

5.3 Conclusions

In this chapter, I have explored whether larvae can form operant memory after pairing bends or forward crawls with *Ddc* neuron activation. While no change in behaviour was observed in the bend paradigm, there was evidence for strong operant conditioning in the forward crawl paradigm. Paired training resulted in an increased forward crawl rate, a decreased duration of forward crawl periods and a slower velocity of movement.

The results indicate that operant conditioning in *Drosophila* larvae is not limited to the bend direction paradigm but can also occur when the US is paired with other behaviours such as forward crawls. However, I also show that not all behaviours can be reinforced through pairing with optogenetic activation of *Ddc* neurons, since the bend rate during test does not increase when bends to both sides are paired with the US.

The expression pattern of *Ddc-Gal4* is broadly expressed in dopaminergic and serotonergic neurons across the CNS (Li et al., 2000; Lundell and Hirsh, 1994). In the following chapters, I will aim to narrow down which of these neurons are involved in operant memory formation. Both the bend direction paradigm and the forward crawl paradigm would be suited to investigate which group of neurons is sufficient to convey valence for operant conditioning.

However, it is hard to interpret what the larvae have learned in the forward crawl paradigm: pairing forward crawls with *Ddc* neuron activation resulted in an increased number of individual forward crawling events. However, there is no difference in the total time spent in a forward crawling state during post-training test between the contingent group and the yoked control. The observed change in behaviour would therefore not enable the larvae to maximise cumulative reward over time. Furthermore, it is unclear why larvae from the contingent group learned to move at a lower velocity than the yoked control. This makes it difficult to understand the immediate effect of optogenetic activation of *Ddc* neurons paired with forward crawls.

Therefore, I will focus on the bend direction paradigm to better understand the neural mechanisms underlying operant conditioning.

6 The Role of the Brain and the Mushroom Body in Operant Conditioning

6.1 Introduction

In Chapters 4 and 5, I have shown that activation of *Ddc* neurons is sufficient to act as a US for operant conditioning. *Ddc* is expressed in a wide range of dopaminergic and serotonergic neurons in the brain, the SEZ and the VNC (Lundell and Hirsh, 1994). It is unclear which of these neurons mediate the observed operant conditioning effect, and whether two or more distinct subsets of *Ddc* neurons need to interact in order for memory to be formed.

In this chapter, I will show that *Ddc-Gal4* expression in the larval brain contains the PAM cluster dopaminergic neurons, which innervate the mushroom body and are both necessary and sufficient to signal reward in classical conditioning (Liu et al., 2012; Rohwedder et al., 2016; Vogt et al., 2014). While previous studies in adult flies suggest that the mushroom body is dispensable for operant conditioning (Booker and Quinn, 1981; Colomb and Brembs, 2010, 2016; Wolf et al., 1998), it is unclear to what extent this is the case in larvae. Therefore, I will then focus on the bend direction paradigm introduced in Chapter 4 to investigate whether i) the *Ddc* neurons of the brain and the SEZ, and ii) the PAM cluster dopaminergic neurons innervating the mushroom body are sufficient to induce operant conditioning.

6.2 Results

In order to get an overview of which neurons may be mediating the formation of an operant memory, I have analysed the *Ddc* expression pattern in *Ddc-Gal4 x UAS-CsChrimson*

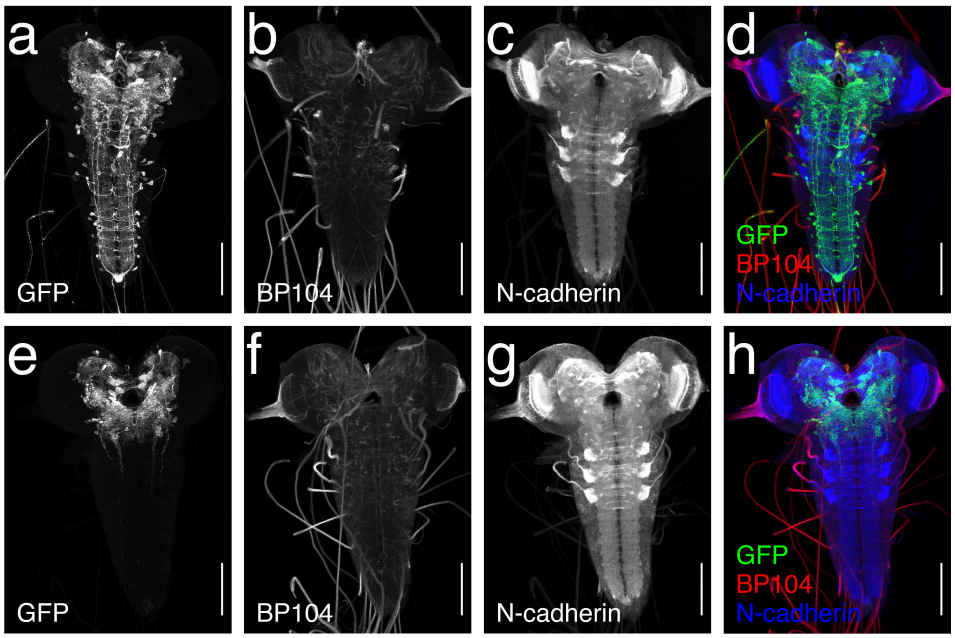

Figure 6.1: Expression pattern of *Ddc-Gal4* without and with restriction by *tsh-Gal80*. Confocal images obtained after immunohistochemical staining against the *mVenus* tag of *CsChrimson* (**a**, **e**; green in **d** and **h**), BP104 (**b**, **f**; red in **d** and **h**) and N-cadherin (**c**, **g**; blue in **d** and **h**). **a–d.** *Ddc-Gal4 x UAS-CsChrimson* larvae, **e–h.** *Ddc-Gal4 x UAS-CsChrimson; tsh-LexA, LexAop-Gal80* larvae. Plan-Apochromat 20x objective, resolution: 592 x 800 pixels, scale bar: 100 µm. Image courtesy of the HHMI Janelia FlyLight team.

larvae. *CsChrimson* contains an *mVenus* tag, which can be targeted by a GFP antibody (Klapoetke et al., 2014). Dissections, stainings and confocal imaging were performed by the HHMI Janelia FlyLight team.

I manually counted the cell bodies in the image stacks and found more than 200 GFP-positive neurons, located in the brain, the SEZ and the VNC ($n = 2$, Fig. 6.1a–d). The expression pattern includes the dopaminergic neurons of the PAM cluster, which innervate the mushroom body (Fig. 6.1a, d). This confirms that *Ddc-Gal4* is indeed driving broad expression across the CNS (Li et al., 2000; Lundell and Hirsh, 1994). Since it is likely that not all *Ddc* neurons are involved in the operant learning process, I investigated whether smaller subsets of neurons contained in the *Ddc-Gal4* expression pattern can sufficiently act as a US in the bend direction paradigm.

GAL80 expression under control of the *tsh* promoter suppresses the expression of GAL4 in the VNC, but not in the brain or in the SEZ (Clyne and Miesenböck, 2008; Fushiki et al., 2016; Heckscher et al., 2015). Indeed, no GFP-positive neurons were found in the VNC of *Ddc-Gal4 x UAS-CsChrimson; tsh-LexA, LexAop-Gal80* larvae ($n = 6$, Fig. 6.1e–h).

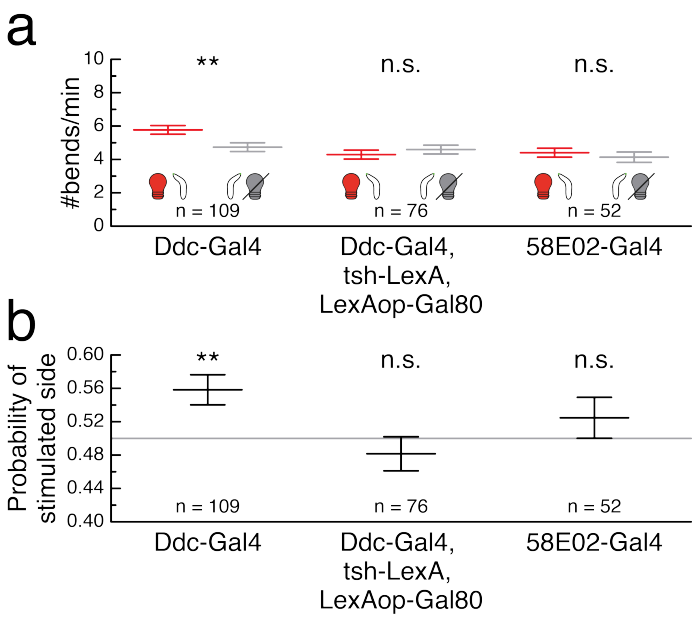

Figure 6.2: Single-larva operant conditioning of bend direction with restriction of *CsChrimson* expression to subsets of the *Ddc-Gal4* expression pattern. Experiments are performed using the protocol described in Fig. 4.1. All larvae express *UAS-CsChrimson* under control of the specified driver. Data is shown for the test after training. Data from *Ddc-Gal4 x UAS-CsChrimson* larvae is replotted from Fig. 4.2. **a.** The graph shows the bend rate in number of bends per minute split up by bend direction. The bend rate to the stimulated side (depicted as a left bend with a red light bulb for simplicity) is shown in red and the bend rate to the other side (depicted as a right bend with a grey light bulb for simplicity) is shown in grey. **b.** The graph shows the probability that a given bend is directed towards the stimulated side. The grey line indicates equal probability of 0.5 for bends to either side. **a–b.** All data is shown as (mean $\pm$ s. e. m.). Statistical differences are tested with a two-sided Wilcoxon signed-rank test; n. s. $p \geq 0.05$ (not significant), ** $p < 0.01$.

Furthermore, there were no GFP-positive neurons in the brain or the SEZ which could be consistently identified in *Ddc-Gal4 x UAS-CsChrimson* larvae, but not in *Ddc-Gal4 x UAS-CsChrimson; tsh-LexA, LexAop-Gal80* larvae (each $n = 3$), indicating that brain and SEZ expression indeed remained largely unaffected (Fig. 6.1).

To test whether the *Ddc* neurons of the brain and the SEZ are sufficient to induce a directional preference for bends to one, but not the other side, I trained *Ddc-Gal4 x UAS-CsChrimson; tsh-LexA, LexAop-Gal80* larvae using the single-larva closed-loop tracker and the training protocol developed in Chapter 4 (Fig. 4.1). Contrary to the result obtained with *Ddc-Gal4 x UAS-CsChrimson* larvae, in the one-minute test after training *Ddc-Gal4 x UAS-CsChrimson; tsh-LexA, LexAop-Gal80* larvae were equally as likely to bend towards the side where they had received the optogenetic stimulus during training as they were to bend towards the other side (Fig. 6.2). This indicates that activation of

the brain and SEZ subset of *Ddc* neurons is not sufficient to act as a rewarding US in this operant conditioning paradigm. Therefore, the VNC subset of *Ddc* neurons must play a role in memory formation.

Next, I assessed the role of a group of neurons innervating the mushroom body in operant conditioning. *58E02-Gal4* drives expression in the majority of PAM cluster dopaminergic neurons (Rohwedder et al., 2016). *58E02-Gal4 x UAS-CsChrimson* larvae did not develop any directional preference for bend following training (Fig. 6.2), indicating that activation of the dopaminergic reward neurons innervating the mushroom body is not sufficient to induce operant conditioning. Since the mushroom body is located in the brain, this is consistent with the observation that *Ddc* neurons of the VNC are necessary to induce the observed bend direction preference.

These experiments were kindly repeated by Elise Croteau-Chonka using the high-throughput paradigm (Fig. 4.3). Again, neither optogenetic stimulation of the brain and SEZ subset of *Ddc* neurons nor activation of the PAM cluster dopaminergic neurons paired with bends to one predefined side was sufficient to induce a learned preference for bends to this side (Fig. 6.3). Together, these results suggest that operant conditioning of bend direction cannot be induced by exclusive activity of the PAM cluster neurons innervating the mushroom body, as is the case for classical conditioning, but that it instead requires the dopaminergic or serotonergic neurons of the VNC. At this point, it remains unclear whether *Ddc* neurons in the VNC are sufficient to serve as a US or whether combined activity with a group of neurons in the brain or SEZ is needed.

6.3 Conclusions

Larvae can be operantly conditioned to develop a directional preference for bends using activation of *Ddc* neurons as a US. Here, I have shown that this operant conditioning effect is lost when the optogenetic stimulation is restricted to the brain and SEZ subsets of *Ddc* neurons. This indicates that dopaminergic or serotonergic neurons in the VNC are necessary for the formation of a bend direction preference. However, it cannot be concluded that they are sufficient, since it is possible that two or more distinct groups of *Ddc* neurons need to be collectively activated during bends to the reinforced side in order for a memory to be formed.

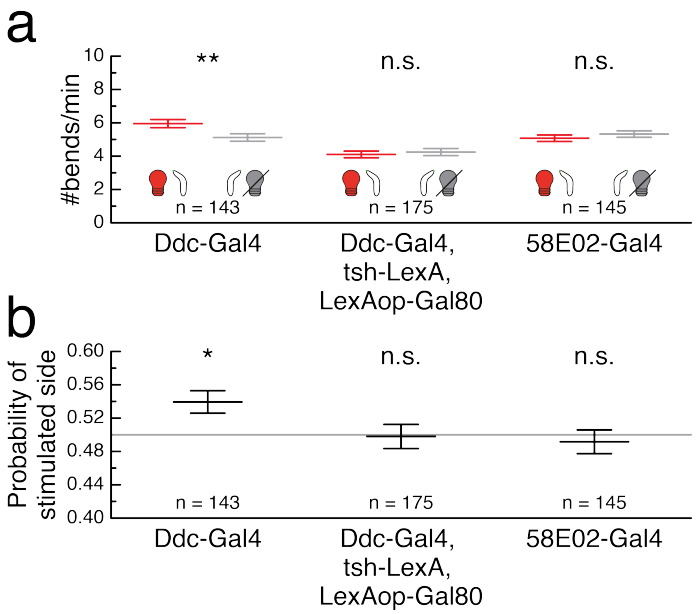

Figure 6.3: High-throughput operant conditioning of bend direction with restriction of *CsChrimson* expression to subsets of the *Ddc-Gal4* expression pattern. Experiments are performed using the protocol described in Fig. 4.3. All larvae express *UAS-CsChrimson* under control of the specified driver. Data is shown for the test after training. Data from *Ddc-Gal4 x UAS-CsChrimson* larvae is replotted from Fig. 4.4. **a.** The graph shows the bend rate in number of bends per minute split up by bend direction. The bend rate to the stimulated side (depicted as a left bend with a red light bulb for simplicity) is shown in red and the bend rate to the other side (depicted as a right bend with a grey light bulb for simplicity) is shown in grey. **b.** The graph shows the probability that a given bend is directed towards the stimulated side. The grey line indicates equal probability of 0.5 for bends to either side. **a–b.** All data is shown as (mean $\pm$ s. e. m.). Statistical differences are tested with a two-sided Wilcoxon signed-rank test; n. s. $p \geq 0.05$ (not significant), * $p < 0.05$, ** $p < 0.01$.

The dopaminergic neurons of the PAM cluster are *Ddc*-positive neurons located in the brain (Fig. 6.1a, d). Given the finding that the brain and SEZ *Ddc* neurons are not sufficient to induce operant conditioning, it is not surprising that activation of the PAM cluster neurons alone could not act as a rewarding US in this paradigm. While it is unclear whether the PAM cluster neurons are involved in the memory formation process by interacting with other *Ddc* neurons, the results presented here further support the idea that operant conditioning in *Drosophila* may not be mediated by the mushroom body.

7 Neural Circuits of Reward and Punishment

7.1 Introduction

In Chapter 4, I have shown for the first time that *Drosophila* larvae are capable of operant conditioning. This experimental paradigm was using optogenetic activation of neurons under control of the *Ddc-Gal4* driver as a US. Since the *Ddc-Gal4* expression pattern is very broad, including more than 200 dopaminergic and serotonergic neurons in the brain, the SEZ and the VNC (Li et al., 2000; Lundell and Hirsh, 1994; Sitaraman et al., 2008; Fig. 6.1a–d), I have used activation of smaller subsets of *Ddc* neurons as a US for operant conditioning in Chapter 6 to narrow down which neurons are involved in memory formation.

The PAM cluster dopaminergic neurons have been shown to play an important role in classical conditioning: when paired with an odour, activation of these neurons is sufficient to induce strong appetitive olfactory memory. On the other hand, inhibition of these neurons impairs the formation of appetitive olfactory memory of an odour which is paired with natural sugar, indicating that they are also necessary for olfactory conditioning (Liu et al., 2012; Rohwedder et al., 2016; Vogt et al., 2014).

I have found that activation of the PAM cluster neurons is not sufficient to serve as a US for operant conditioning. This result is remarkable in two ways. First, it shows that the neural circuits signalling reward for operant conditioning differ from those that mediate classical conditioning. Second, it further supports the idea that operant conditioning is independent of the mushroom body.

Little is known about the neural circuits which signal reward or punishment relevant for associative learning outside the mushroom body. While it is generally accepted that natural sugar can serve as a reward for olfactory conditioning (Apostolopoulou et al., 2013;

Honjo and Furukubo-Tokunaga, 2005; Rohwedder et al., 2012; Schipanski et al., 2008; Schleyer et al., 2015; Weiglein et al., 2019), it has to my knowledge not been attempted in the larva to deliver the US in form of activation of gustatory neurons. In this chapter, I will present the results of an olfactory conditioning screen conducted to identify driver lines for neurons conveying positive or negative valence in a learning context. Because I was ultimately interested in comparing neurons that could convey positive or negative valence in classical and operant conditioning paradigms, I started by performing a classical conditioning screen for their potential to act as a US. In Chapter 8, I will test whether activation of the valence-conveying neurons identified in this olfactory conditioning screen is sufficient to substitute for reward or punishment in the operant bend direction paradigm presented in Chapter 4.

7.2 Results

In the initial screen, I have crossed 26 GAL4 lines to *UAS-CsChrimson* and tested whether pairing of optogenetic activation with an odour could induce olfactory memory (Section 2.5). Learning scores were compared to a negative control, w^{1118} *x UAS-CsChrimson*, which does not contain any GAL4 and did not exhibit a learning phenotype (Fig. 7.1). *58E02-Gal4*, which drives expression in the PAM cluster dopaminergic neurons (Rohwedder et al., 2016), was used as a positive control. Consistent with previous results (Almeida-Carvalho et al., 2017; Eichler et al., 2017; Rohwedder et al., 2016), *58E02-Gal4 x UAS-CsChrimson* larvae showed strong appetitive olfactory learning with a significantly higher learning score than w^{1118} *x UAS-CsChrimson* larvae (Fig. 7.1).

All other examined driver lines were classified as labelling either sensory neurons (Table 7.1), gustatory interneurons (Table 7.2), neuropeptide F (NPF)-positive interneurons or aminergic interneurons (Table 7.3) based on previous data on function and expression pattern, and are known to be expressed in larvae unless indicated as adult-specific.

15 GAL4 lines labelling sensory neurons encoding a variety of chemosensory and thermosensory modalities in larval and adult *Drosophila* were tested. None of these lines showed significant appetitive or aversive olfactory learning compared to the negative control (Fig. 7.2). Similarly, no memory was induced using two lines driving expression

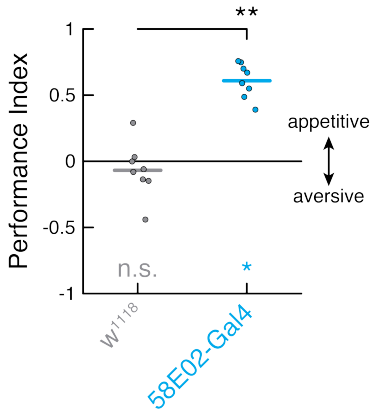

Figure 7.1: Negative and positive controls for classical conditioning. Performance indices after olfactory conditioning (raw data points and mean). *w^{1118} x UAS-CsChrimson* larvae are used as a negative control (grey, n = 8), *58E02-Gal4 x UAS-CsChrimson* larvae are used as a positive control (blue, n = 8). Statistical differences between the two groups are tested with a two-sided Mann-Whitney *U* test with Bonferroni correction; ** $p < 0.01/26$. Significances compared to zero were tested with a two-sided Wilcoxon signed-rank test with Bonferroni correction; n. s. $p \geq 0.05/2$ (not significant), * $p < 0.05/2$.

in adult *Drosophila* sweet taste projection neurons, which process gustatory information downstream of sugar-sensing neurons (Kim et al., 2017b; Fig. 7.3).

Next, I tested a single line driving expression in peptidergic interneurons, the NPF neurons (Shen and Cai, 2001). These neurons can relay reward in olfactory conditioning in adult flies (Shao et al., 2017; Shohat-Ophir et al., 2012), and have been shown to be involved in reward signalling in the larva as well (Pu et al., 2018; Rohwedder et al., 2015; Wang et al., 2013). However, in an experiment using larvae performed by Rohwedder et al. (2015), optogenetic activation of NPF neurons paired with an odour did not result in memory formation. Consistently, pairing optogenetic activation of NPF neurons with the odour did not induce learning in this screen (Fig. 7.4).

Finally, I screened a couple of lines specific to neurons expressing biogenic amines such as octopamine, dopamine or serotonin as neurotransmitters (Fig. 7.5). *Tdc2-Gal4 x UAS-CsChrimson* larvae, which express *CsChrimson* in octopaminergic neurons (Cole et al., 2005), did not show any learning phenotype. By contrast, pairing the odour with activation of neurons targeted by *Ddc-Gal4*, which covers most dopaminergic and serotonergic neurons (Li et al., 2000; Sitaraman et al., 2008), induced strong appetitive olfactory memory with a learning score comparable to the positive control ($p = 0.1304$, two-sided Mann-Whitney *U* test). This result is perhaps not surprising, since the *Ddc-Gal4*

Table 7.1: Driver lines targeting sensory neurons.

Line	Targeted neurons
C1-Gal4	terminal organ neuron C1 (bitter sensing) (Kim et al., 2016; Kwon et al., 2011)
C5-Gal4	terminal organ neuron C5 (Kwon et al., 2011)
C6-Gal4	terminal organ neuron C6 (CO_2 sensing) (Faucher et al., 2006; Jones et al., 2007; Kwon et al., 2007, 2011)
dp2-Gal4	pharyngeal gustatory receptor neuron DP2 (Choi et al., 2016; Kwon et al., 2011)
Gr2a-Gal4	adult *Drosophila* pharyngeal gustatory receptor neuron (high salt avoidance) (Kim et al., 2017a)
Gr5a-Gal4	adult *Drosophila* sugar-sensing neurons (Chyb et al., 2003; Dahanukar et al., 2001)
Gr43a-Gal4 (two lines)	sugar-sensing neurons (Mishra et al., 2013)
Gr64a-Gal4	adult *Drosophila* sugar-sensing neurons (Dahanukar et al., 2007; Jiao et al., 2007)
Gr64f-Gal4	adult *Drosophila* sugar-sensing neurons (Dahanukar et al., 2007)
Ir25a-Gal4	dorsal organ (cool avoidance) (Ni et al., 2016)
Ir76b-Gal4	terminal organ (amino acid sensing) (Croset et al., 2016; Ganguly et al., 2017)
Ir94e-Gal4	terminal organ (putative amino acid sensing) (Croset et al., 2016)
ppk11-Gal4	terminal organ (salt taste) (Liu et al., 2003)
ppk19-Gal4	terminal organ (salt taste) (Liu et al., 2003)

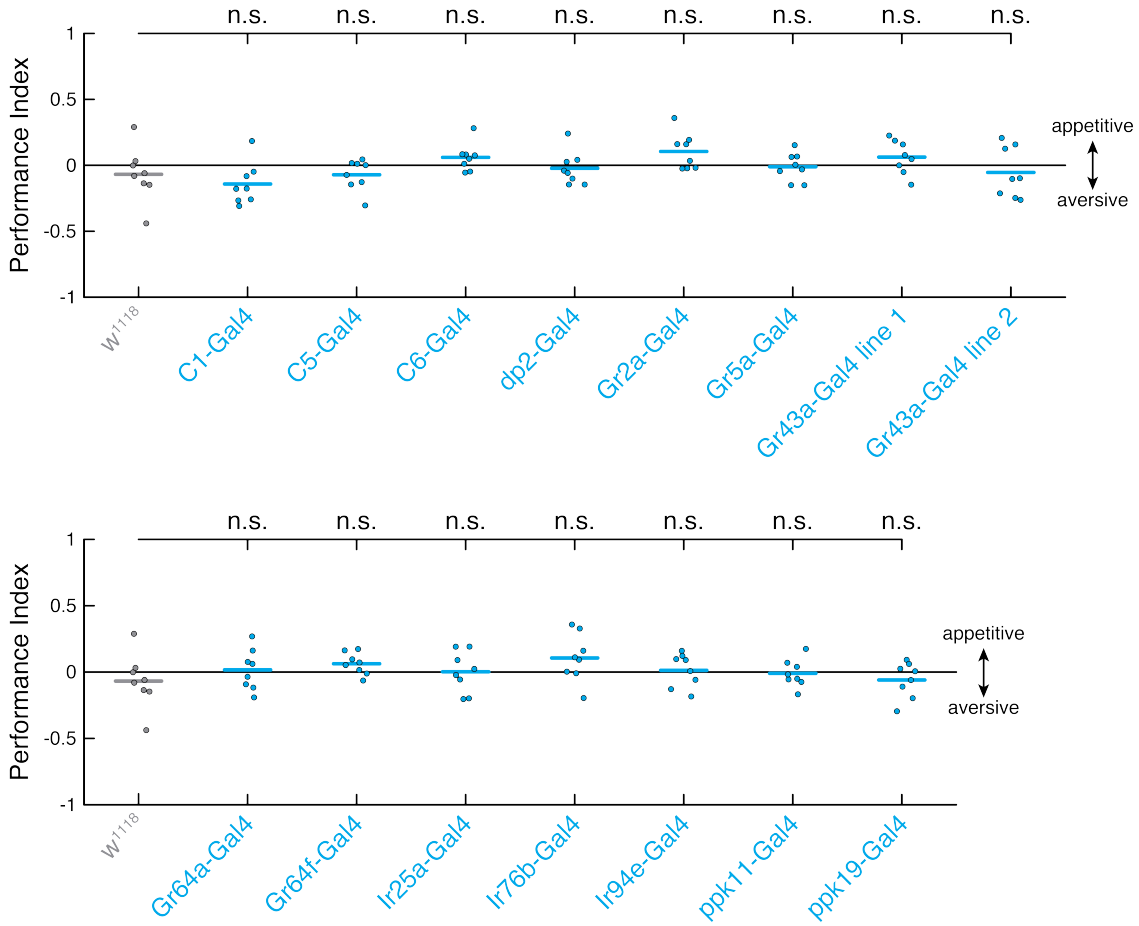

Figure 7.2: Classical conditioning by pairing activation of sensory neurons with an odour. Performance indices after olfactory conditioning (raw data points and mean). Larvae express *UAS-CsChrimson* under control of the specified driver (blue). w^{1118} *x UAS-CsChrimson* larvae are used as a negative control (grey). Statistical differences compared to the negative control are tested with a two-sided Mann-Whitney *U* test with Bonferroni correction; n = 8, n. s. $p \geq 0.05/26$ (not significant).

Table 7.2: Driver lines targeting gustatory interneurons.

Line	Targeted neurons
30A08-Gal4	adult *Drosophila* sweet taste projection neuron TPN1 (Kim et al., 2017b)
VT57358	adult *Drosophila* sweet taste projection neuron TPN2 (Kim et al., 2017b)

expression pattern includes the PAM cluster neurons (Chapter 6). To get a more detailed insight into which neurons contribute to this phenotype, I screened a small number of sparser driver lines which are specific to either dopaminergic or serotonergic neurons.

TH-Gal4 is a broad driver which covers most dopaminergic neurons, but not the PAM cluster neurons (Rohwedder et al., 2016). Consistent with previous studies (Schroll et al., 2006), *TH-Gal4 x UAS-CsChrimson* larvae exhibited significant aversive olfactory learning in this paradigm. This effect may be explained by punishment-signalling dopaminergic neurons which project to the vertical lobes of the mushroom body and are contained in the *TH-Gal4* expression pattern (Eschbach et al., 2019; Selcho et al., 2009). There is a lack of sparse driver lines targeting dopaminergic neurons which do not innervate the mushroom body in the larva. To assess the potential role of dopaminergic neurons in other brain regions, I tested *c346-Gal4*. In adult *Drosophila*, this line drives expression in the dopaminergic neurons of the PPM3 cluster, which innervate the central complex (Kong et al., 2010). However, the expression pattern in larvae has not been thoroughly studied. In this classical conditioning paradigm, no learning phenotype was observed using this line.

No learning phenotype was observed when expressing *CsChrimson* under control of eg^{Mz360}*-Gal4*. *eagle* (*eg*) is a differentiation factor of serotonergic neurons (Dittrich et al., 1997; Lundell and Hirsh, 1998), and eg^{Mz360}*-Gal4* has been reported to drive expression in serotonergic and corazonergic neurons in early larval stages (Dittrich et al., 1997; Sykes and Condron, 2005).

Next, I tested *Trh-Gal4* and *Tph-Gal4*, two driver lines which are known to drive expression in the majority of serotonergic neurons in third-instar larvae (Huser et al., 2012). Larvae expressing *CsChrimson* under control of either of these driver lines formed

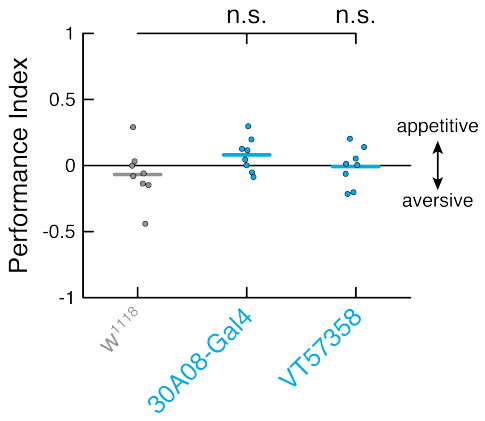

Figure 7.3: Classical conditioning by pairing activation of gustatory interneurons with an odour. Performance indices after olfactory conditioning (raw data points and mean). Larvae express *UAS-CsChrimson* under control of the specified driver (blue). w^{1118} *x UAS-CsChrimson* larvae are used as a negative control (grey). Statistical differences compared to the negative control are tested with a two-sided Mann-Whitney *U* test with Bonferroni correction; n $=$ 8, n. s. p $\geq$ 0.05/26 (not significant).

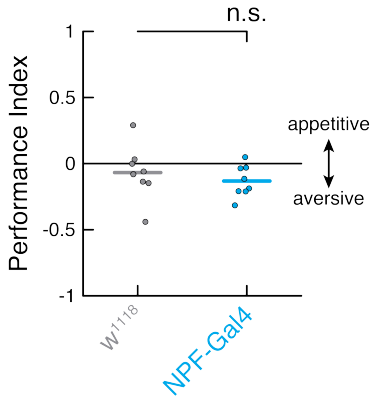

Figure 7.4: Classical conditioning by pairing activation of NPF neurons with an odour. Performance indices after olfactory conditioning (raw data points and mean). Larvae express *UAS-CsChrimson* under control of *NPF-Gal4* (blue). w^{1118} *x UAS-CsChrimson* larvae are used as a negative control (grey). Statistical differences compared to the negative control are tested with a two-sided Mann-Whitney *U* test with Bonferroni correction; n $=$ 8, n. s. p $\geq$ 0.05/26 (not significant).

Table 7.3: Driver lines targeting aminergic interneurons.

Line	Targeted neurons
c346-Gal4	adult *Drosophila* PPM3 dopaminergic neurons (Kong et al., 2010)
Ddc-Gal4	dopaminergic and serotonergic neurons (Li et al., 2000; Lundell and Hirsh, 1994; Sitaraman et al., 2008)
eg^{Mz360}-Gal4	serotonergic and corazonergic neurons during early larval development (Couch et al., 2004; Dittrich et al., 1997; Lundell and Hirsh, 1998)
Tdc2-Gal4	octopaminergic and tyraminergic neurons (Cole et al., 2005)
TH-Gal4	dopaminergic neurons (Friggi-Grelin et al., 2003)
Tph-Gal4	serotonergic neurons (Huser et al., 2012; Park et al., 2006)
Trh-Gal4	serotonergic neurons (Alekseyenko et al., 2010; Huser et al., 2012)

very strong appetitive olfactory memory. Since the expression pattern of these two driver lines is very similar, but *Tph-Gal4* is more specific to serotonergic neurons and drives expression in a smaller number of neurons than *Trh-Gal4*, I decided to use *Tph-Gal4* for the next experiment.

There are approximately 51 neurons per hemisphere covered by *Tph-Gal4*, out of which 29 are located in either the brain or the SEZ (Huser et al., 2012). To narrow down which serotonergic neurons signal reward relevant for associative learning, I restricted *CsChrimson* expression under *Tph-Gal4* using *tsh-Gal80*, which eliminates all GAL4 expression in the VNC, but not in the brain or in the SEZ (Clyne and Miesenböck, 2008; Fushiki et al., 2016; Heckscher et al., 2015). Activation of the brain and SEZ subset of *Tph* neurons was sufficient to induce stable appetitive memory (Fig. 7.6). This result is remarkable, because in larvae, the mushroom bodies are not directly innervated by serotonergic neurons (Huser et al., 2012). It hence brings up the question whether there are alternative learning mechanisms bypassing the mushroom body, or whether serotonergic neurons are indirectly connected to dopaminergic neurons which innervate the mushroom body.

To my knowledge, no sparse driver lines specific to serotonergic neurons in the brain have been identified so far. One previously described serotonergic brain neuron which is

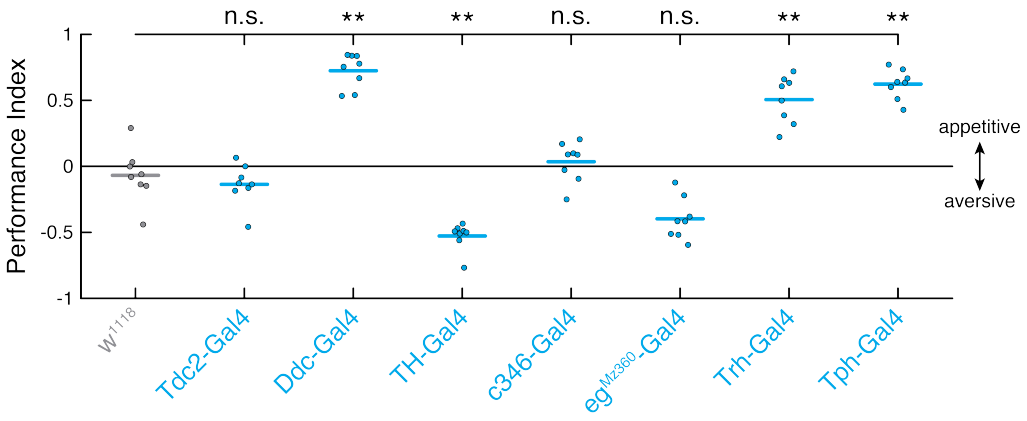

Figure 7.5: Classical conditioning by pairing activation of aminergic interneurons with an odour. Performance indices after olfactory conditioning (raw data points and mean). Larvae express *UAS-CsChrimson* under control of the specified driver (blue). w^{1118} *x UAS-CsChrimson* larvae are used as a negative control (grey). Statistical differences compared to the negative control are tested with a two-sided Mann-Whitney *U* test with Bonferroni correction; n = 8, n. s. $p \geq 0.05/26$ (not significant), ** $p < 0.01/26$.

part of the *Tph-Gal4* expression pattern (Huser et al., 2012) is the contralaterally projecting serotonin-immunoreactive deutocerebral (CSD) neuron (Roy et al., 2007). This neuron is known to closely innervate the antennal lobe, and only a few indirect pathways to the mushroom body exist (Berck et al., 2016). Based on anatomical features from previous EM reconstruction (Berck et al., 2016), available lineage information (Jim Truman) and thanks to the assistance of Dr Michael Winding, I have identified a split-GAL4 line (*SS01989*) which exclusively drives expression in the CSD neuron (Fig. 7.7). Pairing activation of the CSD neuron with an odour was not sufficient to induce olfactory memory (Fig. 7.6), suggesting that the observed learning phenotype is mediated by a least one other group of serotonergic neurons in the brain or SEZ.

7.3 Conclusions

In total, 26 GAL4 lines were assessed for their potential to convey positive or negative valence in this classical conditioning screen. None of the drivers targeting sensory neurons or interneurons processing sweet taste showed any evidence of acting as a rewarding or punishing US. This is surprising, since there is firm evidence for gustatory stimuli serving as a reinforcer in associative learning. Previous studies have shown that a variety of natural sugars can signal reward in larval olfactory conditioning (Neuser et al., 2005;

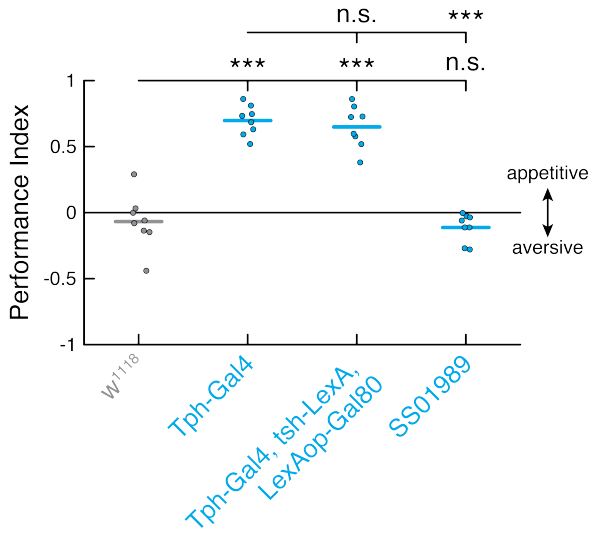

Figure 7.6: Classical conditioning by pairing activation of different subsets of serotonergic neurons with an odour. Performance indices after olfactory conditioning (raw data points and mean). Larvae express *UAS-CsChrimson* under control of the specified driver (blue). w^{1118} *x UAS-CsChrimson* larvae are used as a negative control (grey). Statistical differences between two groups are tested with a two-sided Mann-Whitney *U* test with Bonferroni correction; n = 8, n. s. $p \geq 0.05/5$ (not significant), *** $p < 0.001/5$.

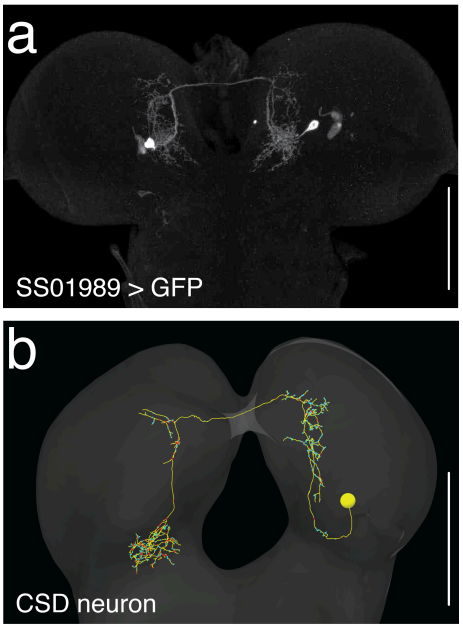

Figure 7.7: SS01989 exclusively drives expression in the CSD neuron. a. Confocal image of the CNS of a third-instar *SS01989 x UAS-GFP* larva obtained after immunohistochemical staining against *GFP*. C-Apochromat 40x objective, resolution: 975 x 651 pixels, scale bar: 100 µm. Image courtesy of the HHMI Janelia FlyLight team. **b.** Electron microscopy reconstruction of the CSD neuron from the CNS of a first-instar larva (Berck et al., 2016). Scale bar: 50 µm. Image courtesy of Dr Michael Winding.

Rohwedder et al., 2012; Scherer et al., 2003; Schipanski et al., 2008). In addition, salt can serve as a US for both appetitive and aversive olfactory memory depending on the concentration (Niewalda et al., 2008), and amino acids are known to be rewarding in larval olfactory conditioning (Kudow et al., 2017). In adult flies, activation of sugar-sensing neurons substitutes for reward in classical conditioning (McGinnis et al., 2016). *Gr43a* neurons, which are the only known sugar-sensing neurons in larvae, are both necessary and sufficient for mediating innate sugar preference (Mishra et al., 2013). Two different *Gr43a-Gal4* drivers were tested in this screen, but none of them displayed a learning phenotype. Similarly, no learning was observed using the activation of driver lines targeting other chemosensory neurons, cold-sensing neurons or gustatory interneurons as a US.

Eschbach et al. (2019) have shown that optogenetic activation of nociceptive neurons or interneurons which integrate nociception and mechanosensation paired with an odour is sufficient to induce aversive olfactory memory. This indicates that larvae are in principal capable of sensing valence through the activity of a distinct set of sensory neurons or interneurons combining information from multiple sensory modalities. However, a large number of gustatory and chemosensory receptors exist in the larva (Kwon et al., 2011). It is thus possible that synergistic activity of multiple classes of chemosensory neurons as induced by natural gustatory stimuli is needed to provide a signal relevant to learning, which could explain why optogenetic activation of small groups of chemosensory neurons was insufficient to trigger learning in this screen.

Optogenetic excitation of NPF neurons paired with the odour did not induce any memory in this screen. This result is consistent with a similar experiment previously performed in larvae, where one of two odours was paired with activation of NPF neurons (Rohwedder et al., 2015). Notably, in the same study, appetitive olfactory conditioning in larvae was impaired when NPF signalling was disrupted (Rohwedder et al., 2015). By contrast, in adult *Drosophila*, activation of NPF neurons paired with an odour is sufficient for the formation of appetitive memory (Shao et al., 2017; Shohat-Ophir et al., 2012). A possible explanation is that NPF neurons in larvae are necessary, but not sufficient to convey reward in classical conditioning, and hence carry a different function than in adult flies.

No olfactory memory was induced when pairing the odour with activation of octopaminergic neurons. This result stands in contrast to previous studies using different paradigms

for odour associative learning in both larval (Honda et al., 2014; Schroll et al., 2006) and adult (Burke et al., 2012) *Drosophila*, in which stimulation of octopaminergic neurons was sufficient to act as a rewarding US. This inconsistency suggests that variations in the experimental procedures for olfactory conditioning can lead to different learning scores.

In addition to the positive control, only four GAL4 lines exhibited appetitive or aversive memory in this screen. All of these lines drive expression in a subset of the dopaminergic and the serotonergic neurons. Strong appetitive olfactory memory was detected when pairing activation of neurons covered by *Ddc-Gal4* with the odour, confirming previous results from adult flies (Aso et al., 2012; Liu et al., 2012; Shyu et al., 2017). These are the same neurons which were also sufficient to induce the operant learning phenotype shown in Chapter 4. This result therefore confirms that dopaminergic and serotonergic neurons can together mediate both classical and operant conditioning in larvae.

Another driver covering a large group of dopaminergic neurons, *TH-Gal4*, showed strong aversive learning. This is consistent with previous substitution experiments for classical conditioning in the larva (Schroll et al., 2006), but also in adult *Drosophila* (Aso et al., 2012; Claridge-Chang et al., 2009; Liu et al., 2012).

This screen has shown for the first time that activation of serotonergic neurons paired with a CS is sufficient to induce memory in flies. This result was obtained using two different driver lines, *Trh-Gal4* and *Tph-Gal4*, which target very similar groups of serotonergic neurons, but no dopaminergic neurons (Huser et al., 2012). Further restriction of *CsChrimson* expression revealed that this effect can sufficiently be explained by the brain and SEZ subset of the serotonergic neurons but is not mediated by the CSD neuron alone.

Serotonergic signalling has been shown to be required for associative learning in both larval (Huser et al., 2017) and adult (Johnson et al., 2011; Sitaraman et al., 2012) *Drosophila*. In the sea slug *Aplysia*, serotonin can substitute for the US in classical conditioning (Hawkins and Byrne, 2015). However, to my knowledge, it has not been previously observed in *Drosophila* that activity of serotonergic neurons is sufficient to act as a US. This result suggests an interesting previously undiscovered role of serotonin. Also, since the mushroom bodies in larvae do not receive direct serotonergic inputs (Huser et al., 2012), it suggests that serotonergic neurons may signal reward elsewhere in the brain or SEZ.

Unfortunately, sparse driver lines targeting small subsets of serotonergic neurons do not yet exist. To further investigate the proposed novel role of serotonin in signalling reward in a learning context, expression patterns of the serotonergic driver lines used in this screen would need to be thoroughly analysed and sparse lines targeting small subsets of serotonergic neurons would need to be generated.

In the next chapter, I will address the role of dopaminergic and serotonergic neurons in operant conditioning of bend direction by expressing *CsChrimson* under control of some of the drivers which were associated with strong learning phenotypes in this screen.

8 The Role of Dopaminergic and Serotonergic Neurons in Operant Conditioning

8.1 Introduction

In Chapters 4 and 5, I have shown that pairing of an action with activation of a large group of dopaminergic and serotonergic neurons is sufficient to induce operant conditioning. My results from Chapter 6 imply that the VNC subset of these neurons is essential for memory formation in the paradigm for conditioning a bend direction preference. However, it remains an open question whether this type of learning is mediated by dopaminergic neurons, serotonergic neurons or a combination of both.

In Chapter 7, I have shown for the first time that activation of serotonergic neurons using the *Tph-Gal4* driver is sufficient to act as a rewarding US for classical conditioning in flies, suggesting a previously undescribed role of serotonin in learning. I have further confirmed results from previous studies indicating that dopaminergic neurons covered by the broad *TH-Gal4* driver can provide a learning signal.

In this chapter, I will use these two drivers to independently investigate the roles of dopaminergic and serotonergic neurons in operant conditioning of bend direction.

8.2 Results

To investigate whether activation of the dopaminergic neurons covered by the *TH-Gal4* driver in correlation with behaviour is sufficient to induce operant conditioning, I trained *TH-Gal4 x UAS-CsChrimson* larvae using the high-throughput training protocol for conditioning a bend direction preference developed in Chapter 4 (Fig. 4.3). No difference between the bend rates to the stimulated side and to the other side was detected in the one-minute

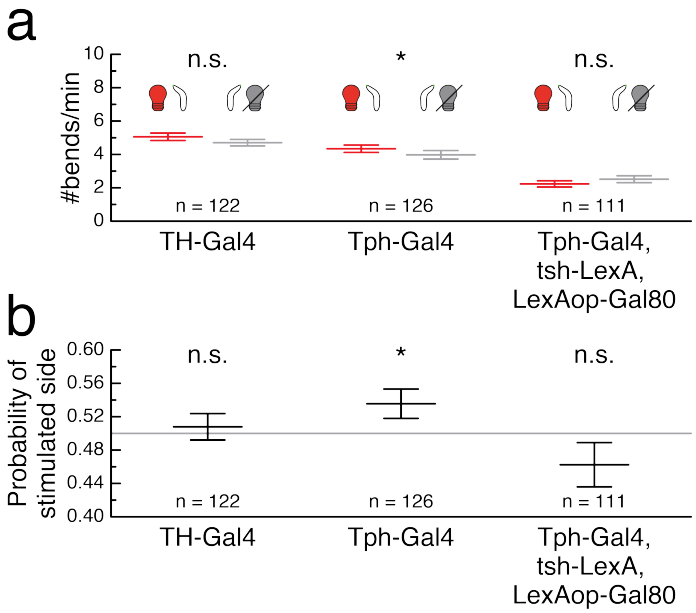

Figure 8.1: High-throughput operant conditioning of bend direction with restriction of *CsChrimson* expression to dopaminergic or serotonergic neurons. Experiments are performed using the protocol described in Fig. 4.3. All larvae express *UAS-CsChrimson* under control of the specified driver. Data is shown for the test after training. **a.** The graph shows the bend rate in number of bends per minute split up by bend direction. The bend rate to the stimulated side (depicted as a left bend with a red light bulb for simplicity) is shown in red and the bend rate to the other side (depicted as a right bend with a grey light bulb for simplicity) is shown in grey. **b.** The graph shows the probability that a given bend is directed towards the stimulated side. The grey line indicates equal probability of 0.5 for bends to either side. **a–b.** All data is shown as (mean $\pm$ s. e. m.). Statistical differences are tested with a two-sided Wilcoxon signed-rank test; n. s. $p \geq 0.05$ (not significant), * $p < 0.05$.

test period following training (Fig. 8.1a). Furthermore, the probability for any given bend to be directed towards the side which was associated with the optogenetic stimulus during training was not significantly different from 50% (Fig. 8.1b). Together, these results suggest that activation of the *TH*-positive dopaminergic neurons paired with bends to one side is not sufficient to induce operant conditioning.

Next, I expressed *CsChrimson* under control of the *Tph-Gal4* driver and tested whether operant conditioning of bend direction can be induced exclusively by serotonergic neurons. Indeed, activation of *Tph* neurons paired with bends to one side resulted in a significantly higher rate of bends to the stimulated side than towards the side without the stimulus during test. The probability of choosing to bend in the direction which was previously paired with the stimulus was also significantly elevated (Fig. 8.1). Therefore, activation of

the *Tph*-positive serotonergic neurons paired with bends to one side is sufficient for the formation of a learned directional preference.

In Chapter 6, I have shown that operant conditioning using *Ddc* neuron activation is impaired when *CsChrimson* expression is restricted to the brain and SEZ subsets of *Ddc* neurons. The result that activation of *Tph* neurons is sufficient to induce operant conditioning suggests that the serotonergic neurons of the VNC are necessary for memory formation in this paradigm. Since both *Ddc-Gal4* and *Tph-Gal4* are very broad driver lines, I cannot exclude the possibility that the expression pattern of *Tph-Gal4* contains brain or SEZ neurons which are not included in the *Ddc-Gal4* expression pattern, which could potentially induce learning through a second mechanism independent from the one which explains memory formation following *Ddc* neuron activation. To assess whether the serotonergic neurons of the VNC are necessary for the observed operant conditioning effect, I restricted the expression pattern of *Tph-Gal4* to the brain and the SEZ using *tsh-Gal80*. Indeed, pairing the optogenetic stimulus with bends to one direction was not sufficient to induce operant conditioning in *Tph-Gal4 x UAS-CsChrimson; tsh-LexA, LexAop-Gal80* larvae (Fig. 8.1).

8.3 Conclusions

Here, I have shown that activation of serotonergic, but not dopaminergic neurons paired with bends to one side is sufficient to induce operant conditioning. Furthermore, my results indicate that the VNC subset of serotonergic neurons is necessary to produce this effect.

The expression pattern of *Tph-Gal4* contains two neurons per hemisegment in the VNC, all of which are serotonergic with the exception of a single neuron in each A8 abdominal hemisegment (Huser et al., 2012). The remaining number of candidate neurons for operant conditioning in the VNC is therefore relatively small. However, based on the data presented here, it cannot be concluded whether the effect only relies on the VNC serotonergic neurons or whether synergistic activity from both VNC neurons and brain or SEZ neurons is needed. To my knowledge, there are currently no sparse driver lines available which exclusively target serotonergic neurons of the VNC to test these hypotheses.

In Chapter 7, I have used a classical conditioning paradigm to show for the first time that there exist learning pathways in *Drosophila* which rely on serotonergic instead of dopaminergic neurons and which do not directly innervate the mushroom body. In this chapter, I show that serotonergic neurons are also sufficient to induce operant conditioning. While activation of the brain and SEZ subset of serotonergic neurons is sufficient to act as a US for classical conditioning, the VNC neurons are essential for operant conditioning. Therefore, different circuit mechanisms underlie classical and operant conditioning mediated by serotonergic neurons.

9 Discussion

9.1 High-throughput tracker

In this thesis, I have introduced a novel high-throughput tracker for multiple *Drosophila* larvae, with real-time detection of behaviours such as left and right bend, forward crawl, roll and back-up, as well as closed-loop control of optogenetic and thermogenetic stimuli. Tracking algorithms for multiple *Drosophila* larvae have already existed before (Ohyama et al., 2013; Swierczek et al., 2011), and simple real-time behaviour detection methods have been available and applied to administer optogenetic stimuli to single larvae in closed loop (Schulze et al., 2015). However, the tracker presented in Chapter 3 combines for the first time FPGA-based real-time tracking with robust online detection of complex behaviours in multiple freely moving animals.

Furthermore, existing multi-animal experiment designs require heating up or illuminating all animals simultaneously to achieve thermogenetic or optogenetic stimulation, respectively (Honda et al., 2016; Klein et al., 2015; Ohyama et al., 2015; Vogelstein et al., 2014). Using the novel high-throughput tracker, optogenetic red light stimuli can be reliably targeted at individual larvae by projecting small spots onto the plate with DMDs. Two-axis galvanometers, which were used in previous studies to project a laser beam onto a single adult fly (Bath et al., 2014; Wu et al., 2014), were controlled to rapidly cycle between several larvae on this tracker, eliminating the need of installing one two-axis galvanometer per animal. Both additional DMDs and galvanometers would be suitable to potentially upgrade the tracker for future use with light stimuli of different wavelengths, e. g. blue light for activation of neurons expressing *Channelrhodopsin-2-XXL* (Dawydow et al., 2014) or *Chronos* (Klapoetke et al., 2014).

This novel set-up allows to efficiently address complex scientific questions. In this project, I have demonstrated that it is useful to investigate the neural circuits of operant conditioning at high throughput, since rewarding stimuli can be delivered to multiple larvae directly in response to behaviour. Other research topics which could benefit from this system include, but are not limited to, chemotaxis (Gomez-Marin et al., 2011; Schulze et al., 2015), decision making (DasGupta et al., 2014; Krajbich, 2019) or spatial navigation and memory (Haberkern et al., 2019; Neuser et al., 2008).

9.2 Operant conditioning in *Drosophila* larvae

Here, I have shown for the first time that *Drosophila* larvae are capable of operant conditioning. I have found that larvae can learn a bend direction preference when bends to one side are paired with activation of dopaminergic and serotonergic neurons. There are strong parallels between this paradigm and the experimental design used by Nuwal et al. (2012) to study operant conditioning in adult *Drosophila*. Flies were fixed onto a metal stick to walk on a rotating ball and turning movements to one direction were rewarded with optogenetic activation of sugar-sensing neurons. As a consequence, the animals learned to increase the number turning movements to this side.

An important difference between the larval and the adult fly paradigms for conditioning a directional preference lies in the nature of the US. I have made initial unsuccessful attempts to operantly condition larvae using activation of sugar-sensing neurons as a US. It is conceivable that sugar cannot serve as a rewarding US for operant conditioning in larvae. However, pairing activation of sugar-sensing neurons, as defined by two different *Gr43a-Gal4* drivers, with an odour was also not sufficient for memory formation in my olfactory conditioning screen, despite extensive evidence that natural sugar can serve as a rewarding US for classical conditioning in larvae (Neuser et al., 2005; Rohwedder et al., 2012; Scherer et al., 2003; Schipanski et al., 2008). A possible explanation for these discrepancies would be that multiple groups of sensory neurons need to be active at the same time in order to relay a meaningful reward signal. Alternatively, adjustments to the temporal pattern or intensity of the optogenetic stimulus may be needed.

I have also introduced a second operant conditioning paradigm, in which larvae modify their behaviour pattern after receiving stimulation paired with forward crawls. However,

attempts to modulate the overall bend rate by pairing bends to both sides with the US failed. This brings up the question whether there are other behaviours which can be paired with reward or punishment to induce operant conditioning.

A challenge when operantly conditioning larval actions such as roll, hunch or back-up is that these actions do not occur frequently in naïve, freely behaving animals. Rolls only ever occur in the presence of a noxious stimulus (Ohyama et al., 2013, 2015; Robertson et al., 2013; Tracey et al., 2003). Similarly, back-up and hunch can only be observed at very low rates (Jovanic et al., 2017, 2016; Ohyama et al., 2013). The amount of the US which animals experience during paired training is therefore very small, making the formation of detectable memory much harder.

The high-throughput tracker could make it possible to study additional operant conditioning paradigms: actions such as back-up or roll could be evoked probabilistically by activating command neurons using thermogenetics (Carreira-Rosario et al., 2018; Ohyama et al., 2015). An optogenetic reward would be administered to those larvae which respond to the stimulus by performing the desired action.

There are several issues which need to be resolved in order to be able to test such paradigms. To achieve independent optogenetic and thermogenetic stimulation of two different sets of neurons, another binary system such as the LexA system (Lai and Lee, 2006) or the Q system (Potter et al., 2010) would need to be employed in addition to the GAL4-UAS system. Therefore, suitable driver lines in the respective systems would need to be created, and one would need to ensure that the effectors can be driven at sufficient strength.

Preliminary tests with thermogenetic stimulation through the LexA system using *pJFRC25-13xLexAop2-IVS-dTrpA1* (Pfeiffer et al., 2010, 2012) suggest that heat-driven activation of *LexAop-dTrpA1* is much weaker compared to *UAS-dTrpA1*. In order to evoke an action, either the intensity of the IR stimulus has to be dramatically increased, to an extent where permanent tissue damage is caused, or the time period of heating has to be extended considerably. However, in this case it is unclear how a reinforcing US is perceived in the context of a prolonged period of heat-induced pain. On the other hand, when using weaker effectors for optogenetics, activation levels could be enhanced by raising the light intensity without harming the animals. This could either be achieved by

adding more DMDs to the set-up or by increasing the amount of light which is fed into each of the existing DMDs.

Due to the available genetic tools and the emerging connectome, the *Drosophila* larva has unique advantages as a model system for neuroscience. The bend direction and forward crawl paradigms presented in this thesis provide a foundation for studying the neural mechanisms underlying operant conditioning. They facilitate both the experiments presented in this thesis, aimed at identifying the neurons which are sufficient to signal reward, as well as future studies to better understand processes such as memory formation and retrieval at both circuit and cellular level.

9.3 Neural circuits of operant conditioning

With a high-throughput operant conditioning paradigm at hand, the neural circuits involved in memory formation could be investigated. I have found that activation of all serotonergic neurons across the CNS can serve as a reinforcing US in operant conditioning. Furthermore, the effect is lost when restricting stimulation to the brain and the SEZ. Therefore, serotonergic neurons of the VNC play a critical role in operant conditioning of bend direction.

From the available data, it cannot be concluded whether the brain and the SEZ are dispensable for operant conditioning in *Drosophila* larvae. There are examples from both vertebrate (Grau et al., 1998) and invertebrate (Booker and Quinn, 1981; Horridge, 1962) species where the spinal cord or the VNC is sufficient for learning, suggesting that there exist conserved mechanisms for brain-independent operant conditioning across species. However, this does not exclude the possibility that there are alternative learning pathways using the brain. In mammals (Balleine et al., 2009; Redgrave et al., 2011) and birds (Fee and Goldberg, 2011), brain correlates of operant conditioning have been identified. It is unclear where in the brain such pathways would be located in insects. Both the experiments presented here and previous studies in adult flies (Booker and Quinn, 1981; Colomb and Brembs, 2010, 2016; Wolf et al., 1998) support the idea that operant conditioning is independent of the mushroom body, such that other learning centres might exist. To determine whether operant conditioning can be fully mediated by the VNC in the larva or whether the brain or SEZ are necessary, new driver lines would need to be

created. A collection of sparse split-GAL4 lines, each specific to a small distinct group of serotonergic neurons, could help to identify the minimum subset of neurons necessary for conveying the US in the bend direction paradigm.

Even if the learning signal for operant conditioning can be mapped to a small number of serotonergic neurons, there will still remain many open questions regarding the mechanisms by which these neurons drive learning. They could act on their immediate output sites by driving synaptic plasticity or modulating the intrinsic excitability of their postsynaptic partners. Another possibility would be that the learning signal is propagated further downstream, such that learning correlates could be found elsewhere in the network.

Furthermore, in order for a memory to be formed, the US needs to be integrated with information about the occurrence of the reinforced action. This movement signal could be transmitted to higher-level circuits by motor feedback, e. g. through efference copy (Fee, 2014; Webb, 2004), where it could converge with the valence-encoding US. Alternatively, proprioceptive inputs could convey information about body posture, which is related to the animal's behaviour. Finally, if memory formation occurred at the level of motor output, the action-specific signal could be integrated with valence locally inside the motor or premotor neuron without the need for feedback loops.

Indeed, Lorenzetti et al. (2008) have proposed intracellular mechanisms for modulating the intrinsic excitability of the premotor neuron B51 in *Aplysia*, which is mediated by the highly conserved PKC. Work by Colomb and Brembs (2016) suggests that operant self-learning in adult flies relies on PKC signalling in motor neurons. If evidence for PKC-induced motor neuron plasticity could be detected in the larva as well, reconstruction of the pathways between the serotonergic neurons of the VNC and the PKC-positive motor neurons from the larval EM volume (Ohyama et al., 2015) could provide further insight into the mechanisms of memory formation and retrieval.

9.4 Serotonin as a learning signal

This project has revealed that serotonergic neurons can convey a learning signal in *Drosophila*. In the case of olfactory conditioning, optogenetic stimulation of the serotonergic neurons in the brain and the SEZ paired with an odour was sufficient to induce strong appetitive learning. On the other hand, the serotonergic neurons of the VNC are neces-

sary for the formation of operant memory, although it is possible that the serotonergic neurons of the brain and the SEZ are also involved. This indicates that different groups of serotonergic neurons play a role in classical and operant conditioning.

Serotonin was previously shown to be involved in associative learning in *Drosophila*. Sitaraman et al. (2012) have shown that synaptic transmission from serotonergic neurons is essential for appetitive olfactory conditioning in adult flies. Formation of aversive olfactory memory is impaired in flies which are fed with a tryptophan hydroxylase inhibitor, which blocks serotonin biosynthesis (Lee et al., 2011). Furthermore, serotonin receptor signalling is required for memory formation in classical conditioning tasks (Johnson et al., 2011). In larvae, ablation of serotonergic neurons during development or mutations in a serotonin receptor gene impair aversive olfactory conditioning (Huser et al., 2017).

Not many studies exist in which serotonergic signalling was found to be sufficient to induce learning. Optogenetic stimulation of serotonergic neurons in the dorsal raphe nucleus serves as reinforcement in both an olfactory learning and an associative nose-poking task in mice (Liu et al., 2014). In the sea slug *Aplysia*, serotonin can serve as a punishing US in classical conditioning (Hawkins and Byrne, 2015). To the best of my knowledge, there is no prior evidence of serotonergic neuron activation being sufficient as a US in insects. However, dopamine and serotonin receptors are necessary for different types of classical conditioning tasks in honeybees, suggesting that the two neurotransmitters may carry out separate functions (Wright et al., 2010).

The mechanisms by which serotonin mediates learning in larvae are not clear. The mushroom body plays a central role in classical conditioning in *Drosophila* (Aso et al., 2014a; de Belle and Heisenberg, 1994; Heisenberg, 2003; Heisenberg et al., 1985; Owald and Waddell, 2015; Rohwedder et al., 2016; Saumweber et al., 2018; Vogt et al., 2014). In adult flies, the serotonergic dorsal paired medium (DPM) neuron, which innervates the mushroom body, is necessary for memory consolidation in olfactory learning (Keene et al., 2006, 2004; Yu et al., 2005). However, this neuron does not exist in larvae (Pauls et al., 2010), and there are no other serotonergic neurons which innervate the mushroom body (Huser et al., 2012). Activation of the serotonergic CSD neuron, which has projections to the mushroom body calyx in adult flies but not in larvae (Roy et al., 2007), paired with the odour was on its own not sufficient for olfactory memory formation (Chapter 7), indicating that the activity of other serotonergic neurons in the brain or SEZ is needed.

Furthermore, olfactory conditioning requires expression of serotonin receptors in the Kenyon cells of the mushroom body (Lee et al., 2011). There is only limited expression of some serotonin receptors in the larval mushroom body (Huser et al., 2017). The serotonin receptor *5-HT2A*, which is not expressed in the mushroom body, has been shown to be involved in the formation of olfactory memory (Huser et al., 2017). Together, these findings support the idea that there exist serotonergic mechanisms for classical conditioning outside the mushroom body.

To further assess the role of serotonin in olfactory learning, it would be useful to develop new sparse driver lines specific to serotonergic neurons to identify the minimal subset of neurons which provide the serotonergic learning signal. In a next step, these neurons and their connective pathways to the mushroom body could be identified from the larval connectome. One could then test whether learning as induced by the serotonergic US remains intact when these pathways are silenced. In addition, the expression pattern of serotonin receptors could give a clue about how the serotonergic signal triggers learning. Furthermore, one should consider the possibility that learning is not induced by serotonin itself, but by other neurotransmitters which could be coexpressed by certain serotonergic neurons. This could be assessed by suppressing serotonin biosynthesis in the desired subset of neurons.

Because operant conditioning relies on activation of the VNC subset of the serotonergic neurons, it is mediated by mechanisms which differ from the ones underlying classical conditioning. However, since it is unclear to what extent serotonergic neurons in the brain and SEZ are involved in the observed operant conditioning effect, it is possible that some neurons play a role in both forms of associative learning. More investigation would be needed to better understand the function of serotonin in memory formation.

9.5 Concluding remarks

This thesis has uncovered novel circuit mechanisms of operant and classical conditioning in *Drosophila*, with a common role of serotonergic signalling as a reinforcing US in both types of learning. However, it is important to keep in mind that the single one mechanism defining learning may not exist. While distinct types of learning may share

many similarities, including the same neurotransmitters or even circuit components, there may still be fundamental differences at functional and circuit level.

Finally, it is not unlikely that even a single instance of learning leads to a variety of changes across the nervous system. In the case of operant conditioning, higher brain centres, motor command neurons, premotor circuits and motor neurons would all qualify as potential learning sites. Much work remains to be done to fully comprehend the processes which are involved in operant memory formation. The work presented here may contribute to our understanding of some of these mechanisms.

References

Abramson, C. I., Dinges, C. W., and Wells, H. (2016). Operant Conditioning in Honey Bees (Apis mellifera L.): The Cap Pushing Response. *PLoS ONE*, 11(9):e0162347.

Aceves-Piña, E. O. and Quinn, W. G. (1979). Learning in normal and mutant Drosophila larvae. *Science*, 206(4414):93–96.

Alekseyenko, O. V., Lee, C., and Kravitz, E. A. (2010). Targeted Manipulation of Serotonergic Neurotransmission Affects the Escalation of Aggression in Adult Male Drosophila melanogaster. *PLoS ONE*, 5(5):e10806.

Alexander, J., Audesirk, T. E., and Audesirk, G. J. (1984). One-trial reward learning in the snail Lymnea stagnalis. *Journal of Neurobiology*, 15(1):67–72.

Almeida-Carvalho, M. J., Berh, D., Braun, A., Chen, Y.-C., Eichler, K., Eschbach, C., Fritsch, P. M. J., Gerber, B., Hoyer, N., Jiang, X., Kleber, J., Klämbt, C., König, C., Louis, M., Michels, B., Miroschnikow, A., Mirth, C., Miura, D., Niewalda, T., Otto, N., Paisios, E., Pankratz, M. J., Petersen, M., Ramsperger, N., Randel, N., Risse, B., Saumweber, T., Schlegel, P., Schleyer, M., Soba, P., Sprecher, S. G., Tanimura, T., Thum, A. S., Toshima, N., Truman, J. W., Yarali, A., and Zlatic, M. (2017). The Ol1mpiad: concordance of behavioural faculties of stage 1 and stage 3 Drosophila larvae. *The Journal of Experimental Biology*, 220(13):2452–2475.

Amano, H. and Maruyama, I. N. (2011). Aversive olfactory learning and associative long-term memory in Caenorhabditis elegans. *Learning & Memory*, 18(10):654–665.

Andreatta, M. and Pauli, P. (2015). Appetitive vs. Aversive conditioning in humans. *Frontiers in Behavioral Neuroscience*, 9:128.

Apostolopoulou, A. A., Mazija, L., Wüst, A., and Thum, A. S. (2014). The neuronal and molecular basis of quinine-dependent bitter taste signaling in Drosophila larvae. *Frontiers in Behavioral Neuroscience*, 8:6.

Apostolopoulou, A. A., Widmann, A., Rohwedder, A., Pfitzenmaier, J. E., and Thum, A. S. (2013). Appetitive Associative Olfactory Learning in Drosophila Larvae. *Journal of Visualized Experiments*, e4334(72):1–11.

Asano, S., Maruyama, T., and Yamaguchi, Y. (2009). Performance comparison of FPGA, GPU and CPU in image processing. In *International Conference on Field Programmable Logic and Applications*, pages 126–131. IEEE.

Aso, Y., Hattori, D., Yu, Y., Johnston, R. M., Iyer, N. A., Ngo, T.-T. B., Dionne, H., Abbott, L. F., Axel, R., Tanimoto, H., and Rubin, G. M. (2014a). The neuronal architecture of the mushroom body provides a logic for associative learning. *eLife*, 3:e04577.

Aso, Y., Herb, A., Ogueta, M., Siwanowicz, I., Templier, T., Friedrich, A. B., Ito, K., Scholz, H., and Tanimoto, H. (2012). Three Dopamine pathways induce aversive odor memories with different stability. *PLoS Genetics*, 8(7):e1002768.

Aso, Y., Sitaraman, D., Ichinose, T., Kaun, K. R., Vogt, K., Belliart-Guérin, G., Plaçais, P.-Y., Robie, A. A., Yamagata, N., Schnaitmann, C., Rowell, W. J., Johnston, R. M., Ngo, T.-T. B., Chen, N., Korff, W., Nitabach, M. N., Heberlein, U., Preat, T., Branson, K. M., Tanimoto, H., and Rubin, G. M. (2014b). Mushroom body output neurons encode valence and guide memory-based action selection in Drosophila. *eLife*, 3:e04580.

Austin, A. J. and Duka, T. (2010). Mechanisms of attention for appetitive and aversive outcomes in Pavlovian conditioning. *Behavioural Brain Research*, 213(1):19–26.

Balleine, B. W., Liljeholm, M., and Ostlund, S. B. (2009). The integrative function of the basal ganglia in instrumental conditioning. *Behavioural Brain Research*, 199(1):43–52.

Balleine, B. W., Morris, R. W., and Leung, B. K. (2015). Thalamocortical integration of instrumental learning and performance and their disintegration in addiction. *Brain Research*, 1628(Pt A):104–116.

Bate, M., Goodman, C. S., and Spitzer, N. C. (1981). Embryonic development of identified neurons: segment-specific differences in the H cell homologues. *The Journal of Neuroscience*, 1(1):103–106.

Bath, D. E., Stowers, J. R., Hörmann, D., Poehlmann, A., Dickson, B. J., and Straw, A. D. (2014). FlyMAD: rapid thermogenetic control of neuronal activity in freely walking Drosophila. *Nature Methods*, 11(7):756–762.

Berck, M. E., Khandelwal, A., Claus, L., Hernandez-Nunez, L., Si, G., Tabone, C. J., Li, F., Truman, J. W., Fetter, R. D., Louis, M., Samuel, A. D., and Cardona, A. (2016). The wiring diagram of a glomerular olfactory system. *eLife*, 5:e14859.

Bitterman, M. E., Menzel, R., Fietz, A., and Schäfer, S. (1983). Classical conditioning of proboscis extension in honeybees (Apis mellifera). *Journal of Comparative Psychology*, 97(2):107–119.

Booker, R. and Quinn, W. G. (1981). Conditioning of leg position in normal and mutant Drosophila. *Neurobiology*, 78(6):3940–3944.

Bouton, M. E. and Peck, C. A. (1989). Context effects on conditioning, extinction, and reinstatement in an appetitive conditioning preparation. *Animal Learning & Behavior*, 17(2):188–198.

Boyden, E. S., Zhang, F., Bamberg, E., Nagel, G., and Deisseroth, K. (2005). Millisecond-timescale, genetically targeted optical control of neural activity. *Nature Neuroscience*, 8(9):1263–1268.

Brand, A. H. and Perrimon, N. (1993). Targeted gene expression as a means of altering cell fates and generating dominant phenotypes. *Development*, 118(2):401–415.

Branson, K., Robie, A. A., Bender, J., Perona, P., and Dickinson, M. H. (2009). High-throughput ethomics in large groups of Drosophila. *Nature Methods*, 6(6):451–457.

Braubach, O. R., Wood, H.-D., Gadbois, S., Fine, A., and Croll, R. P. (2009). Olfactory conditioning in the zebrafish (Danio rerio). *Behavioural Brain Research*, 198(1):190–198.

Brembs, B. (2003). Operant conditioning in invertebrates. *Current Opinion in Neurobiology*, 13(6):710–717.

Brembs, B. (2011). Spontaneous decisions and operant conditioning in fruit flies. *Behavioural Processes*, 87(1):157–164.

Brembs, B., Lorenzetti, F. D., Reyes, F. D., Baxter, D. a., and Byrne, J. H. (2002). Operant reward learning in Aplysia: neuronal correlates and mechanisms. *Science*, 296(5573):1706–1709.

Brembs, B. and Plendl, W. (2008). Double Dissociation of PKC and AC Manipulations on Operant and Classical Learning in Drosophila. *Current Biology*, 18(15):1168–1171.

Brown, J. S., Kalish, H. I., and Farber, I. E. (1951). Conditioned fear as revealed by magnitude of startle response to an auditory stimulus. *Journal of Experimental Psychology*, 41(5):317–328.

Burke, C. J., Huetteroth, W., Owald, D., Perisse, E., Krashes, M. J., Das, G., Gohl, D., Silies, M., Certel, S., and Waddell, S. (2012). Layered reward signalling through octopamine and dopamine in Drosophila. *Nature*, 492(7429):433–437.

Campbell, R. A. A., Honegger, K. S., Qin, H., Li, W., Demir, E., and Turner, G. C. (2013). Imaging a Population Code for Odor Identity in the Drosophila Mushroom Body. *Journal of Neuroscience*, 33(25):10568–10581.

Caroni, P. (2015). Inhibitory microcircuit modules in hippocampal learning. *Current Opinion in Neurobiology*, 35:66–73.

Carreira-Rosario, A., Zarin, A. A., Clark, M. Q., Manning, L., Fetter, R. D., Cardona, A., and Doe, C. Q. (2018). MDN brain descending neurons coordinately activate backward and inhibit forward locomotion. *eLife*, 7:e38554.

Chen, Y.-J., Li, Y.-C., Huang, K.-N., and Young, M.-S. (2005). The Implementation of a Stand-alone Video Tracking and Analysis System for Animal Behavior Measurement in Morris Water Maze. In *IEEE Engineering in Medicine and Biology 27th Annual Conference*, pages 1766–1768. IEEE.

Chiuchisan, I. (2013). A new FPGA-based real-time configurable system for medical image processing. In *E-Health and Bioengineering Conference (EHB)*, pages 1–4. IEEE.

Choi, J., van Giesen, L., Choi, M. S., Kang, K., Sprecher, S. G., and Kwon, J. Y. (2016). A Pair of Pharyngeal Gustatory Receptor Neurons Regulates Caffeine-Dependent Ingestion in Drosophila Larvae. *Frontiers in Cellular Neuroscience*, 10:181.

Chyb, S., Dahanukar, A., Wickens, A., and Carlson, J. R. (2003). Drosophila Gr5a encodes a taste receptor tuned to trehalose. *Proceedings of the National Academy of Sciences*, 100(suppl. 2):14526–14530.

Claridge-Chang, A., Roorda, R. D., Vrontou, E., Sjulson, L., Li, H., Hirsh, J., and Miesenböck, G. (2009). Writing Memories with Light-Addressable Reinforcement Circuitry. *Cell*, 139(2):405–415.

Clyne, J. D. and Miesenböck, G. (2008). Sex-Specific Control and Tuning of the Pattern Generator for Courtship Song in Drosophila. *Cell*, 133(2):354–363.

Cognigni, P., Felsenberg, J., and Waddell, S. (2018). Do the right thing: neural network mechanisms of memory formation, expression and update in Drosophila. *Current Opinion in Neurobiology*, 49:51–58.

Cole, S. H., Carney, G. E., McClung, C. A., Willard, S. S., Taylor, B. J., and Hirsh, J. (2005). Two Functional but Noncomplementing Drosophila Tyrosine Decarboxylase Genes. *Journal of Biological Chemistry*, 280(15):14948–14955.

Colomb, J. and Brembs, B. (2010). The biology of psychology. *Communicative & Integrative Biology*, 3(2):142–145.

Colomb, J. and Brembs, B. (2016). PKC in motorneurons underlies selflearning, a form of motor learning in Drosophila. *PeerJ*, 2016(4):e1971.

Cong, L., Wang, Z., Chai, Y., Hang, W., Shang, C., Yang, W., Bai, L., Du, J., Wang, K., and Wen, Q. (2017). Rapid whole brain imaging of neural activity in freely behaving larval zebrafish (Danio rerio). *eLife*, 6:e28158.

Corbett, D. and Wise, R. A. (1980). Intracranial self-stimulation in relation to the ascending dopaminergic systems of the midbrain: A moveable electrode mapping study. *Brain Research*, 185(1):1–15.

Couch, J. A., Chen, J., Rieff, H. I., Uri, E. M., and Condron, B. G. (2004). robo2 and robo3 interact with eagle to regulate serotonergic neuron differentiation. *Development*, 131(5):997–1006.

Croset, V., Schleyer, M., Arguello, J. R., Gerber, B., and Benton, R. (2016). A molecular and neuronal basis for amino acid sensing in the Drosophila larva. *Scientific Reports*, 6(1):34871.

Curcio, J. A. and Petty, C. C. (1951). The near infrared absorption spectrum of liquid water. *Journal of the Optical Society of America*, 41(5):302–304.

Dahanukar, A., Foster, K., van der Goes van Naters, W. M., and Carlson, J. R. (2001). A Gr receptor is required for response to the sugar trehalose in taste neurons of Drosophila. *Nature Neuroscience*, 4(12):1182–1186.

Dahanukar, A., Lei, Y.-T., Kwon, J. Y., and Carlson, J. R. (2007). Two Gr Genes Underlie Sugar Reception in Drosophila. *Neuron*, 56(3):503–516.

Dankert, H., Wang, L., Hoopfer, E. D., Anderson, D. J., and Perona, P. (2009). Automated monitoring and analysis of social behavior in Drosophila. *Nature Methods*, 6(4):297–303.

DasGupta, S., Ferreira, C. H., and Miesenböck, G. (2014). FoxP influences the speed and accuracy of a perceptual decision in Drosophila. *Science*, 344(6186):901–904.

Davis, R. L. (2005). Olfactory Memory Formation in Drosophila: From Molecular to Systems Neuroscience. *Annual Review of Neuroscience*, 28:275–302.

Dawydow, A., Gueta, R., Ljaschenko, D., Ullrich, S., Hermann, M., Ehmann, N., Gao, S., Fiala, A., Langenhan, T., Nagel, G., and Kittel, R. J. (2014). Channelrhodopsin-2-XXL, a powerful optogenetic tool for low-light applications. *Proceedings of the National Academy of Sciences*, 111(38):13972–13977.

de Belle, J. S. and Heisenberg, M. (1994). Associative odor learning in Drosophila abolished by chemical ablation of mushroom bodies. *Science*, 263(5147):692–695.

Denisov, G., Ohyama, T., Jovanic, T., and Zlatic, M. (2013). Model-based Detection and Analysis of Animal Behaviors using Signals Extracted by Automated Tracking. In *BIOSIGNALS*, pages 175–181.

Dickinson, A. (1981). Conditioning and Associative Learning. *British Medical Bulletin*, 37(2):165–168.

Dittrich, R., Bossing, T., Gould, A. P., Technau, G. M., and Urban, J. (1997). The differentiation of the serotonergic neurons in the Drosophila ventral nerve cord depends on the combined function of the zinc finger proteins Eagle and Huckebein. *Development*, 124(13):2515–25.

Donelson, N., Kim, E. Z., Slawson, J. B., Vecsey, C. G., Huber, R., and Griffith, L. C. (2012). High-Resolution Positional Tracking for Long-Term Analysis of Drosophila Sleep and Locomotion Using the "Tracker" Program. *PLoS ONE*, 7(5):e37250.

Dong, Y., Green, T., Saal, D., Marie, H., Neve, R., Nestler, E. J., and Malenka, R. C. (2006). CREB modulates excitability of nucleus accumbens neurons. *Nature Neuroscience*, 9(4):475–477.

Draper, B. A., Beveridge, J. R., Bohm, A. P. W., Ross, C., and Chawathe, M. (2003). Accelerated image processing on FPGAs. *IEEE Transactions on Image Processing*, 12(12):1543–1551.

Drash, P. W. and Leibowitz, J. M. (1973). Operant Conditioning of Speech and Language in the Nonverbal Retarded Child. Recent Advances. *Pediatric Clinics of North America*, 20(1):233–243.

Eichler, K., Li, F., Litwin-Kumar, A., Park, Y., Andrade, I., Schneider-Mizell, C. M., Saumweber, T., Huser, A., Eschbach, C., Gerber, B., Fetter, R. D., Truman, J. W., Priebe, C. E., Abbott, L. F., Thum, A. S., Zlatic, M., and Cardona, A. (2017). The complete connectome of a learning and memory centre in an insect brain. *Nature*, 548(7666):175–182.

Erber, J., Pribbenow, B., Kisch, J., and Faensen, D. (2000). Operant conditioning of antennal muscle activity in the honey bee (Apis mellifera L.). *Journal of Comparative Physiology A*, 186(6):557–565.

Eschbach, C., Cano, C., Haberkern, H., Schraut, K., Guan, C., Triphan, T., and Gerber, B. (2011). Associative learning between odorants and mechanosensory punishment in larval Drosophila. *Journal of Experimental Biology*, 214(23):3897–3905.

Eschbach, C., Fushiki, A., Winding, M., Schneider-Mizell, C., Shao, M., Arruda, R., Eichler, K., Valdes-Aleman, J., Ohyama, T., Thum, A. S., Gerber, B., Fetter, R. D., Truman, J. W., Cardona, A., and Zlatic, M. (2019). Multilayered recurrent architecture for adaptive regulation of learning in the insect brain. *bioRxiv*.

Everitt, B. J., Giuliano, C., and Belin, D. (2018). Addictive behaviour in experimental animals: prospects for translation. *Philosophical Transactions of the Royal Society B*, 373(1742):20170027.

Faucher, C., Forstreuter, M., Hilker, M., and de Bruyne, M. (2006). Behavioral responses of Drosophila to biogenic levels of carbon dioxide depend on life-stage, sex and olfactory context. *The Journal of Experimental Biology*, 209(Pt 14):2739–48.

Fee, M. S. (2014). The role of efference copy in striatal learning. *Current Opinion in Neurobiology*, 25(4):194–200.

Fee, M. S. and Goldberg, J. H. (2011). A hypothesis for basal ganglia-dependent reinforcement learning in the songbird. *Neuroscience*, 198:152–170.

Fernando, A. B. P., Mar, A. C., Urcelay, G. P., Dickinson, A., and Robbins, T. W. (2015). Avoidance behavior: A free-operant lever-press avoidance task for the assessment of the effects of safety signals. *Current Protocols in Neuroscience*, 70:8.32.1–8.32.12.

Fischer, J. A., Giniger, E., Maniatis, T., and Ptashne, M. (1988). GAL4 activates transcription in Drosophila. *Nature*, 332(6167):853–856.

Friggi-Grelin, F., Coulom, H., Meller, M., Gomez, D., Hirsh, J., and Birman, S. (2003). Targeted gene expression in Drosophila dopaminergic cells using regulatory sequences from tyrosine hydroxylase. *Journal of Neurobiology*, 54(4):618–627.

Fry, S. N., Rohrseitz, N., Straw, A. D., and Dickinson, M. H. (2008). TrackFly: Virtual reality for a behavioral system analysis in free-flying fruit flies. *Journal of Neuroscience Methods*, 171(1):110–117.

Fushiki, A., Zwart, M. F., Kohsaka, H., Fetter, R. D., Cardona, A., and Nose, A. (2016). A circuit mechanism for the propagation of waves of muscle contraction in Drosophila. *eLife*, 5:e13253.

Ganguly, A., Pang, L., Duong, V. K., Lee, A., Schoniger, H., Varady, E., and Dahanukar, A. (2017). A Molecular and Cellular Context-Dependent Role for Ir76b in Detection of Amino Acid Taste. *Cell Reports*, 18(3):737–750.

Gerber, B. and Hendel, T. (2006). Outcome expectations drive learned behaviour in larval Drosophila. *Proceedings of the Royal Society B*, 273(1604):2965–2968.

Gerber, B., Scherer, S., Neuser, K., Michels, B., Hendel, T., Stocker, R. F., and Heisenberg, M. (2004). Visual learning in individually assayed Drosophila larvae. *The Journal of Experimental Biology*, 207(Pt 1):179–188.

Gershow, M., Berck, M., Mathew, D., Luo, L., Kane, E. A., Carlson, J. R., and Samuel, A. D. T. (2012). Controlling airborne cues to study small animal navigation. *Nature Methods*, 9(3):290–296.

Giurfa, M. (2006). Associative Learning: The Instructive Function of Biogenic Amines. *Current Biology*, 16(20):R892–R895.

Giurfa, M., Fabre, E., Flaven-Pouchon, J., Groll, H., Oberwallner, B., Vergoz, V., Roussel, E., and Sandoz, J. C. (2009). Olfactory conditioning of the sting extension reflex in honeybees: Memory dependence on trial number, interstimulus interval, intertrial interval, and protein synthesis. *Learning & Memory*, 16(12):761–765.

Gomez-Marin, A., Stephens, G. J., and Louis, M. (2011). Active sampling and decision making in Drosophila chemotaxis. *Nature Communications*, 2:441.

Gómez-Pinilla, F., Huie, J. R., Ying, Z., Ferguson, A. R., Crown, E. D., Baumbauer, K. M., Edgerton, V. R., and Grau, J. W. (2007). BDNF and learning: Evidence that instrumental training promotes learning within the spinal cord by up-regulating BDNF expression. *Neuroscience*, 148(4):893–906.

Grau, J. W., Barstow, D. G., and Joynes, R. L. (1998). Instrumental learning within the spinal cord: I. Behavioral Properties. *Behavioral Neuroscience*, 112(6):1366–1386.

Groszer, M., Keays, D. A., Deacon, R. M. J., de Bono, J. P., Prasad-Mulcare, S., Gaub, S., Baum, M. G., French, C. A., Nicod, J., Coventry, J. A., Enard, W., Fray, M., Brown, S. D. M., Nolan, P. M., Pääbo, S., Channon, K. M., Costa, R. M., Eilers, J., Ehret, G.,

Rawlins, J. N. P., and Fisher, S. E. (2008). Impaired Synaptic Plasticity and Motor Learning in Mice with a Point Mutation Implicated in Human Speech Deficits. *Current Biology*, 18(5):354–362.

Grover, D., Tower, J., and Tavaré, S. (2008). O fly, where art thou? *Journal of the Royal Society Interface*, 5(27):1181–1191.

Gründemann, J. and Lüthi, A. (2015). Ensemble coding in amygdala circuits for associative learning. *Current Opinion in Neurobiology*, 35:200–206.

Haberkern, H., Basnak, M. A., Ahanonu, B., Schauder, D., Cohen, J. D., Bolstad, M., Bruns, C., and Jayaraman, V. (2019). Visually Guided Behavior and Optogenetically Induced Learning in Head-Fixed Flies Exploring a Virtual Landscape. *Current Biology*, 29(10):1647–1659.e8.

Haesler, S., Rochefort, C., Georgi, B., Licznerski, P., Osten, P., and Scharff, C. (2007). Incomplete and inaccurate vocal imitation after knockdown of FoxP2 in songbird basal ganglia nucleus Area X. *PLoS Biology*, 5(12):2885–2897.

Hamada, F. N., Rosenzweig, M., Kang, K., Pulver, S. R., Ghezzi, A., Jegla, T. J., and Garrity, P. A. (2008). An internal thermal sensor controlling temperature preference in Drosophila. *Nature*, 454(7201):217–220.

Hawkins, R. D. and Byrne, J. H. (2015). Associative Learning in Invertebrates. *Cold Spring Harbor Perspectives in Biology*, 7(5):a021709.

Hazelrigg, T., Levis, R., and Rubin, G. M. (1984). Transformation of white locus DNA in Drosophila: Dosage compensation, zeste interaction, and position effects. *Cell*, 36(2):469–481.

He, J., Wei, J., Rizak, J. D., Chen, Y., Wang, J., Hu, X., and Ma, Y. (2015). An odor detection system based on automatically trained mice by relative go no-go olfactory operant conditioning. *Scientific Reports*, 5:10019.

Heckscher, E. S., Lockery, S. R., and Doe, C. Q. (2012). Characterization of Drosophila Larval Crawling at the Level of Organism, Segment, and Somatic Body Wall Musculature. *Journal of Neuroscience*, 32(36):12460–12471.

Heckscher, E. S., Zarin, A. A., Faumont, S., Clark, M. Q., Manning, L., Fushiki, A., Schneider-Mizell, C. M., Fetter, R. D., Truman, J. W., Zwart, M. F., Landgraf, M., Cardona, A., Lockery, S. R., and Doe, C. Q. (2015). Even-Skipped+ Interneurons Are Core Components of a Sensorimotor Circuit that Maintains Left-Right Symmetric Muscle Contraction Amplitude. *Neuron*, 88(2):314–329.

Heisenberg, M. (2003). Mushroom body memoir: from maps to models. *Nature Reviews Neuroscience*, 4(4):266–75.

Heisenberg, M., Borst, A., Wagner, S., and Byers, D. (1985). Drosophila Mushroom Body Mutants are Deficient in Olfactory Learning. *Journal of Neurogenetics*, 2(1):1–30.

Hendel, T., Michels, B., Neuser, K., Schipanski, A., Kaun, K., Sokolowski, M. B., Marohn, F., Michel, R., Heisenberg, M., and Gerber, B. (2005). The carrot, not the stick: Appetitive rather than aversive gustatory stimuli support associative olfactory learning in individually assayed Drosophila larvae. *Journal of Comparative Physiology A*, 191(3):265–279.

Holland, P. C. and Rescorla, R. A. (1975). The effect of two ways of devaluing the unconditioned stimulus after first- and second-order appetitive conditioning. *Journal of Experimental Psychology: Animal Behavior Processes*, 1(4):355–363.

Honda, T., Lee, C.-Y., Honjo, K., and Furukubo-Tokunaga, K. (2016). Artificial Induction of Associative Olfactory Memory by Optogenetic and Thermogenetic Activation of Olfactory Sensory Neurons and Octopaminergic Neurons in Drosophila Larvae. *Frontiers in Behavioral Neuroscience*, 10:137.

Honda, T., Lee, C.-Y., Yoshida-Kasikawa, M., Honjo, K., and Furukubo-Tokunaga, K. (2014). Induction of Associative Olfactory Memory by Targeted Activation of Single Olfactory Neurons in Drosophila Larvae. *Scientific Reports*, 4:4798.

Honegger, K. S., Campbell, R. A. A., and Turner, G. C. (2011). Cellular-Resolution Population Imaging Reveals Robust Sparse Coding in the Drosophila Mushroom Body. *Journal of Neuroscience*, 31(33):11772–11785.

Honjo, K. and Furukubo-Tokunaga, K. (2005). Induction of cAMP Response Element-Binding Protein-Dependent Medium-Term Memory by Appetitive Gustatory Reinforcement in Drosophila Larvae. *Journal of Neuroscience*, 25(35):7905–7913.

Honjo, K. and Furukubo-Tokunaga, K. (2009). Distinctive Neuronal Networks and Biochemical Pathways for Appetitive and Aversive Memory in Drosophila Larvae. *Journal of Neuroscience*, 29(3):852–862.

Horridge, G. A. (1962). Learning of Leg Position by the Ventral Nerve Cord in Headless Insects. *Proceedings of the Royal Society B*, 157(966):33–52.

Hoyer, S. C., Eckart, A., Herrel, A., Zars, T., Fischer, S. A., Hardie, S. L., and Heisenberg, M. (2008). Octopamine in Male Aggression of Drosophila. *Current Biology*, 18(3):159–167.

Hoyle, G. (1979). Mechanisms of simple motor learning. *Trends in Neurosciences*, 2:153–155.

Huang, K.-M., Cosman, P., and Schafer, W. R. (2006). Machine vision based detection of omega bends and reversals in C. elegans. *Journal of Neuroscience Methods*, 158(2):323–336.

Huser, A., Eschment, M., Güllü, N., Collins, K. A. N., Böpple, K., Pankevych, L., Rolsing, E., and Thum, A. S. (2017). Anatomy and behavioral function of serotonin receptors in Drosophila melanogaster larvae. *PLoS ONE*, 12(8):e0181865.

Huser, A., Rohwedder, A., Apostolopoulou, A. A., Widmann, A., Pfitzenmaier, J. E., Maiolo, E. M., Selcho, M., Pauls, D., von Essen, A., Gupta, T., Sprecher, S. G., Birman, S., Riemensperger, T., Stocker, R. F., and Thum, A. S. (2012). The Serotonergic Central Nervous System of the Drosophila Larva: Anatomy and Behavioral Function. *PLoS ONE*, 7(10):e47518.

Hwang, R. Y., Zhong, L., Xu, Y., Johnson, T., Zhang, F., Deisseroth, K., and Tracey, W. D. (2007). Nociceptive Neurons Protect Drosophila Larvae from Parasitoid Wasps. *Current Biology*, 17(24):2105–2116.

Jefferis, G. S. X. E., Potter, C. J., Chan, A. M., Marin, E. C., Rohlfing, T., Maurer, Jr., C. R., and Luo, L. (2007). Comprehensive Maps of Drosophila Higher Olfactory Centers: Spatially Segregated Fruit and Pheromone Representation. *Cell*, 128(6):1187–1203.

Jenett, A., Rubin, G. M., Ngo, T.-T. B., Shepherd, D., Murphy, C., Dionne, H., Pfeiffer, B. D., Cavallaro, A., Hall, D., Jeter, J., Iyer, N., Fetter, D., Hausenfluck, J. H., Peng, H.,

Trautman, E. T., Svirskas, R. R., Myers, E. W., Iwinski, Z. R., Aso, Y., DePasquale, G. M., Enos, A., Hulamm, P., Lam, S. C. B., Li, H. H., Laverty, T. R., Long, F., Qu, L., Murphy, S. D., Rokicki, K., Safford, T., Shaw, K., Simpson, J. H., Sowell, A., Tae, S., Yu, Y., and Zugates, C. T. (2012). A GAL4-Driver Line Resource for Drosophila Neurobiology. *Cell Reports*, 2(4):991–1001.

Jiao, Y., Moon, S. J., and Montell, C. (2007). A Drosophila gustatory receptor required for the responses to sucrose, glucose, and maltose identified by mRNA tagging. *Proceedings of the National Academy of Sciences*, 104(35):14110–14115.

Jin, X. and Costa, R. M. (2010). Start/stop signals emerge in nigrostriatal circuits during sequence learning. *Nature*, 466(7305):457–462.

Joel, D. (2006). The signal attenuation rat model of obsessive-compulsive disorder: a review. *Psychopharmacology*, 186(4):487–503.

Johnson, O., Becnel, J., and Nichols, C. (2011). Serotonin receptor activity is necessary for olfactory learning and memory in Drosophila melanogaster. *Neuroscience*, 192:372–381.

Jones, S. V., Heldt, S. A., Davis, M., and Ressler, K. J. (2005). Olfactory-Mediated Fear Conditioning in Mice: Simultaneous Measurements of Fear-Potentiated Startle and Freezing. *Behavioral Neuroscience*, 119(1):329–335.

Jones, W. D., Cayirlioglu, P., Grunwald Kadow, I., and Vosshall, L. B. (2007). Two chemosensory receptors together mediate carbon dioxide detection in Drosophila. *Nature*, 445(7123):86–90.

Jovanic, T., Masson, J.-B., Truman, J. W., and Zlatic, M. (2017). Mapping neurons and brain regions underlying sensorimotor decisions and sequences. *bioRxiv*.

Jovanic, T., Schneider-Mizell, C. M., Shao, M., Masson, J.-B., Denisov, G., Fetter, R. D., Mensh, B. D., Truman, J. W., Cardona, A., and Zlatic, M. (2016). Competitive Disinhibition Mediates Behavioral Choice and Sequences in Drosophila. *Cell*, 167(3):858–870.e19.

Jovanic, T., Winding, M., Cardona, A., Truman, J. W., Gershow, M., Zlatic, M., Jovanic, T., Winding, M., Cardona, A., Truman, J. W., and Gershow, M. (2019). Neural Sub-

strates of Drosophila Larval Anemotaxis Article Neural Substrates of Drosophila Larval Anemotaxis. *Current Biology*, 29(4):554–566.

Joynes, R. L., Janjua, K., and Grau, J. W. (2004). Instrumental learning within the spinal cord: VI: The NMDA receptor antagonist, AP5, disrupts the acquisition and maintenance of an acquired flexion response. *Behavioural Brain Research*, 154(2):431–438.

Kabra, M., Robie, A. A., Rivera-Alba, M., Branson, S., and Branson, K. (2013). JAABA: interactive machine learning for automatic annotation of animal behavior. *Nature Methods*, 10(1):64–67.

Kane, E. A., Gershow, M., Afonso, B., Larderet, I., Klein, M., Carter, A. R., de Bivort, B. L., Sprecher, S. G., and Samuel, A. D. T. (2013). Sensorimotor structure of Drosophila larva phototaxis. *Proceedings of the National Academy of Sciences*, 110(40):E3868–E3877.

Karagyozov, D., Mihovilovic Skanata, M., Lesar, A., and Gershow, M. (2018). Recording Neural Activity in Unrestrained Animals with Three-Dimensional Tracking Two-Photon Microscopy. *Cell Reports*, 25(5):1371–1383.e10.

Katsov, A. Y. and Clandinin, T. R. (2008). Motion Processing Streams in Drosophila Are Behaviorally Specialized. *Neuron*, 59(2):322–335.

Kauffman, A. L., Ashraf, J. M., Corces-Zimmerman, M. R., Landis, J. N., and Murphy, C. T. (2010). Insulin Signaling and Dietary Restriction Differentially Influence the Decline of Learning and Memory with Age. *PLoS Biology*, 8(5):e1000372.

Keene, A. C., Krashes, M. J., Leung, B., Bernard, J. A., and Waddell, S. (2006). Drosophila Dorsal Paired Medial Neurons Provide a General Mechanism for Memory Consolidation. *Current Biology*, 16(15):1524–1530.

Keene, A. C., Stratmann, M., Keller, A., Perrat, P. N., Vosshall, L. B., and Waddell, S. (2004). Diverse odor-conditioned memories require uniquely timed dorsal paired medial neuron output. *Neuron*, 44(3):521–533.

Kernan, M., Cowan, D., and Zuker, C. (1994). Genetic dissection of mechanosensory transduction: mechanoreception-defective mutations of Drosophila. *Neuron*, 12(6):1195–206.

Kershaw, J. C. and Running, C. A. (2018). Conditioning of human salivary flow using a visual cue for sour candy. *Archives of Oral Biology*, 92:90–95.

Khurana, S., AbuBaker, M. B., and Siddiqi, O. (2009). Odour avoidance learning in the larva of Drosophila melanogaster. *Journal of Biosciences*, 34(4):621–631.

Khurana, S., Robinson, B. G., Wang, Z., Shropshire, W. C., Zhong, A. C., Garcia, L. E., Corpuz, J., Chow, J., Hatch, M. M., Precise, E. F., Cady, A., Godinez, R. M., Pulpanyawong, T., Nguyen, A. T., Li, W.-k., Seiter, M., Jahanian, K., Sun, J. C., Shah, R., Rajani, S., Chen, W. Y., Ray, S., Ryazanova, N. V., Wakou, D., Prabhu, R. K., and Atkinson, N. S. (2012). Olfactory Conditioning in the Third Instar Larvae of Drosophila melanogaster Using Heat Shock Reinforcement. *Behavior Genetics*, 42(1):151–161.

Kim, H., Choi, M. S., Kang, K., and Kwon, J. Y. (2016). Behavioral Analysis of Bitter Taste Perception in Drosophila Larvae. *Chemical Senses*, 41(1):85–94.

Kim, H., Jeong, Y. T., Choi, M. S., Choi, J., Moon, S. J., and Kwon, J. (2017a). Involvement of a Gr2a-Expressing Drosophila Pharyngeal Gustatory Receptor Neuron in Regulation of Aversion to High-Salt Foods. *Molecules and Cells*, 40(5):331–338.

Kim, H., Kirkhart, C., and Scott, K. (2017b). Long-range projection neurons in the taste circuit of Drosophila. *eLife*, 6:e23386.

Kisch, J. and Erber, J. (1999). Operant conditioning of antennal movements in the honey bee. *Behavioural Brain Research*, 99(1):93–102.

Kitamoto, T. (2001). Conditional modification of behavior in Drosophila by targeted expression of a temperature-sensitive shibire allele in defined neurons. *Journal of Neurobiology*, 47(2):81–92.

Klapoetke, N. C., Murata, Y., Kim, S. S., Pulver, S. R., Birdsey-Benson, A., Cho, Y. K., Morimoto, T. K., Chuong, A. S., Carpenter, E. J., Tian, Z., Wang, J., Xie, Y., Yan, Z., Zhang, Y., Chow, B. Y., Surek, B., Melkonian, M., Jayaraman, V., Constantine-Paton, M., Wong, G. K.-S., and Boyden, E. S. (2014). Independent optical excitation of distinct neural populations. *Nature Methods*, 11(3):338–346.

Klein, M., Afonso, B., Vonner, A. J., Hernandez-Nunez, L., Berck, M., Tabone, C. J., Kane, E. A., Pieribone, V. A., Nitabach, M. N., Cardona, A., Zlatic, M., Sprecher, S. G., Gershow, M., Garrity, P. A., and Samuel, A. D. T. (2015). Sensory determinants of behavioral dynamics in Drosophila thermotaxis. *Proceedings of the National Academy of Sciences*, 112(2):E220–E229.

Kong, E. C., Woo, K., Li, H., Lebestky, T., Mayer, N., Sniffen, M. R., Heberlein, U., Bainton, R. J., Hirsh, J., and Wolf, F. W. (2010). A Pair of Dopamine Neurons Target the D1-Like Dopamine Receptor DopR in the Central Complex to Promote Ethanol-Stimulated Locomotion in Drosophila. *PLoS ONE*, 5(4):e9954.

Krajbich, I. (2019). Accounting for attention in sequential sampling models of decision making. *Current Opinion in Psychology*, 29:6–11.

Kudow, N., Miura, D., Schleyer, M., Toshima, N., Gerber, B., and Tanimura, T. (2017). Preference for and learning of amino acids in larval Drosophila. *Biology Open*, 6(3):365–369.

Kwon, J. Y., Dahanukar, A., Weiss, L. A., and Carlson, J. R. (2007). The molecular basis of CO2 reception in Drosophila. *Proceedings of the National Academy of Sciences*, 104(9):3574–3578.

Kwon, J. Y., Dahanukar, A., Weiss, L. A., and Carlson, J. R. (2011). Molecular and Cellular Organization of the Taste System in the Drosophila Larva. *Journal of Neuroscience*, 31(43):15300–15309.

Lahiri, S., Shen, K., Klein, M., Tang, A., Kane, E., Gershow, M., Garrity, P., and Samuel, A. D. T. (2011). Two Alternating Motor Programs Drive Navigation in Drosophila Larva. *PLoS ONE*, 6(8):e23180.

Lai, C. S. L., Fisher, S. E., Hurst, J. A., Vargha-Khadem, F., and Monaco, A. P. (2001). A forkhead-domain gene is mutated in a severe speech and language disorder. *Nature*, 413(6855):519–523.

Lai, S.-L. and Lee, T. (2006). Genetic mosaic with dual binary transcriptional systems in Drosophila. *Nature Neuroscience*, 9(5):703–709.

Larderet, I., Fritsch, P. M. J., Gendre, N., Neagu-Maier, G. L., Fetter, R. D., Schneider-Mizell, C. M., Truman, J. W., Zlatic, M., Cardona, A., and Sprecher, S. G. (2017). Organization of the Drosophila larval visual circuit. *eLife*, 6:e28387.

Lee, P. T., Lin, H. W., Chang, Y. H., Fu, T. F., Dubnau, J., Hirsh, J., Lee, T., and Chiang, A. S. (2011). Serotonin-mushroom body circuit modulating the formation of anesthesia-resistant memory in Drosophila. *Proceedings of the National Academy of Sciences*, 108(33):13794–13799.

Lee, T. and Luo, L. (1999). Mosaic analysis with a repressible cell marker for studies of gene function in neuronal morphogenesis. *Neuron*, 22(3):451–461.

Li, H., Chaney, S., Forte, M., and Hirsh, J. (2000). Ectopic G-protein expression in dopamine and serotonin neurons blocks cocaine sensitization in Drosophila melanogaster. *Current Biology*, 10(4):211–214.

Li, H.-H., Kroll, J. R., Lennox, S. M., Ogundeyi, O., Jeter, J., Depasquale, G., and Truman, J. W. (2014). A GAL4 driver resource for developmental and behavioral studies on the larval CNS of Drosophila. *Cell Reports*, 8(3):897–908.

Li, Y., Yao, Q., Tian, B., and Xu, W. (2011). Fast double-parallel image processing based on FPGA. In *IEEE International Conference on Vehicular Electronics and Safety*, pages 97–102. IEEE.

Lima, S. Q. and Miesenböck, G. (2005). Remote control of behavior through genetically targeted photostimulation of neurons. *Cell*, 121(1):141–152.

Lin, S., Owald, D., Chandra, V., Talbot, C., Huetteroth, W., and Waddell, S. (2014). Neural correlates of water reward in thirsty Drosophila. *Nature Neuroscience*, 17(11):1536–1542.

Liu, C., Plaçais, P.-Y., Yamagata, N., Pfeiffer, B. D., Aso, Y., Friedrich, A. B., Siwanowicz, I., Rubin, G. M., Preat, T., and Tanimoto, H. (2012). A subset of dopamine neurons signals reward for odour memory in Drosophila. *Nature*, 488(7412):512–516.

Liu, L., Leonard, A. S., Motto, D. G., Feller, M. A., Price, M. P., Johnson, W. A., and Welsh, M. J. (2003). Contribution of Drosophila DEG/ENaC Genes to Salt Taste. *Neuron*, 39(1):133–146.

Liu, Z., Zhou, J., Li, Y., Hu, F., Lu, Y., Ma, M., Feng, Q., Zhang, J.-e., Wang, D., Zeng, J., Bao, J., Kim, J.-Y., Chen, Z.-F., El Mestikawy, S., and Luo, M. (2014). Dorsal Raphe Neurons Signal Reward through 5-HT and Glutamate. *Neuron*, 81(6):1360–1374.

Lorenzetti, F. D., Baxter, D. A., and Byrne, J. H. (2008). Molecular Mechanisms Underlying a Cellular Analog of Operant Reward Learning. *Neuron*, 59(5):815–828.

Lovell, J. M., Mylius, J., Scheich, H., and Brosch, M. (2015). Stimulation of the dopaminergic midbrain as a behavioral reward in instrumentally conditioned monkeys. *Brain Stimulation*, 8(5):868–874.

Lovinger, D. M. (2010). Neurotransmitter Roles in Synaptic Modulation, Plasticity and Learning in the Dorsal Striatum. *Neuropharmacology*, 58(7):951–961.

Luan, H., Peabody, N. C., Vinson, C. R., and White, B. H. (2006). Refined Spatial Manipulation of Neuronal Function by Combinatorial Restriction of Transgene Expression. *Neuron*, 52(3):425–436.

Lundell, M. J. and Hirsh, J. (1994). Temporal and Spatial Development of Serotonin and Dopamine Neurons in the Drosophila CNS. *Developmental Biology*, 165(2):385–396.

Lundell, M. J. and Hirsh, J. (1998). eagle is required for the specification of serotonin neurons and other neuroblast 7-3 progeny in the Drosophila CNS. *Development*, 125(3):463–472.

Luo, L., Gershow, M., Rosenzweig, M., Kang, K., Fang-Yen, C., Garrity, P. A., and Samuel, A. (2010). Navigational decision-making in Drosophila thermotaxis. *Journal of Neuroscience*, 30(12):4261–4272.

Marin, E. C., Jefferis, G. S. X. E., Komiyama, T., Zhu, H., and Luo, L. (2002). Representation of the Glomerular Olfactory Map in the Drosophila Brain. *Cell*, 109:243–255.

Masek, P. and Scott, K. (2010). Limited taste discrimination in Drosophila. *Proceedings of the National Academy of Sciences*, 107(33):14833–14838.

Masson, J.-B., Voisinne, G., Wong-Ng, J., Celani, A., and Vergassola, M. (2012). Noninvasive inference of the molecular chemotactic response using bacterial trajectories. *Proceedings of the National Academy of Sciences*, 109(5):1802–1807.

McDannald, M. A., Lucantonio, F., Burke, K. A., Niv, Y., and Schoenbaum, G. (2011). Ventral Striatum and Orbitofrontal Cortex Are Both Required for Model-Based, But Not Model-Free, Reinforcement Learning. *Journal of Neuroscience*, 31(7):2700–2705.

McGinnis, J. P., Jiang, H., Agha, M. A., Sanchez, C. P., Lange, J., Yu, Z., Marion-Poll, F., and Si, K. (2016). Immediate perception of a reward is distinct from the reward's long-term salience. *eLife*, 5:e22283.

Mendoza, E., Colomb, J., Rybak, J., Pflüger, H. J., Zars, T., Scharff, C., and Brembs, B. (2014). Drosophila FoxP mutants are deficient in operant self-learning. *PLoS ONE*, 9(6):e100648.

Meneses, A. and Liy-Salmeron, G. (2012). Serotonin and emotion, learning and memory. *Reviews in the Neurosciences*, 23(5-6):543–553.

Menne, D. and Spatz, H.-C. (1977). Colour Vision in Drosophila melanogaster. *Journal of Comparative Physiology A*, 114(3):301–312.

Mirat, O., Sternberg, J. R., Severi, K. E., and Wyart, C. (2013). ZebraZoom: an automated program for high-throughput behavioral analysis and categorization. *Frontiers in Neural Circuits*, 7:107.

Mischiati, M., Lin, H.-T., Herold, P., Imler, E., Olberg, R., and Leonardo, A. (2015). Internal models direct dragonfly interception steering. *Nature*, 517(7534):333–338.

Mishra, D., Miyamoto, T., Rezenom, Y. H., Broussard, A., Yavuz, A., Slone, J., Russell, D. H., and Amrein, H. (2013). The Molecular Basis of Sugar Sensing in Drosophila Larvae. *Current Biology*, 23(15):1466–1471.

Miyamoto, T., Slone, J., Song, X., and Amrein, H. (2012). A Fructose Receptor Functions as a Nutrient Sensor in the Drosophila Brain. *Cell*, 151(5):1113–1125.

Mora, F., Avrith, D. B., Phillips, A. G., and Rolls, E. T. (1979). Effects of satiety on self-stimulation of the orbitofrontal cortex in the rhesus monkey. *Neuroscience Letters*, 13(2):141–145.

Mueller, K. P. and Neuhauss, S. C. F. (2012). Automated visual choice discrimination learning in zebrafish (Danio rerio). *Journal of Integrative Neuroscience*, 11(1):73–85.

Nargeot, R., Baxter, D. A., and Byrne, J. H. (1997). Contingent-dependent enhancement of rhythmic motor patterns: an in vitro analog of operant conditioning. *The Journal of Neuroscience*, 17(21):8093–8105.

Nargeot, R., Le Bon-Jego, M., and Simmers, J. (2009). Cellular and Network Mechanisms of Operant Learning-Induced Compulsive Behavior in Aplysia. *Current Biology*, 19(12):975–984.

Nern, A., Pfeiffer, B. D., and Rubin, G. M. (2015). Optimized tools for multicolor stochastic labeling reveal diverse stereotyped cell arrangements in the fly visual system. *Proceedings of the National Academy of Sciences*, 112(22):E2967–E2976.

Neuser, K., Husse, J., Stock, P., and Gerber, B. (2005). Appetitive olfactory learning in Drosophila larvae: effects of repetition, reward strength, age, gender, assay type and memory span. *Animal Behaviour*, 69(4):891–898.

Neuser, K., Triphan, T., Mronz, M., Poeck, B., and Strauss, R. (2008). Analysis of a spatial orientation memory in Drosophila. *Nature*, 453(7199):1244–1247.

Ni, L., Klein, M., Svec, K. V., Budelli, G., Chang, E. C., Ferrer, A. J., Benton, R., Samuel, A. D. T., and Garrity, P. A. (2016). The Ionotropic Receptors IR21a and IR25a mediate cool sensing in Drosophila. *eLife*, 5:e13254.

Niewalda, T., Singhal, N., Fiala, A., Saumweber, T., Wegener, S., and Gerber, B. (2008). Salt Processing in Larval Drosophila: Choice, Feeding, and Learning Shift from Appetitive to Aversive in a Concentration-Dependent Way. *Chemical Senses*, 33(8):685–692.

Nishijima, S. and Maruyama, I. N. (2017). Appetitive Olfactory Learning and Long-Term Associative Memory in Caenorhabditis elegans. *Frontiers in Behavioral Neuroscience*, 11:80.

Nottebohm, F. (1991). Reassessing the mechanisms and origins of vocal learning in birds. *Trends in Neurosciences*, 14(5):206–211.

Nurvitadhi, E., Sheffield, D., Jaewoong Sim, Mishra, A., Venkatesh, G., and Marr, D. (2016). Accelerating Binarized Neural Networks: Comparison of FPGA, CPU, GPU, and ASIC.

In *International Conference on Field-Programmable Technology (FPT)*, pages 77–84. IEEE.

Nuwal, N., Stock, P., Hiemeyer, J., Schmid, B., Fiala, A., and Buchner, E. (2012). Avoidance of Heat and Attraction to Optogenetically Induced Sugar Sensation as Operant Behavior in Adult Drosophila. *Journal of Neurogenetics*, 26(3-4):298–305.

Ohyama, T., Jovanic, T., Denisov, G., Dang, T. C., Hoffmann, D., Kerr, R. A., and Zlatic, M. (2013). High-Throughput Analysis of Stimulus-Evoked Behaviors in Drosophila Larva Reveals Multiple Modality-Specific Escape Strategies. *PLoS ONE*, 8(8):e71706.

Ohyama, T., Schneider-Mizell, C. M., Fetter, R. D., Aleman, J. V., Franconville, R., Rivera-Alba, M., Mensh, B. D., Branson, K. M., Simpson, J. H., Truman, J. W., Cardona, A., and Zlatic, M. (2015). A multilevel multimodal circuit enhances action selection in Drosophila. *Nature*, 520(7549):633–639.

Olds, J. and Milner, P. (1954). Positive reinforcement produced by electrical stimulation of septal area and other regions of rat brain. *Journal of Comparative and Physiological Psychology*, 47(6):419–427.

Owald, D., Felsenberg, J., Talbot, C. B., Das, G., Perisse, E., Huetteroth, W., and Waddell, S. (2015). Activity of defined mushroom body output neurons underlies learned olfactory behavior in Drosophila. *Neuron*, 86(2):417–427.

Owald, D. and Waddell, S. (2015). Olfactory learning skews mushroom body output pathways to steer behavioral choice in Drosophila. *Current Opinion in Neurobiology*, 35:178–184.

Park, J., Lee, S. B., Lee, S., Kim, Y., Song, S., Kim, S., Bae, E., Kim, J., Shong, M., Kim, J.-M., and Chung, J. (2006). Mitochondrial dysfunction in Drosophila PINK1 mutants is complemented by parkin. *Nature*, 441(7097):1157–1161.

Pauls, D., Pfitzenmaier, J. E. R., Krebs-Wheaton, R., Selcho, M., Stocker, R. F., and Thum, A. S. (2010). Electric shock-induced associative olfactory learning in Drosophila larvae. *Chemical Senses*, 35(4):335–346.

Pavlov, I. P. (1927). *Conditioned reflexes: an investigation of the physiological activity of the cerebral cortex*. Oxford University Press, Oxford.

Perisse, E., Owald, D., Barnstedt, O., Talbot, C. B., Huetteroth, W., and Waddell, S. (2016). Aversive Learning and Appetitive Motivation Toggle Feed-Forward Inhibition in the Drosophila Mushroom Body. *Neuron*, 90(5):1086–1099.

Pfeiffer, B. D., Jenett, A., Hammonds, A. S., Ngo, T.-T. B., Misra, S., Murphy, C., Scully, A., Carlson, J. W., Wan, K. H., Laverty, T. R., Mungall, C., Svirskas, R., Kadonaga, J. T., Doe, C. Q., Eisen, M. B., Celniker, S. E., and Rubin, G. M. (2008). Tools for neuroanatomy and neurogenetics in Drosophila. *Proceedings of the National Academy of Sciences*, 105(28):9715–9720.

Pfeiffer, B. D., Ngo, T.-T. B., Hibbard, K. L., Murphy, C., Jenett, A., Truman, J. W., and Rubin, G. M. (2010). Refinement of Tools for Targeted Gene Expression in Drosophila. *Genetics*, 186(2):735–755.

Pfeiffer, B. D., Truman, J. W., and Rubin, G. M. (2012). Using translational enhancers to increase transgene expression in Drosophila. *Proceedings of the National Academy of Sciences*, 109(17):6626–6631.

Pickett, E., Pullara, O., O'Grady, J., and Gordon, B. (2009). Speech Acquisition in Older Nonverbal Individuals With Autism. *Cognitive and Behavioral Neurology*, 22(1):1–21.

Plaçais, P. Y., Trannoy, S., Friedrich, A. B., Tanimoto, H., and Preat, T. (2013). Two pairs of mushroom body efferent neurons are required for appetitive long-term memory retrieval in drosophila. *Cell Reports*, 5(3):769–780.

Potter, C. J., Tasic, B., Russler, E. V., Liang, L., and Luo, L. (2010). The Q System: A Repressible Binary System for Transgene Expression, Lineage Tracing, and Mosaic Analysis. *Cell*, 141(3):536–548.

Pu, Y., Zhang, Y., Zhang, Y., and Shen, P. (2018). Two Drosophila Neuropeptide Y-like Neurons Define a Reward Module for Transforming Appetitive Odor Representations to Motivation. *Scientific Reports*, 8:11658.

Redgrave, P., Vautrelle, N., and Reynolds, J. N. J. (2011). Functional properties of the basal ganglia's re-entrant loop architecture: selection and reinforcement. *Neuroscience*, 198:138–151.

Rescorla, R. A. (1988). Behavioral Studies of Pavlovian Conditioning. *Annual Review of Neuroscience*, 11:329–352.

Reynolds, J. N. J. and Wickens, J. R. (2002). Dopamine-dependent plasticity of corticostriatal synapses. *Neural Networks*, 15(4-6):507–521.

Robertson, J. L., Tsubouchi, A., and Tracey, W. D. (2013). Larval Defense against Attack from Parasitoid Wasps Requires Nociceptive Neurons. *PLoS ONE*, 8(10):e78704.

Robie, A. A., Hirokawa, J., Edwards, A. W., Umayam, L. A., Lee, A., Phillips, M. L., Card, G. M., Korff, W., Rubin, G. M., Simpson, J. H., Reiser, M. B., and Branson, K. (2017). Mapping the Neural Substrates of Behavior. *Cell*, 170(2):393–406.

Rohwedder, A., Pfitzenmaier, J. E., Ramsperger, N., Apostolopoulou, A. A., Widmann, A., and Thum, A. S. (2012). Nutritional Value-Dependent and Nutritional Value-Independent Effects on Drosophila melanogaster Larval Behavior. *Chemical Senses*, 37(8):711–721.

Rohwedder, A., Selcho, M., Chassot, B., and Thum, A. S. (2015). Neuropeptide F neurons modulate sugar reward during associative olfactory learning of Drosophila larvae. *Journal of Comparative Neurology*, 523(18):2637–2664.

Rohwedder, A., Wenz, N. L., Stehle, B., Huser, A., Yamagata, N., Zlatic, M., Truman, J. W., Tanimoto, H., Saumweber, T., Gerber, B., and Thum, A. S. (2016). Four Individually Identified Paired Dopamine Neurons Signal Reward in Larval Drosophila. *Current Biology*, 26(5):661–669.

Rosenegger, D. and Lukowiak, K. (2010). The participation of NMDA receptors, PKC, and MAPK in the formation of memory following operant conditioning in Lymnaea. *Molecular Brain*, 3(1):24.

Roy, B., Singh, A. P., Shetty, C., Chaudhary, V., North, A., Landgraf, M., VijayRaghavan, K., and Rodrigues, V. (2007). Metamorphosis of an identified serotonergic neuron in the Drosophila olfactory system. *Neural Development*, 2(1):20.

Saumweber, T., Husse, J., and Gerber, B. (2011). Innate attractiveness and associative learnability of odors can be dissociated in larval Drosophila. *Chemical Senses*, 36(3):223–235.

Saumweber, T., Rohwedder, A., Schleyer, M., Eichler, K., Chen, Y.-c., Aso, Y., Cardona, A., Eschbach, C., Kobler, O., Voigt, A., Durairaja, A., Mancini, N., Zlatic, M., Truman, J. W., Thum, A. S., and Gerber, B. (2018). Functional architecture of reward learning in mushroom body extrinsic neurons of larval Drosophila. *Nature Communications*, 9(1):1104.

Sawin-McCormack, E. P., Sokolowski, M. B., and Campos, A. R. (1995). Characterization and Genetic Analysis of Drosophila Melanogaster Photobehavior During Larval Development. *Journal of Neurogenetics*, 10(2):119–135.

Scherer, S., Stocker, R. F., and Gerber, B. (2003). Olfactory Learning in Individually Assayed Drosophila Larvae. *Learning & Memory*, 10(3):217–225.

Schipanski, A., Yarali, A., Niewalda, T., and Gerber, B. (2008). Behavioral Analyses of Sugar Processing in Choice, Feeding, and Learning in Larval Drosophila. *Chemical Senses*, 33(6):563–573.

Schlegel, P., Texada, M. J., Miroschnikow, A., Schoofs, A., Hückesfeld, S., Peters, M., Schneider-Mizell, C. M., Lacin, H., Li, F., Fetter, R. D., Truman, J. W., Cardona, A., and Pankratz, M. J. (2016). Synaptic transmission parallels neuromodulation in a central food-intake circuit. *eLife*, 5:e16799.

Schleyer, M., Miura, D., Tanimura, T., and Gerber, B. (2015). Learning the specific quality of taste reinforcement in larval Drosophila. *eLife*, 4:e04711.

Schleyer, M., Saumweber, T., Nahrendorf, W., Fischer, B., von Alpen, D., Pauls, D., Thum, A., and Gerber, B. (2011). A behavior-based circuit model of how outcome expectations organize learned behavior in larval Drosophila. *Learning & Memory*, 18(10):639–653.

Schnaitmann, C., Vogt, K., Triphan, T., and Tanimoto, H. (2010). Appetitive and aversive visual learning in freely moving Drosophila. *Frontiers in Behavioral Neuroscience*, 4:10.

Schroll, C., Riemensperger, T., Bucher, D., Ehmer, J., Völler, T., Erbguth, K., Gerber, B., Hendel, T., Nagel, G., Buchner, E., and Fiala, A. (2006). Light-Induced Activation of Distinct Modulatory Neurons Triggers Appetitive or Aversive Learning in Drosophila Larvae. *Current Biology*, 16(17):1741–1747.

Schulze, A., Gomez-Marin, A., Rajendran, V. G., Lott, G., Musy, M., Ahammad, P., Deogade, A., Sharpe, J., Riedl, J., Jarriault, D., Trautman, E. T., Werner, C., Venkadesan, M., Druckmann, S., Jayaraman, V., and Louis, M. (2015). Dynamical feature extraction at the sensory periphery guides chemotaxis. *eLife*, 4:e06694.

Schwaerzel, M., Monastirioti, M., Scholz, H., Friggi-Grelin, F., Birman, S., and Heisenberg, M. (2003). Dopamine and Octopamine Differentiate between Aversive and Appetitive Olfactory Memories in Drosophila. *The Journal of Neuroscience*, 23(33):10495–10502.

Séjourné, J., Plaçais, P.-Y., Aso, Y., Siwanowicz, I., Trannoy, S., Thoma, V., Tedjakumala, S. R., Rubin, G. M., Tchénio, P., Ito, K., Isabel, G., Tanimoto, H., and Preat, T. (2011). Mushroom body efferent neurons responsible for aversive olfactory memory retrieval in Drosophila. *Nature Neuroscience*, 14(7):903–910.

Selcho, M., Pauls, D., Han, K.-A., Stocker, R. F., and Thum, A. S. (2009). The Role of Dopamine in Drosophila Larval Classical Olfactory Conditioning. *PLoS ONE*, 4(6):e5897.

Shao, L., Saver, M., Chung, P., Ren, Q., Lee, T., Kent, C. F., and Heberlein, U. (2017). Dissection of the Drosophila neuropeptide F circuit using a high-throughput two-choice assay. *Proceedings of the National Academy of Sciences*, 114(38):E8091–E8099.

Shen, P. and Cai, H. N. (2001). Drosophila neuropeptide F mediates integration of chemosensory stimulation and conditioning of the nervous system by food. *Journal of Neurobiology*, 47(1):16–25.

Shen, W., Hamilton, S. E., Nathanson, N. M., and Surmeier, D. J. (2005). Cholinergic Suppression of KCNQ Channel Currents Enhances Excitability of Striatal Medium Spiny Neurons. *Journal of Neuroscience*, 25(32):7449–7458.

Shirvaikar, M. and Bushnaq, T. (2009). A comparison between DSP and FPGA platforms for real-time imaging applications. In Kehtarnavaz, N. and Carlsohn, M. F., editors, *Real-Time Image and Video Processing*, volume 7244, page 724406. International Society for Optics and Photonics.

Shohat-Ophir, G., Kaun, K. R., Azanchi, R., Mohammed, H., and Heberlein, U. (2012). Sexual Deprivation Increases Ethanol Intake in Drosophila. *Science*, 335(6074):1351–1355.

Shyu, W.-H., Chiu, T.-H., Chiang, M.-H., Cheng, Y.-C., Tsai, Y.-L., Fu, T.-F., Wu, T., and Wu, C.-L. (2017). Neural circuits for long-term water-reward memory processing in thirsty Drosophila. *Nature Communications*, 8:15230.

Sison, M. and Gerlai, R. (2010). Associative learning in zebrafish (Danio rerio) in the plus maze. *Behavioural Brain Research*, 207(1):99–104.

Sitaraman, D., LaFerriere, H., Birman, S., and Zars, T. (2012). Serotonin is Critical for Rewarded Olfactory Short-Term Memory in Drosophila. *Journal of Neurogenetics*, 26(2):238–244.

Sitaraman, D., Zars, M., LaFerriere, H., Chen, Y.-C., Sable-Smith, A., Kitamoto, T., Rottinghaus, G. E., and Zars, T. (2008). Serotonin is necessary for place memory in Drosophila. *Proceedings of the National Academy of Sciences*, 105(14):5579–5584.

Skeath, J. B. and Thor, S. (2003). Genetic control of Drosophila nerve cord development. *Current Opinion in Neurobiology*, 13(1):8–15.

Skinner, B. F. (1938). *The Behavior of Organisms: An Experimental Analysis*. NY: Appleton-Century-Crofts, New York.

Soares dos Santos, M. P. and Ferreira, J. (2014). Novel intelligent real-time position tracking system using FPGA and fuzzy logic. *ISA Transactions*, 53(2):402–414.

St Johnston, D. (2002). The art and design of genetic screens: Drosophila melanogaster. *Nature Reviews Genetics*, 3(3):176–188.

Stowers, J. R., Hofbauer, M., Bastien, R., Griessner, J., Higgins, P., Farooqui, S., Fischer, R. M., Nowikovsky, K., Haubensak, W., Couzin, I. D., Tessmar-Raible, K., and Straw, A. D. (2017). Virtual reality for freely moving animals. *Nature Methods*, 14(10):995–1002.

Straw, A. D., Branson, K., Neumann, T. R., and Dickinson, M. H. (2011). Dimensional Tracking of Multiple Flying Animals. *Journal of the Royal Society Interface*, 8(56):395–409.

Straw, A. D. and Dickinson, M. H. (2009). Motmot, an open-source toolkit for realtime video acquisition and analysis. *Source Code for Biology and Medicine*, 4:5.

Sturdy, C. B. and Nicoladis, E. (2017). How Much of Language Acquisition Does Operant Conditioning Explain? *Frontiers in Psychology*, 8:1918.

Surmeier, D. J., Ding, J., Day, M., Wang, Z., and Shen, W. (2007). D1 and D2 dopamine-receptor modulation of striatal glutamatergic signaling in striatal medium spiny neurons. *Trends in Neurosciences*, 30(5):228–235.

Swierczek, N. A., Giles, A. C., Rankin, C. H., and Kerr, R. A. (2011). High-throughput behavioral analysis in C. elegans. *Nature Methods*, 8(7):592–598.

Sykes, P. A. and Condron, B. G. (2005). Development and sensitivity to serotonin of Drosophila serotonergic varicosities in the central nervous system. *Developmental Biology*, 286(1):207–216.

Takeda, K. (1961). Classical conditioned response in the honey bee. *Journal of Insect Physiology*, 6:169–179.

Tastekin, I., Riedl, J., Schilling-Kurz, V., Gomez-Marin, A., Truman, J. W., and Louis, M. (2015). Role of the subesophageal zone in sensorimotor control of orientation in Drosophila larva. *Current Biology*, 25(11):1448–1460.

Thorndike, E. L. (1911). *Animal intelligence; experimental studies*. The Macmillan company, New York.

Tonegawa, S., Pignatelli, M., Roy, D. S., and Ryan, T. J. (2015). Memory engram storage and retrieval. *Current Opinion in Neurobiology*, 35:101–109.

Topál, J., Byrne, R. W., Miklósi, Á., and Csányi, V. (2006). Reproducing human actions and action sequences: "Do as I do!" in a dog. *Animal Cognition*, 9(4):355–367.

Tracey, W. D., Wilson, R. I., Laurent, G., and Benzer, S. (2003). painless, a Drosophila Gene Essential for Nociception. *Cell*, 113(2):261–273.

Tsubouchi, A., Caldwell, J. C., and Tracey, W. D. (2012). Dendritic filopodia, ripped pocket, NOMPC, and NMDARs contribute to the sense of touch in Drosophila larvae. *Current Biology*, 22:2124–2134.

Tully, T., Cambiazo, V., and Kruse, L. (1994). Memory through Metamorphosis. *Journal of Neuroscience*, 14(1):68–74.

Tully, T. and Quinn, W. G. (1985). Classical conditioning and retention in normal and mutant Drosophila melanogaster. *Journal of Comparative Physiology A*, 157(2):263–277.

Turner, G. C., Bazhenov, M., and Laurent, G. (2008). Olfactory Representations by Drosophila Mushroom Body Neurons. *Journal of Neurophysiology*, 99(2):734–746.

Uzun, I. S., Amira, A., and Bouridane, A. (2005). FPGA implementations of fast Fourier transforms for real-time signal and image processing. *IEE Proceedings - Vision, Image, and Signal Processing*, 152(3):283–296.

Veeraraghavan, A., Chellappa, R., and Srinivasan, M. (2008). Shape-and-Behavior Encoded Tracking of Bee Dances. *IEEE Transactions on Pattern Analysis and Machine Intelligence*, 30(3):463–476.

Vinauger, C., Lutz, E. K., and Riffell, J. A. (2014). Olfactory learning and memory in the disease vector mosquito Aedes aegypti. *Journal of Experimental Biology*, 217(13):2321–2330.

Vogelstein, J. T., Park, Y., Ohyama, T., Kerr, R. A., Truman, J. W., Priebe, C. E., and Zlatic, M. (2014). Discovery of Brainwide Neural-Behavioral Maps via Multiscale Unsupervised Structure Learning. *Science*, 344(6182):386–392.

Vogt, K., Schnaitmann, C., Dylla, K. V., Knapek, S., Aso, Y., Rubin, G. M., and Tanimoto, H. (2014). Shared mushroom body circuits underlie visual and olfactory memories in Drosophila. *eLife*, 3:e02395.

von Essen, A. M. H. J., Pauls, D., Thum, A. S., and Sprecher, S. G. (2011). Capacity of Visual Classical Conditioning in Drosophila Larvae. *Behavioral Neuroscience*, 125(6):921–929.

Waddell, S. (2013). Reinforcement signalling in Drosophila; dopamine does it all after all. *Current Opinion in Neurobiology*, 23(3):324–329.

Wang, Y., Pu, Y., and Shen, P. (2013). Neuropeptide-Gated Perception of Appetitive Olfactory Inputs in Drosophila Larvae. *Cell Reports*, 3(3):820–830.

Webb, B. (2004). Neural mechanisms for prediction: Do insects have forward models? *Trends in Neurosciences*, 27(5):278–282.

Weiglein, A., Gerstner, F., Mancini, N., Schleyer, M., and Gerber, B. (2019). One-trial learning in larval Drosophila. *Learning & Memory*, 26(4):109–120.

Wen, J. Y. M., Kumar, N., Morrison, G., Rambaldini, G., Runciman, S., Rousseau, J., and van der Kooy, D. (1997). Mutations that prevent associative learning in C. elegans. *Behavioral Neuroscience*, 111(2):354–368.

Wen, T., Parrish, C. A., Xu, D., Wu, Q., and Shen, P. (2005). Drosophila neuropeptide F and its receptor, NPFR1, define a signaling pathway that acutely modulates alcohol sensitivity. *Proceedings of the National Academy of Sciences*, 102(6):2141–2146.

White, J. G., Southgate, E., Thomson, J. N., and Brenner, S. (1986). The Structure of the Nervous System of the Nematode Caenorhabditis elegans. *Philosophical Transactions of the Royal Society B*, 314(1165):1–340.

Wirtz, R. A. and Semey, H. G. (1982). The Drosophila kitchen-equipment, media preparation, and supplies. *Drosophila Information Service*, 58:176–180.

Wolf, R. and Heisenberg, M. (1991). Basic organization of operant behavior as revealed in Drosophila flight orientation. *Journal of Comparative Physiology A*, 169(6):699–705.

Wolf, R., Wittig, T., Liu, L., Wustmann, G., Eyding, D., and Heisenberg, M. (1998). Drosophila mushroom bodies are dispensable for visual, tactile, and motor learning. *Learning & Memory*, 5(1-2):166–78.

Wong, A. M., Wang, J. W., and Axel, R. (2002). Spatial representation of the glomerular map in the Drosophila protocerebrum. *Cell*, 109(2):229–241.

Wright, G. A., Mustard, J. A., Simcock, N. K., Ross-Taylor, A. A. R., McNicholas, L. D., Popescu, A., and Marion-Poll, F. (2010). Parallel reinforcement pathways for conditioned food aversions in the honeybee. *Current Biology*, 20(24):2234–2240.

Wu, M.-C., Chu, L.-A., Hsiao, P.-Y., Lin, Y.-Y., Chi, C.-C., Liu, T.-H., Fu, C.-C., and Chiang, A.-S. (2014). Optogenetic control of selective neural activity in multiple freely moving Drosophila adults. *Proceedings of the National Academy of Sciences*, 111(14):5367–5372.

Xiang, Y., Yuan, Q., Vogt, N., Looger, L. L., Jan, L. Y., and Jan, Y. N. (2010). Light-avoidance-mediating photoreceptors tile the Drosophila larval body wall. *Nature*, 468(7326):921–926.

Yasukawa, S., Okuno, H., Ishii, K., and Yagi, T. (2016). Real-time object tracking based on scale-invariant features employing bio-inspired hardware. *Neural Networks*, 81:29–38.

Yu, D., Keene, A. C., Srivatsan, A., Waddell, S., and Davis, R. L. (2005). Drosophila DPM neurons form a delayed and branch-specific memory trace after olfactory classical conditioning. *Cell*, 123(5):945–957.

Zabala, F., Polidoro, P., Robie, A., Branson, K., Perona, P., and Dickinson, M. H. (2012). A Simple Strategy for Detecting Moving Objects during Locomotion Revealed by Animal-Robot Interactions. *Current Biology*, 22(14):1344–1350.

Zemelman, B. V., Lee, G. A., Ng, M., and Miesenböck, G. (2002). Selective photostimulation of genetically chARGed neurons. *Neuron*, 33(1):15–22.

Zhang, C., Liang, T., Mok, P. K. T., and Yu, W. (2017). FPGA Implementation of the Coupled Filtering Method and the Affine Warping Method. *IEEE Transactions on Nanobioscience*, 16(5):314–325.

Zwillinger, D. (2003). *CRC Standard Mathematical Tables and Formulae*. CRC Press, Boca Raton, 31 edition.